

---

Monticello Nuclear Power Plant

Qualification of Reactor Physics  
Methods for Application to Monticello  
Revision 3

NSPNAD-8609-A Revision 3

---

October 1995

Northern States Power Company  
Nuclear Analysis & Design

9601170268 960110  
PDR ADOCK 05000263  
P PDR





---

Monticello Nuclear Power Plant

**Qualification of Reactor Physics  
Methods for Application to Monticello  
Revision 3**

NSPNAD-8609-A Revision 3

---

October 1995

Northern States Power Company  
Nuclear Analysis & Design

9601170268 960110  
PDR ABCK 05000263  
PDR



UNITED STATES  
NUCLEAR REGULATORY COMMISSION

WASHINGTON, D.C. 20555-0001

September 11, 1995

Mr. Roger O. Anderson, Director  
Licensing and Management Issues  
Northern States Power Company  
414 Nicollet Mall  
Minneapolis, Minnesota 55401

SUBJECT: MONTICELLO NUCLEAR GENERATING PLANT - REVIEW OF TOPICAL REPORT  
NSPNAD-8609, REVISION 2, "QUALIFICATION OF REACTOR PHYSICS METHODS  
FOR APPLICATION TO MONTICELLO" (TAC NO. M90277)

Dear Mr. Anderson:

By letter dated August 23, 1994, Northern States Power Company submitted, for the staff review and approval, a Revision 2 of the Topical Report NSPNAD-8609, "Qualification of Reactor Physics Methods for Application to Monticello." This submittal describes the new qualification of new methods based on CASMO-3/SIMULATE-3, for application to operations and reload safety evaluations for the Monticello plant.

The staff has reviewed the submittal and concluded that the application of CASMO-3/SIMULATE-3 is acceptable for use in the Monticello boiling-water reactor reload analyses. Details of our review are provided in the enclosed safety evaluation. This action closes TAC No. M90277. If you have any questions concerning this action please call me at (301) 415-1392.

Sincerely,

A handwritten signature in cursive script, appearing to read "Tae Kim".

Tae Kim, Project Manager  
Project Directorate III-1  
Division of Reactor Projects - III/IV  
Office of Nuclear Reactor Regulation

Docket No. 50-263

Enclosure: Safety Evaluation

cc w/encl: See next page

Mr. Roger O. Anderson, Director  
Northern States Power Company

Monticello Nuclear Generating Plant

cc:

J. E. Silberg, Esquire  
Shaw, Pittman, Potts and Trowbridge  
2300 N Street, N. W.  
Washington DC 20037

Adonis A. Neblett  
Assistant Attorney General  
Office of the Attorney General  
445 Minnesota Street  
Suite 900  
St. Paul, Minnesota 55101-2127

U.S. Nuclear Regulatory Commission  
Resident Inspector's Office  
2807 W. County Road 75  
Monticello, Minnesota 55362

Plant Manager  
Monticello Nuclear Generating Plant  
ATTN: Site Licensing  
Northern States Power Company  
2807 West County Road 75  
Monticello, Minnesota 55362-9637

Robert Nelson, President  
Minnesota Environmental Control  
Citizens Association (MECCA)  
1051 South McKnight Road  
St. Paul, Minnesota 55119

Commissioner  
Minnesota Pollution Control Agency  
520 Lafayette Road  
St. Paul, Minnesota 55119

Regional Administrator, Region III  
U.S. Nuclear Regulatory Commission  
801 Warrenville Road  
Lisle, Illinois 60532-4351

Commissioner of Health  
Minnesota Department of Health  
717 Delaware Street, S. E.  
Minneapolis, Minnesota 55440

Darla Groshens, Auditor/Treasurer  
Wright County Government Center  
10 NW Second Street  
Buffalo, Minnesota 55313

Kris Sanda, Commissioner  
Department of Public Service  
121 Seventh Place East  
Suite 200  
St. Paul, Minnesota 55101-2145

January 1995





UNITED STATES  
NUCLEAR REGULATORY COMMISSION  
WASHINGTON, D.C. 20555-0001

SAFETY EVALUATION BY THE OFFICE OF NUCLEAR REACTOR REGULATION  
RELATING TO REVISION 2 OF TOPICAL REPORT NSPNAD-8609  
"QUALIFICATION OF REACTOR PHYSICS METHODS FOR APPLICATION TO MONTICELLO"

FOR

NORTHERN STATES POWER COMPANY

MONTICELLO NUCLEAR GENERATING PLANT

DOCKET NO. 50-263

1.0 INTRODUCTION

By letter dated August 23, 1994 (Ref. 1), the Northern States Power Company (NSP) submitted Revision 2 of the Topical Report NSPNAD-8609, "Qualification of Reactor Physics Methods for Application to Monticello," (Ref. 2) for NRC review. NSPNAD-8609, Rev. 1-A describes the currently approved methodology for the Monticello Nuclear Generating Plant. This revision documents the capability of NSP to implement and apply new methods, based on CASMO-3/SIMULATE-3 methodology, to boiling water reactor (BWR) core reload physics design activities for the Monticello unit. Both the CASMO-3 and SIMULATE-3 computer program packages have been reviewed and accepted for referencing (with certain restrictions) by separate NRC safety evaluations (Refs. 3 and 4) regarding the Yankee Atomic Electric Company (YAEC) Topical Reports YAEC-1363 (Ref. 5) and YAEC-1659 (Ref. 6). Specific limitations imposed on the use of these models at that time were:

- 1) that CASMO-3 is to be used for the core parameter ranges and configurations that were verified; i.e., new fuel designs will require additional validation, and
- 2) that SIMULATE-3 is to be used for steady-state physics analyses only with the approved versions of the CASMO-3 and TABLES-3 codes.

NSP intends to use the CASMO-3/SIMULATE-3 programs in licensing applications, including BWR reload physics design, calculations for startup predictions, generation of physics input for reload safety evaluation (RSE) analyses, core physics data books and setpoint updates for both the reactor protection and monitoring systems.

2.0 SUMMARY OF THE TOPICAL REPORT

Topical Report NSPNAD-8609, Revision 2, describes the NSP qualification of new reactor physics methods (CASMO-3/SIMULATE-3) for application to the Monticello BWR and addresses the reactor model description, qualification and

ENCLOSURE

quantification of reliability factors and applications to operations and reload safety evaluations of Monticello. The qualification benchmarking compares the CASMO-3/SIMULATE-3 model results with measurements obtained from benchmarking data covering operating cycles 11 through 15 of the Monticello unit. The plant analyses were performed over a wide range of conditions from cold (ambient) temperature to hot full power operation. The good agreement between the measured and calculated values presented in the topical report is used to validate the NSP application of these computer programs for analysis of the Monticello BWR unit.

NSP intends to use these methods for steady-state BWR core physics reload design and licensing applications, including fuel bundle and loading pattern analysis; for the generation of core physics control rod worth and startup predictions, reactivity coefficients for transient and safety analyses input; and for the potential support of the process computer core monitoring system.

## 2.1 Overview

Section 1 of the topical report provides introductory and background information and an overview of the scope of the report. The philosophy for determining the calculational uncertainties (and bias) and reliability factors is presented in Appendix A of the topical.

## 2.2 Methodology

Section 2 of the topical report describes the NSP-specific CASMO-3/SIMULATE-3 computer program package methodology, provides references for each of the individual components, and gives a flowchart for the model application.

CASMO-3 is the Studsvik Energiteknik lattice physics code (Ref. 7) used by NSP in determining the neutronics input to SIMULATE-3 for BWR core performance analyses. CASMO-3 uses a binary-format cross section library based on the standard ENDF/B-IV cross-section set with some ENDF/B-V fission spectrum updates.

SIMULATE-3 was also acquired from Studsvik of America (Ref. 8). The code is based on a modified coarse mesh (nodal) diffusion theory calculational technique, with coupled thermal hydraulic and Doppler feedback. The code includes the following modeling capabilities: solution of the two group neutron diffusion equation, fuel assembly homogenization, baffle/reflector modeling, cross-section depletion and pin power reconstruction. In order to ensure the flux continuity at nodal interfaces and perform an accurate determination of the pin-wise power distribution, SIMULATE-3 uses assembly discontinuity factors that are pre-calculated by CASMO-3. These factors are related to the ratio of the nodal surface flux in the actual heterogeneous geometry to the cell averaged flux in an equivalent homogeneous model and are determined for each energy group as a function of exposure, moderator density and control-rod-state.

The two-group model solves the neutron diffusion equation in three dimensions, and the assembly homogenization employs the flux discontinuity correction factors from CASMO-3 to combine the global (nodal) flux shape and the assembly



heterogeneous flux distribution. The flux discontinuity concept is also applied to the baffle/reflector region in both radial and axial directions to eliminate the need for user-supplied albedoes, normalization, or other adjustment at the core/reflector interface.

The SIMULATE-3 fuel depletion model uses tabular and functionalized macroscopic and/or microscopic cross sections to account for fuel exposure without tracking the individual nuclide concentrations. Depletion history effects are calculated by CASMO-3 and then processed by the TABLES-3 code (Ref. 9) for generation of the cross-section library used by SIMULATE-3.

SIMULATE-3 can be used to calculate the three-dimensional pin-by-pin power distribution in a manner that accounts for individual pin burnup and spectral effects. SIMULATE-3 also calculates control rod worth and moderator, Doppler and xenon feedback effects.

SCORE is an Electric Power Research Institute (EPRI) developed computer code (Ref. 10) for predicting best-estimate, steady-state fuel rod performance parameters for light-water reactor (LWR) fuel rods. This program has been previously reviewed and approved (Ref. 11) for use in calculating fuel rod temperatures for input to reload and safety analyses as a function of burnup and power history.

### 2.3 Benchmarking and Model Verification

Section 3 of the topical report discusses benchmarking of the NSP models to the five operating cycles which provided measured plant data from a range of plant startup and normal operation conditions.

### 2.4 Model Applications for Reactor Operating Support

Section 4 of the topical report discusses the application of the NSP models to both predictive and plant monitoring modes.

### 2.5 Model Applications to Safety Evaluation Analyses

Section 5 of the topical report describes the methods used to apply the reliability factors and biases to calculational physics results for safety applications.

## 3.0 TECHNICAL EVALUATION

### Background

The previously approved YAEC topical report (YAEC-1363) for CASMO-3 applications included a detailed description of the neutronics modeling methodology together with the YAEC validation of the code system. The basic nuclear cross-section data, unit cell calculation, two-dimensional transport theory and diffusion theory calculations, and the determination of flux discontinuity factors for use in SIMULATE-3 were described.

The original CASMO-3 validation was carried out by the code developer - Studsvik Energiteknik. This benchmarking included the calculation of a set of pin-cell critical experiments, with varying pin radius and pitch, and fuel enrichments. The YAEC validation was based on comparisons with measured critical experiments, measured fuel isotopics, and measured pin-wise La-140 distributions. These comparisons were intended to exercise and validate the depletion calculation, the spatial transport calculation and the nuclear data library. The fuel depletion calculation was validated by comparisons with the Yankee Core-1 and Zion measured uranium and plutonium isotopics which are industry-standard benchmark sources. These comparisons were performed for a range of pin-cell spectra and indicated good agreement for the fuel isotopics versus burnup. As further validation, a set of uniform critical measurements were also calculated. CASMO-3 reproduced 74 criticals to within 1 percent delta-k/k. The comparisons were analyzed as a function of rod pitch, fuel enrichment, H<sub>2</sub>O/U-ratio, soluble boron, buckling and moderator temperature, and no significant dependence of the calculation/measurement differences was observed.

In addition to the measurement benchmarks, the YAEC CASMO-3 calculation of the Brookhaven National Laboratory (BNL) Fuel Assembly Standard Problem was compared to the BNL reference solution. Comparisons of reactivity defects, control rod worth, boron worth, fuel isotopics, and pin-wise power distributions were made. The agreement was found to be very good, with the observed differences within the stated uncertainty of the BNL reference solution.

The previously approved YAEC topical report (YAEC-1659) for SIMULATE-3 applications focused upon three major areas. The first was application to operating pressurized water reactors (PWRs) and included comparisons of SIMULATE-3 generated parameters to measured data, as well as to the BNL PWR Core Standard Problem. The second application was to operating BWRs and included comparisons to measured data. The third area focused on the pin-by-pin power distribution capabilities of SIMULATE-3. This application compared multi-assembly SIMULATE-3 pin-by-pin power distributions to higher order transport theory solutions. In addition, pin-by-pin power distributions were compared between SIMULATE-3 and previously accepted PDQ-07 methods of pin power distribution calculations.

The statistics from the cold (85°F to 209°F) zero-power comparisons quantify the model accuracy for predicting reactivity for beginning-of-cycle (BOC), xenon-free and in-cycle restart conditions. Thirty-three measurements from the five operating cycles are included. Sixty-eight at-power statepoints with TIP [traversing incore probe] traces are used for reactivity comparison and power distribution reliability factors.

The statistical analysis described in Appendix A was performed on the measured versus the SIMULATE-3 calculated reactivities and TIP reaction rates.

The sample distributions were tested for normality using standard methods. The normality test is used since the standard 95 percent probability at the 95 percent confidence level [95/95] tolerance limit method assumes that the population has a normal distribution. If the distributions are not normal,



but are known, a special treatment (Appendix A) allows equivalent 95/95 statistics to be generated. Parameters not covered by the above are conservatively bounded.

#### Control rod worths

The SIMULATE-3 prediction of control rod worths was compared by NSP with the BOC zero-power startup measurements for the five operating cycles. A statistical analysis of the control rod worth differences determined the bias, standard deviation and the normality of the difference distribution. The SIMULATE-3 capability to predict the shutdown margin with the worst stuck rod was qualified by comparison to local critical measurements as well as in-sequence rod withdrawal criticals.

#### Assembly power distribution

The SIMULATE-3 calculated incore detector reaction rates and assembly power distributions were verified at NSP by comparison with direct incore signal measurements. A total of 68 incore detector (TIP) statepoints were taken at close to Hot-Full-Power (HFP) conditions from Cycles 11 through 15. The predicted reaction rates were compared with the measured signals by individual detector, assembly location, and radial level to determine the mean and standard deviation for the observed differences. The 95/95 tolerance limits for assembly peaking factors were calculated from multiplying the standard deviations by the k-value corresponding to the sample size for all statepoint conditions.

#### 4.0 SUMMARY AND CONCLUSIONS

Northern States Power Company (NSP) has performed extensive benchmarking using the CASMO-3/SIMULATE-3 methodology. This effort consisted of detailed comparisons of calculated key physics parameters with the measurements obtained from five operating cycles of the Monticello BWR plant. These results were used to determine the set of 95/95 (probability/confidence) tolerance limits for application to the calculation of the stated BWR physics parameters. This effort also demonstrated the ability of NSP to use the CASMO-3/SIMULATE-3 computer program package for application to the Monticello BWR unit.

Based on the analyses and results presented in the topical report, the staff concludes that the CASMO-3/SIMULATE-3 methodology as validated by NSP can be applied to steady-state BWR reactor physics calculations for reload applications as discussed in the above technical evaluation. The accuracy of this methodology has been demonstrated to be sufficient for use in licensing applications, including BWR reload core physics analysis, generation of safety and transient analysis inputs, startup and control rod worth predictions, and core monitoring system support.

As in the earlier approvals, application of the approved package is limited to the range of fuel configurations and core design parameters verified and referenced by this topical report; introduction of significantly different fuel designs may require further validation by the licensee.

Principal Contributor: E. Kendrick

Date: September 11, 1995

5.0 REFERENCES

1. Letter from R. O. Anderson (NSP) to Document Control Desk (USNRC), regarding "Revision 2 of Topical Report NSP-8609, 'Qualification of Reactor Physics Methods for Application to Monticello'," dated August 23, 1994.
2. NSPNAD-8609, Rev 2, "Qualification of Reactor Physics Methods for Application to Monticello," Northern States Power Company, August 1994.
3. Letter from A. C. Thadani (USNRC) to G. Papanic, Jr. (YAEC), regarding "Acceptance for Referencing of Topical Report YAEC-1363, 'CASMO-3G Validation'," March 21, 1990.
4. Letter from A. C. Thadani (USNRC) to G. Papanic, Jr. (YAEC), regarding "Acceptance for Referencing of Topical Report YAEC-1659, 'SIMULATE-3, Validation and Verification'," February 20, 1990.
5. YAEC-1363, "CASMO-3G Validation," Yankee Atomic Electric Company, April 1988.
6. YAEC-1659, "SIMULATE-3, Validation and Verification," Yankee Atomic Electric Company, September 1988.
7. M. Edenius, A. Ahlin, B. H. Forssen, "CASMO-3, A Fuel Assembly Burnup Program, User's Manual, Version 4.4," STUDSVIK/NFA-89/3, Studsvik Energiteknik AB, Sweden, November 1989. [Proprietary - Not publicly available]
8. K. S. Smith, J. A. Umbarger, D. M. Ver Planck, "SIMULATE-3, Advanced Three-Dimensional Two-Group Reactor Analysis Code, User's Manual, Version 3.0," STUDSVIK/SOA-89/03, Studsvik of America, Inc., November 1989. [Proprietary - Not publicly available]
9. K. S. Smith, J. A. Umbarger, D. M. Ver Planck, "TABLES-3, Library Preparation Code for SIMULATE-3, User's Manual, Version 3.0," STUDSVIK/SOA-89/05, Studsvik of America, Inc., November 1989. [Proprietary - Not publicly available]
10. "ESCORE - The EPRI Steady-State Core Reload Evaluator Code: General Description," EPRI-NP-5100, February 1987.
11. Letter from A. C. Thadani (USNRC) to C. R. Lehmann (Pennsylvania Power and Light Co.), regarding "Acceptance for Referencing of Licensing Topical Report EPRI-NP-5100, 'ESCORE - The EPRI Steady-State Core Reload Evaluator Code: General Description'," May 23, 1990.





UNITED STATES  
NUCLEAR REGULATORY COMMISSION  
WASHINGTON, D. C. 20555

ENCLOSURE 2

SAFETY EVALUATION BY THE OFFICE OF NUCLEAR REACTOR REGULATION  
RELATING TO NORTHERN STATES POWER COMPANY  
TOPICAL REPORT NSPNAD-8609  
"QUALIFICATION OF REACTOR PHYSICS METHODS FOR  
APPLICATION TO MONTICELLO"  
NORTHERN STATES POWER COMPANY  
MONTICELLO NUCLEAR GENERATING PLANT !  
DOCKET NO. 50-263

1.0 INTRODUCTION

By letter dated October 2, 1986 (Ref. 1), the Northern States Power Company (NSP) submitted for review NSPNAD-8609, "Qualification of Reactor Physics Methods for Application to Monticello." The report describes the reactor model and qualification, quantification of reliability factors, and applications to operations and reload safety evaluations for the Monticello Nuclear Plant (Monticello). The information in this report was supplemented by information submitted with Reference 8 in response to questions from the NRC staff and consultants. The review by the staff of this report and supplemental information was performed with the assistance of consultants from Brookhaven National Laboratory (BNL).

NSP intends to perform the reload and transient calculations required for the operation of Monticello and, in support of this effort, has developed its own reactor physics methodology. The NSP steady state neutronic and thermal-hydraulic methodology is based on two widely used codes: CASMO-II (Ref. 2) for the generation of lattice physics parameters and NDH (Ref. 3) for three-dimensional neutronic/thermal-hydraulic simulation. NDH is a derivative of the FLARE-based EPRI-NODE-B program (Refs. 4 & 5). Normalization parameters and adjustment factors used in the three-dimensional calculation are derived from PDQ7/HARMONY (Refs. 6 & 7). Model verification and reliability factor

determination are presented in the report along with a discussion of the statistical methods used in the determination and application of uncertainties. Applications of the NSP steady state calculational model to reactor operation and safety analysis are also outlined.

## 2.0 REPORT SUMMARY

The CASMO-II and NDH codes are the principal NSP calculational tools for performing reload analyses and for determining input to transient calculations. The NSP application of these codes, the model verification, and determination of reliability factors, are briefly described in the following report summary.

### 2.1 CASMO-II

CASMO-II is used to derive the lattice physics constants which are needed for input to the three-dimensional code NDH. CASMO-II is a multigroup two-dimensional transport theory code which calculates fuel assembly parameters such as reactivities, pin powers, reaction rates and nuclide concentrations at every burnup step. The code provides the standard assembly-averaged two-group macroscopic cross section sets. This code is also used in the generation of constants needed in PDQ/HARMONY for deriving normalization parameters for NDH and generic adjustment factors for local peaking factor generation.

### 2.2 NDH

This code is an expanded version of the FLARE-based EPRI-NODE-B. A modified one-group theory model is used in this code. The key input parameters in NDH are the neutron multiplication,  $K$ -infinity and the migration area,  $M^2$ . These parameters are derived from detailed energy and space-dependent calculations for each fuel assembly type and are entered in the nodal calculation as a function of coolant voids and exposure, including the effects of control, coolant temperature, Doppler and xenon. The fuel assemblies are coupled together in NDH using a transport kernel which is a function of the migration

area and the nodal mesh spacing. The transport kernel plays an important role in the nodal calculations since it, along with the local multiplication and leakage factors, is used by the code in the calculation of the three-dimensional power distribution. The code calculates the transport kernel in each node in the horizontal and vertical directions using input constants which are selected such that the results of the basic model calculations are normalized to a more accurate calculation such as PDO or to measured data. The inlet flow distribution is calculated by EPRI-THERM-B (Ref. 5) in the void iteration loop.

This code calculates the thermal hydraulic parameters of the core including flow distribution, subcooling, void and quality distributions based on total core power, recirculation flow, power distribution, and feedwater flow and temperature. Since the coolant flow distribution through the core is influenced by the void content and the power level, an iterative calculation is required to determine the power and flow distribution.

The flow distribution is obtained by equalizing the pressure drop across each channel. This calculation starts with an initial guess for the coolant velocity in each channel and the pumphead requirements, and proceeds iteratively until coolant velocity converges within a specified tolerance. The process is repeated for each channel. When a distribution is obtained for all of the channels, all individual channel flows are summed and compared to the total core flow. The calculation is complete when the summed flow is within a specified tolerance of the total core flow.

### 2.3 Model Verification and Reliability Factor Determination

The CASMO/NDH model has been benchmarked against Monticello measured data obtained during Cycles 7 through 10. Core reactivity, radial and axial power distributions evaluated at various statepoints spanning four operating cycles, and comparisons with measured data are presented. Results of gamma scan comparisons for selected assemblies at the end of two cycles are also provided. The derivation of reliability factors and biases for the basic



safety parameters such as minimum critical power ratio, linear heat generation rate, void and Doppler coefficients and delayed neutron parameters has been based on the above benchmarking. The model reliability factor for calculating power distributions is based on comparisons of measured and predicted traversing incore probe (TIP) signals. The latter are corrected by the process computer to account for detector sensitivity, drift and background effects. Reliability factors have been determined for local pin powers as well as for total bundle powers and are applied to the calculation of the linear heat generation rate (LHGR), the average planar linear heat generation rate (APLHGR) and the critical power ratio (CPR).

### 3.0 EVALUATION

#### 3.1 Modeling

Nuclear constants for the three-dimensional code NDH are derived from CASMO-II. These constants include infinite neutron multiplication, migration areas and fission rates. The calculation of the Doppler reactivity effect in each node is based on a square root of fuel temperature dependence with appropriate power and moderator density corrections. These representations are known from past reviews to be suitable for the analyses intended to be carried out with NDH. Exposure and void-dependent input reactivities allow the evaluation of nodal exposure effects. Nodal exposure is updated with each exposure step using the nodal power at the start of the step. The nodal calculation accounts for control rod history effects. This exposure and local reactivity modeling in NDH is sufficiently detailed for core follow and reload analyses and is acceptable.

The NDH model has been normalized to the Monticello Cycles 7 through 10 measurement data. Albedos and mixing factors used in simulating normal operating conditions are based on Cycles 5 and 6 data. For cold shutdown conditions the albedos and mixing factors are determined from Cycles 7 through 10 measurements. These determinations are acceptable.

The review concludes that the NSP CASMO/NDH modeling, adopted from well known and/or previously reviewed methodology components, provides an acceptable calculation package for use in Monticello three dimensional steady state core analyses.

### 3.2 Qualification of Methodology

The steady state BWR methods summarized in NSPNAD-8609 have been verified and qualified with measured data obtained during four cycles of operation of the Monticello plant. The qualification process covered both cold zero power and hot operating conditions. In addition, the performance of the code was verified against gamma scan measurements made on selected discharged fuel assemblies at the end of Cycle 8 (EOC-8) and at EOC-9.

#### Cold Reactivity

The NDH cold model has been verified with cold critical measured data from Cycles 7 through 10, at core average exposures ranging from about 10 to about 16 Gwd/MTU and moderator temperatures in the range from 97 to 172° F. Of the 22 cold critical measurements performed, 14 were of the in-sequence type while eight were of the few-rod type.

The NSP results show that the cold NDH model is capable of calculating cold reactivities within  $\pm 0.5\%$  with a standard deviation of about 0.2%.

#### Hot Reactivity

A total of 56 statepoints spanning the operation of Cycles 7 through 10 of Monticello were calculated using the NDH code. The resultant hot critical k-effective was in the range from 0.988 to 0.966. Most of the statepoints represented hot full power operation. Some coastdown operating data was also included in the analysis. The mean hot eigenvalue (k-effective) was 0.992 with a standard deviation of about 0.2%.

It is seen from the NSP results that NDH underpredicts the core reactivity by less than 1% with a standard deviation of about 0.2%.

#### Power Distribution Uncertainties and Reliability Factors

Comparison of measured TIP distributions with NDH-simulated TIP readings provides a measure of the ability of the NDH code to match observed power shapes. In the qualification of the NSP CASMO/NDH model, TIP sets representing 44 statepoints spanning four cycles and spread over a core average exposure range of 0.1 to 7.6 GWd/MTU were calculated and compared with corresponding measured data. However, in the evaluation of the uncertainties associated with the calculation of power distributions, selected TIP readings have been eliminated from the statistical analysis. The deletion of this data is based on the observation that this data results in the largest calculation/measurement differences. With the deletion of these NDH/TIP comparisons, the NDH power distribution calculational uncertainty is 4.7%. NSP provides an alternate analysis in Reference 8 in response to questions in which the NDH calculational uncertainty is determined to be 4.3%. In this second analysis it is assumed (following a discussion presented in Reference 9) that the TIP measurement uncertainty is one-half the measured TIP asymmetry.

Since it has not been demonstrated that the TIP measurement uncertainty is one-half the TIP measurement asymmetry, and since sufficient justification for the deletion of the largest calculation/measurement TIP comparisons has not been provided, the quoted 4.3% calculational uncertainty and resulting power distribution reliability factor are considered to be unacceptable. It is therefore required, until such time as the elimination of some of the TIP readings is acceptably justified and approved, that all TIP comparisons be included in the determination of the NDH power distribution calculation uncertainties and resulting APLHGR, LHGR and MCPR reliability factors. This will increase the CPR, APLHGR and LHGR reliability factors from 8.1, 11.1% and 11.1 to 9.5, 12.3 and 12.3%, respectively.



### Accuracy of the Methodology and Uncertainties

The validity of the CASMO/NDH model was tested by comparing results of calculations with measured data from a broad range of operating states. These states provide a suitable data base for determining NDH uncertainties in predicting basic core parameters. Based on the calculation-to-measurement comparisons for these states, it is concluded that the NSP predictions of cold reactivity are accurate to within 0.5% with a standard deviation of about 0.2% and the hot reactivity predictions are accurate to within about 1% with a standard deviation of about 0.2%. As discussed above, the approach used in determining the uncertainties associated with the calculation of power distributions has been found to be inadequate. However, NSP has agreed that the uncertainties and reliability factors assigned to APLHGP, LHGR and MCPR will, for the present, be based on the entire data base including the eliminated TIP data. The only direct use of the reliability factors in reload safety analysis calculations is for the fuel bundle misloading and control rod withdrawal events, which are done with "steady state" methods. These analyses will use the increased values.

### Applications

The report briefly discusses the approaches to be taken in using the reliability factors in application of the CASMO/NDH methodology to reactor operations, including prediction and monitoring of relevant parameters, and to safety analyses. However, it was not the intent of the report to describe such procedures or methods in detail, and the review thus simply notes that the approach is reasonable, and in the case of startup reactivity predictions, the results are satisfactory. A formal review in this area, presumably related to safety analyses or monitoring (if NSP elects to support the installed GE monitoring system), would have to be in connection with a full submittal of the relevant methodology or its qualification.

5. Advanced Recycle Methodology Program (ARMP) System Documentation, EPRI CCM-3 Research Project 118-1, September 1977.
6. W. R. Cadwell, "PDQ-7 Reference Manual," WAPD-TM-678, Westinghouse Electric Corporation, January 1967.
7. R. Breen, O. Marlowe, and C. Pfeifer, "Harmony: System for Nuclear Reactor Depletion Computation," WAPD-TM-478, Westinghouse Electric Corporation, January 1985.
8. Letter from D. Musolf, NSP, to Director of Nuclear Reactor Regulation, USNRC, "Additional Information to Support the Submission of NSPNAD-8608 and NSPNAD-8609," September 29, 1987.
9. EPRI Report NP-1278, "On-Line Nuclear Power Distribution Measurement," Appendix A.

MONTICELLO NUCLEAR GENERATING PLANT

QUALIFICATION OF REACTOR PHYSICS METHODS  
FOR  
APPLICATION TO MONTICELLO

NSPNAD-8609-A

Revision 3

October 1995

Principal Contributors

Anthony Bockelman, NSP  
Clifford Bonneau, NSP  
David Dean, NSP  
Keith Dehnbostel, NSP  
Thomas Iseman, NSP  
William Lax, NSP  
Ryan Maas, NSP  
Michael Miller, NSP  
Peter Pankratz, NSP  
Richard Rohrer, NSP  
Ralph Rye, NSP  
Richard Streng, NSP  
Scott Vanevenhoven, NSP

Prepared by *D. W. Dean*  
David W. Dean, Principal Engineer

Date *10/16/95*

Reviewed by *Clifford A. Bonneau*  
Clifford A. Bonneau, Process Manager

Date *10/16/95*

Approved by *Louis P. Matis*  
Louis P. Matis, Director Fuel Resources

Date *10/16/95*



#### ABSTRACT

This document is a Topical Report describing the Northern States Power Company (NSP) qualification of reactor physics methods for application to the Monticello Nuclear Plant.

This document addresses the reactor model description, qualification and quantification of reliability factors and applications to operations and reload safety evaluations of the Monticello plant.

#### LEGAL NOTICE

This report was prepared by or on behalf of Northern States Power Company (NSP). It is intended for use by NSP personnel only. Use of any information, apparatus, method, or process disclosed or contained in this report by non-authorized personnel shall be considered unauthorized use, unless said personnel have received prior written permission from NSP to use the contents of this report. With respect to unauthorized use, neither NSP, nor any person acting on behalf of NSP:

a. Makes any warranty or representation, express or implied, with respect to the accuracy, completeness, usefulness, or use of any information, apparatus, method or process disclosed or contained in this report, or that the use of any such information, apparatus, method, or process may not infringe privately owned rights; or

b. Assumes any liabilities with respect to the use of, or for damages resulting from the use of, any information, apparatus, method, or process disclosed in the report.

TABLE OF CONTENTS

	<u>PAGE</u>
1.0 <u>INTRODUCTION</u> . . . . .	6
2.0 <u>GENERAL CHARACTERISTICS OF THE NSP CALCULATIONAL MODEL</u> . . . . .	6
3.0 <u>MODEL VERIFICATION AND RELIABILITY FACTOR DETERMINATION</u> . . . . .	9
3.1 <u>Control Rod Worth</u> . . . . .	11
3.2 <u>Temperature Coefficient</u> . . . . .	18
3.3 <u>Void Coefficient</u> . . . . .	18
3.4 <u>Doppler Coefficient</u> . . . . .	20
3.5 <u>Isotopics</u> . . . . .	20
3.6 <u>Power Distribution Reliability Factor Determination</u> . . . . .	20
3.6.1 <u>Local Power Distribution</u> . . . . .	20
3.6.2 <u>Integrated Power Distribution</u> . . . . .	24
3.6.3 <u>Gamma Scan Comparisons</u> . . . . .	25
3.6.4 <u>Standard Power Distribution Comparison</u> . . . . .	25
3.6.4.1 <u>Axial Power Distribution Comparisons</u> . . . . .	25
3.6.4.2 <u>Radial Power Distribution Comparisons</u> . . . . .	26
3.6.4.3 <u>Nodal Power Distributions Comparisons</u> . . . . .	26
3.7 <u>Delayed Neutron Parameters</u> . . . . .	26
3.8 <u>Effective Neutron Lifetime</u> . . . . .	27
4.0 <u>MODEL APPLICATIONS TO REACTOR OPERATIONS</u> . . . . .	55
4.1 <u>Predictive Applications</u> . . . . .	55
4.1.1 <u>Cold Criticals</u> . . . . .	55
4.1.2 <u>Hot Full Power Criticals</u> . . . . .	55
4.2 <u>Monitoring Applications</u> . . . . .	56
4.2.1 <u>Process Computer</u> . . . . .	56
4.2.2 <u>Isotopic Inventory</u> . . . . .	56
5.0 <u>MODEL APPLICATIONS TO SAFETY EVALUATION CALCULATIONS</u> . . . . .	60
5.1 <u>Linear Heat Generation Rate (LHGR and APLHGR)</u> . . . . .	60
5.2 <u>Critical Power Ratio (CPR)</u> . . . . .	60
5.3 <u>Control Rod Worth</u> . . . . .	60
5.4 <u>Void Reactivity</u> . . . . .	61
5.5 <u>Fuel Temperature (Doppler) Coefficient</u> . . . . .	61
5.6 <u>Delayed Neutrons</u> . . . . .	61
5.7 <u>Prompt Neutron Lifetime</u> . . . . .	61
6.0 <u>REFERENCES</u> . . . . .	62
APPENDIX A <u>Statistical Methods for the Determination and Application of</u> <u>Uncertainties</u> . . . . .	66
A.1 <u>Application of Normal Distribution Statistics</u> . . . . .	67
A.2 <u>Application of Non-Normal Distribution Statistics</u> . . . . .	70
APPENDIX B <u>Computer Code Summary Description</u> . . . . .	76

LIST OF TABLES

<u>TABLE</u>	<u>TITLE</u>	<u>PAGE</u>
3.0.1	Reliability Factors for Monticello . . . . .	10
3.1.1	Measured to Calculated Rod Worth Comparison . . . . .	12
3.3.1	EOC Coastdown Statepoints . . . . .	19
3.6.1	Full Power Statepoints . . . . .	28
3.6.2	Axial Power Distribution Comparison . . . . .	30
3.6.3	Radial Power Distribution Comparisons . . . . .	31
3.6.4	Power Distribution Standard Deviations in 20 Axial Planes . .	32
4.1.1	Few Rod and In-sequence Cold Criticals . . . . .	57
A.1	Single-Sided Tolerance Factors . . . . .	69



LIST OF FIGURES

<u>FIGURE</u>	<u>DESCRIPTION</u>	<u>PAGE</u>
2.0.1	Flow Chart: CASMO-3/SIMULATE-3 Model . . . . .	8
3.1.1	Control Notch Worth Inventory Versus Exposure Cycle 11 . . .	13
3.1.2	Control Notch Worth Inventory Versus Exposure Cycle 12 . . .	14
3.1.3	Control Notch Worth Inventory Versus Exposure Cycle 13 . . .	15
3.1.4	Control Notch Worth Inventory Versus Exposure Cycle 14 . . .	16
3.1.5	Control Notch Worth Inventory Versus Exposure Cycle 15 . . .	17
3.6.1	Measured and Calculated Detector Responses BOC Cycle 11 . . .	33
3.6.2	Measured and Calculated Detector Responses MOC Cycle 11 . . .	34
3.6.3	Measured and Calculated Detector Responses EOC Cycle 11 . . .	35
3.6.4	Measured and Calculated Detector Responses BOC Cycle 12 . . .	36
3.6.5	Measured and Calculated Detector Responses MOC Cycle 12 . . .	37
3.6.6	Measured and Calculated Detector Responses EOC Cycle 12 . . .	38
3.6.7	Measured and Calculated Detector Responses BOC Cycle 13 . . .	39
3.6.8	Measured and Calculated Detector Responses MOC Cycle 13 . . .	40
3.6.9	Measured and Calculated Detector Responses EOC Cycle 13 . . .	41
3.6.10	Measured and Calculated Detector Responses BOC Cycle 14 . . .	42
3.6.11	Measured and Calculated Detector Responses MOC Cycle 14 . . .	43
3.6.12	Measured and Calculated Detector Responses EOC Cycle 14 . . .	44
3.6.13	Measured and Calculated Detector Responses BOC Cycle 15 . . .	45
3.6.14	Measured and Calculated Detector Responses MOC Cycle 15 . . .	46
3.6.15	Measured and Calculated Detector Responses EOC Cycle 15 . . .	47
3.6.16	Observed Differences Density Function Comparison . . . . .	48
3.6.17	Cumulative Distribution Function (CDF) Comparison . . . . .	49
3.6.18	CDF in the Region of the 95th Percentile Model Comparison . .	50
3.6.19	Observed Differences Density Function Integrated Reaction Rates Comparison . . . . .	51
3.6.20	Cumulative Distribution Function (CDF) Integrated Reaction Rates Comparison . . . . .	52
3.6.21	CDF in the Region of the 95th Percentile For Integrated Reaction Rates . . . . .	53
3.6.22	Standard Deviation vs Measured Instrument Response . . . . .	54
4.1.1	Cold Criticals versus Core Average Exposure . . . . .	58
4.1.2	Hot Criticals . . . . .	59

## 1.0 INTRODUCTION

This report addresses the reactor model description, qualification and quantification of reliability factors, applications to operations and reload safety evaluations of the Monticello Nuclear Plant (Mnt). This model, based on the Studsvik CMS system of codes, can be used as a substitute for the CASMO/NDH methods previously approved for use (Reference 2). Adoption of the methods described here does not preclude the use the earlier CASMO/NDH methods as needed.

A summary description of the computer codes is given in Section 2. This report stresses the aspects of implementation of the NSP model; the individual code descriptions are referenced in Appendix B.

Whenever possible, directly observable parameters (such as reactor critical  $k_{eff}$  and measured incore detector fission rates) are utilized. The Mnt data used in this evaluation span cycles 11 through 15. In order to be completely objective in the choice of data to be used for the comparisons, all Mnt cycles 11 through 15 measurements were reviewed and qualified prior to initiating the comparison calculations.

After the measured data to be used in the benchmark process had been defined, the model calculations were performed and comparisons are presented in this report as part of the quantification of the NSP model calculational uncertainties and reliability factors. A statistical approach was used to derive the uncertainties. These uncertainties are consistent with the model application procedures and methodology.

The uncertainties are evaluated by direct comparison to experimental data.

In order to provide a continuing verification of the conservatism of the reliability factors determined by Mnt cycles 11 through 15 data, ongoing comparisons are made each cycle using the statistical methods described in this report. A discussion of the reliability factors is provided in Section 3.

The methods for use of the model and the reliability factors are described relative to reactor operation and reload safety evaluation in Sections 4 and 5.

## 2.0 GENERAL CHARACTERISTICS OF THE NSP CALCULATIONAL MODEL

The Monticello (Mnt) calculational model based on the Studsvik system of codes, is very similar to the calculational model previously approved for use by Yankee Atomic Electric Company for use with Vermont Yankee (see References 4, 5, and 6), and is similar in many respects to the model previously approved for use with Mnt (see Reference 2). A flow diagram of the Monticello model is shown in Figure 2.0.1. The code acronyms used in these figures are defined in Appendix B.

In general, the CASMO-3<sup>7,8</sup> program is used to generate the lattice physics parameters for input to SIMULATE-3<sup>11,12</sup>. MICBURN-3<sup>10</sup> is used to model gadolinia containing fuel pins and provides homogenized Gd cross sections for input to CASMO-3. CASMO-3 produces fission product nuclide concentrations, depletion and product chain data, pin power distributions, microscopic and macroscopic cross sections, and other nuclear data input to TABLES-3<sup>13</sup>. TABLES-3 constructs tables of these nuclear data as functions of local state variables (e.g. water density, fuel temperature etc.) for input to SIMULATE-3.

SIMULATE-3 is a three-dimensional, two-group steady state reactor neutronic and thermal hydraulic simulator. This simulator is used to generate eigenvalues, power distributions, and incore instrument predictions for use in reload safety evaluations, plant support, reload

design, fuel management, and benchmark comparisons.

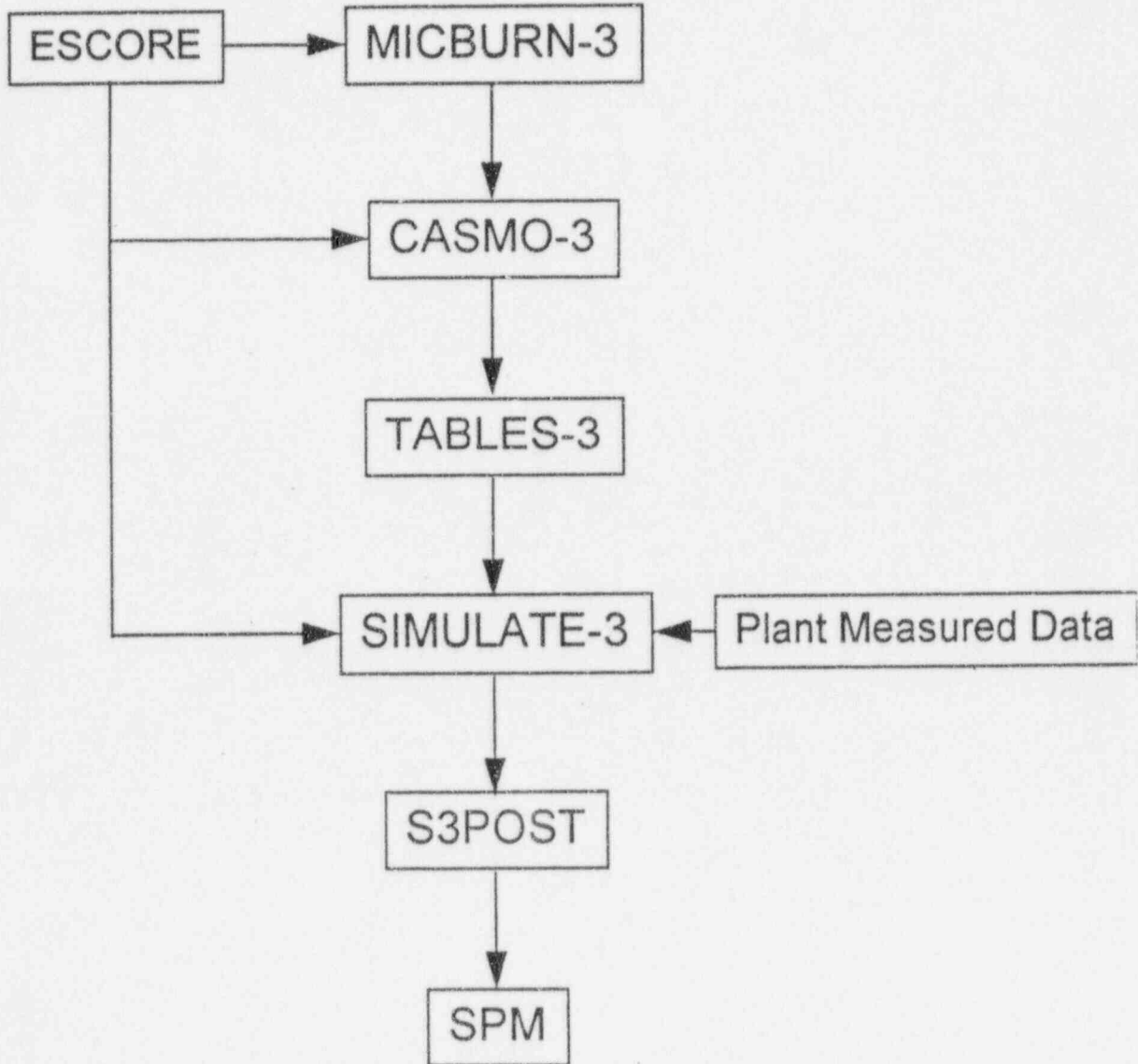
ESCORE<sup>15,16,17,18</sup> is an EPRI computer code for steady state fuel performance analysis. The Monticello methodology uses ESCORE for fuel temperature predictions to be used as input to MICBURN-3, CASMO-3, and SIMULATE-3 for modeling fuel temperature related effects on the nuclear data (i.e. Doppler coefficient and power defect).

The S3POST<sup>14</sup> program summarizes SIMULATE-3 results including the measured and predicted incore reaction rates. SPM, an NSP developed code, then combines all the statepoints to calculate overall uncertainties.

The computer code descriptions are summarized in Appendix B.

Figure 2.0.1

Flow Chart: CASMO-3/SIMULATE-3 Model





### 3.0 MODEL VERIFICATION AND RELIABILITY FACTOR DETERMINATION

The NSP models have been benchmarked against Mnt measurements made during cycles 11 through 15 for the CASMO-3/SIMULATE-3 model to quantify the reliability factors to be used in safety related calculations. The resultant reliability factors and biases are summarized in Table 3.0.1. The remainder of this section is a detailed account of the derivation of these factors.

The term reliability factor (RF) is used to describe the allowances to be used in safety related calculations to assure conservatism. The uncertainty factor ( $1\sigma$ ) is used to describe the actual model accuracy. The reliability factor is always larger than the uncertainty factor.

The term bias is used to describe the statistical difference between an observed or measured distribution and the calculated value.

Appendix A describes the statistical methods used in the evaluation of the uncertainties in the following sections.

During each cycle, measured and calculated parameters will be compared in order to verify and update the reliability factors determined in this section. Results of the verification and an update for each parameter will be documented in the reload safety evaluation for the reload in which the updated values will be used. The updates to the reliability factors will be in accordance with the methods outlined in this section and in Appendix A.

TABLE 3.0.1

## Reliability Factors for Monticello

Parameter	Reliability Factor (expressed as applied)	Reliability Factor (expressed as %)	Bias
APLHGR	$RF_{TPF} = .124$	12.4	0
LHGR	$RF_{TPF} = .124$	12.4	0
MCPR	$RF_{RPF} = .095$	9.5	0
Rod Worth	$RF_{RODS} = .10$	10.0	0
Void Coefficient	$RF_{VOIDS} = .10$	10.0	0
Doppler Coefficient	$RF_{DOP} = .10$	10.0	0
Delayed Neutron Parameters			
$\Lambda$	$RF_{\Lambda} = .04$	4.0	0
$\beta$	$RF_{\beta} = .04$	4.0	0

### 3.1 Control Rod Worth

Control rod worth in a BWR cannot be directly measured. Control rod worth can be inferred from various reactor critical conditions. The approach taken is to benchmark the NSP model to these critical conditions. The data base includes 9 few rod criticals and 24 sequence criticals taken at temperatures ranging from 85 °F to 209 °F. This data represents the actual critical statepoints in cycles 11 through 15. All measured statepoints at temperatures below the boiling point of 212 °F have been included. The results of the comparisons are shown in Table 3.1.1.

The standard deviation of the calculated  $k_{eff}$  at the critical positions is .0027. This difference includes the measurement uncertainty as well as the calculational uncertainty. The typical amount of reactivity being held down by rods is on the order of 10%  $\Delta k$ . Using this value we can calculate an uncertainty in rod worth by dividing the standard deviation by this worth, i.e.  $.27\% \Delta k / 10\% \Delta k = 2.7\%$ . For conservatism the rod worth reliability factor ( $RF_{rods}$ ) is defined as 10%.

Figures 3.1.1 through 3.1.5 present graphs of control rod notch inventory versus cycle exposure for hot critical conditions for cycles 11 through 15. The best estimate is the predicted control rod notch inventory using CASMO-3/SIMULATE-3 with the  $\pm 1\% \Delta K$  reactivity anomaly shown. Measured rod notch inventory is indicated as a dot for each statepoint. All measured values are within the  $\pm 1\% \Delta K$  bounds. This indicates the well behaved prediction of the model and supports the use of the conservative rod worth reliability factor used above.

Table 3.1.1 Measured to Calculated Rod Worth Comparison

Cycle	Notches Withdrawn	Core Ave. Exposure (GWD/MTU)	Temperature (°F)	$k_{eff}$
11	60	12.802	85	0.9921
	64	12.802	106	0.9936
	644	12.802	105	0.9948
	394	12.802	113	0.9936
12	152	13.666	129	0.9964
	1416	13.666	128	0.9928
	728	13.666	128	0.9938
	734	16.922	141	0.9903
	1498	19.926	206	0.9896
13	66	15.025	91	0.9905
	106	15.025	91	0.9904
	978	15.025	91	0.9897
	678	15.025	91	0.9908
	2040	23.878	200	0.9876
	1518	24.789	164	0.9851
14	108	16.683	109	0.9907
	1076	16.683	111	0.9913
	734	16.683	118	0.9936
	108	21.252	122	0.9924
	864	21.252	123	0.9919
	738	22.494	152	0.9895
	892	23.330	209	0.9905
	1502	25.193	154	0.9923
	1542	25.193	142	0.9920
15	118	16.217	108	0.9933
	114	16.217	108	0.9963
	984	16.217	113	0.9939
	774	16.217	107	0.9963
	2560	16.310	200	0.9979
	1516	16.310	147	0.9962
	1632	17.833	181	0.9939
	762	20.368	137	0.9922
	702	22.419	129	0.9928

Mean  $k_{eff}$  = 0.9923  $\sigma$  = .0027



Figure 3.1.1  
Control Notch Worth Inventory Versus Exposure  
Cycle 11

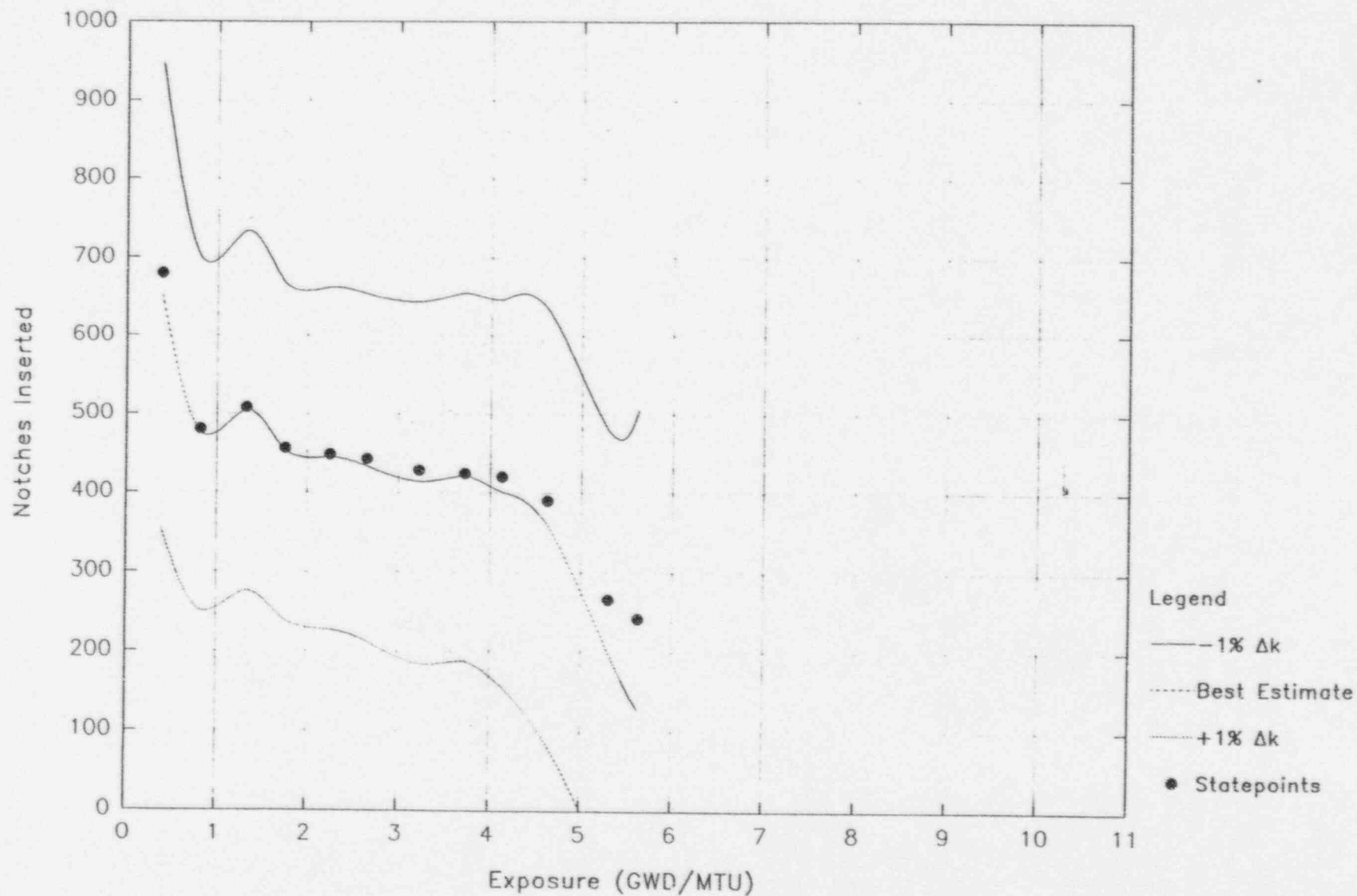


Figure 3.1.2  
Control Notch Worth Inventory Versus Exposure  
Cycle 12

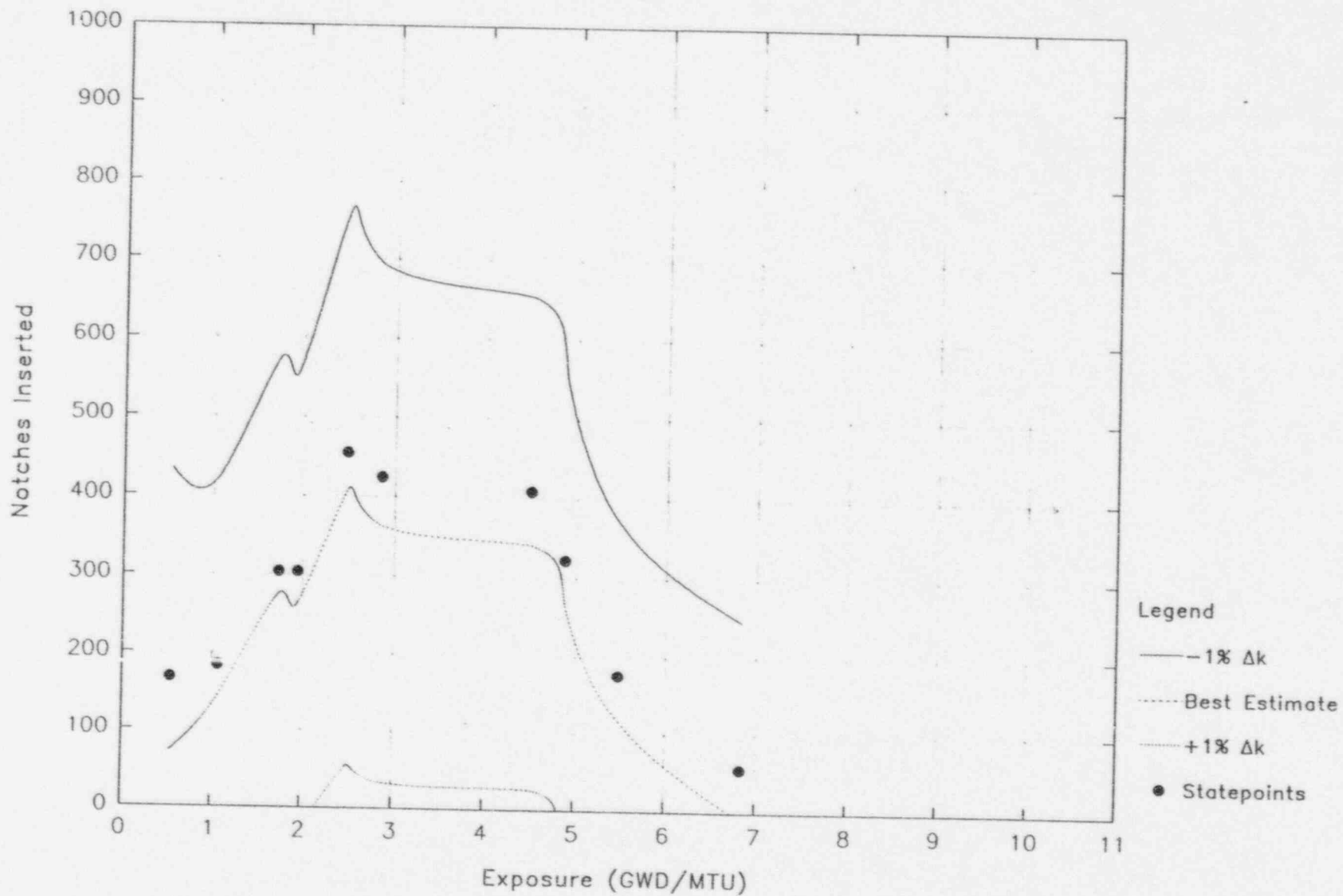


Figure 3.1.3  
Control Notch Worth Inventory Versus Exposure  
Cycle 13

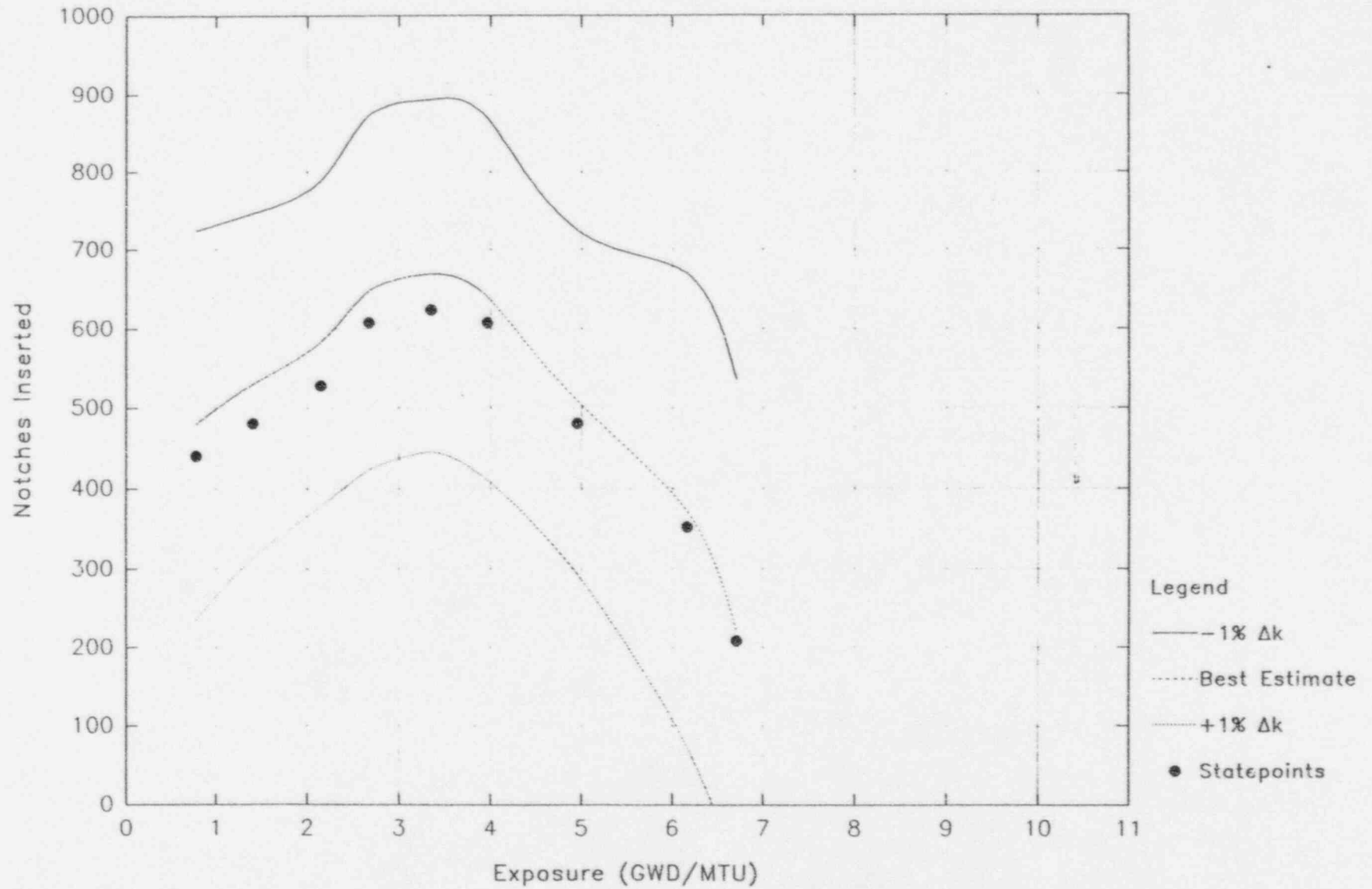


Figure 3.1.4  
Control Notch Worth Inventory Versus Exposure  
Cycle 14

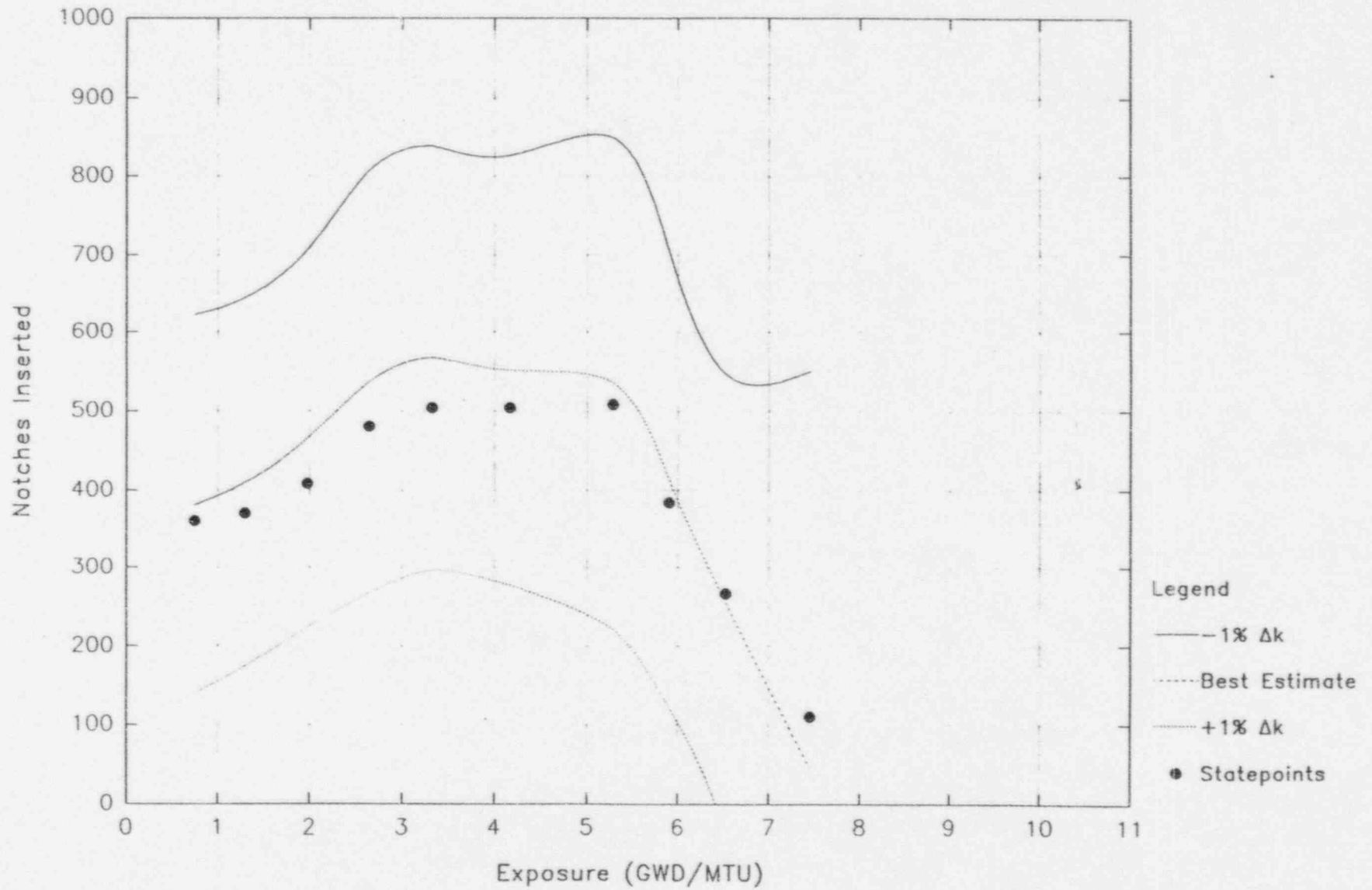
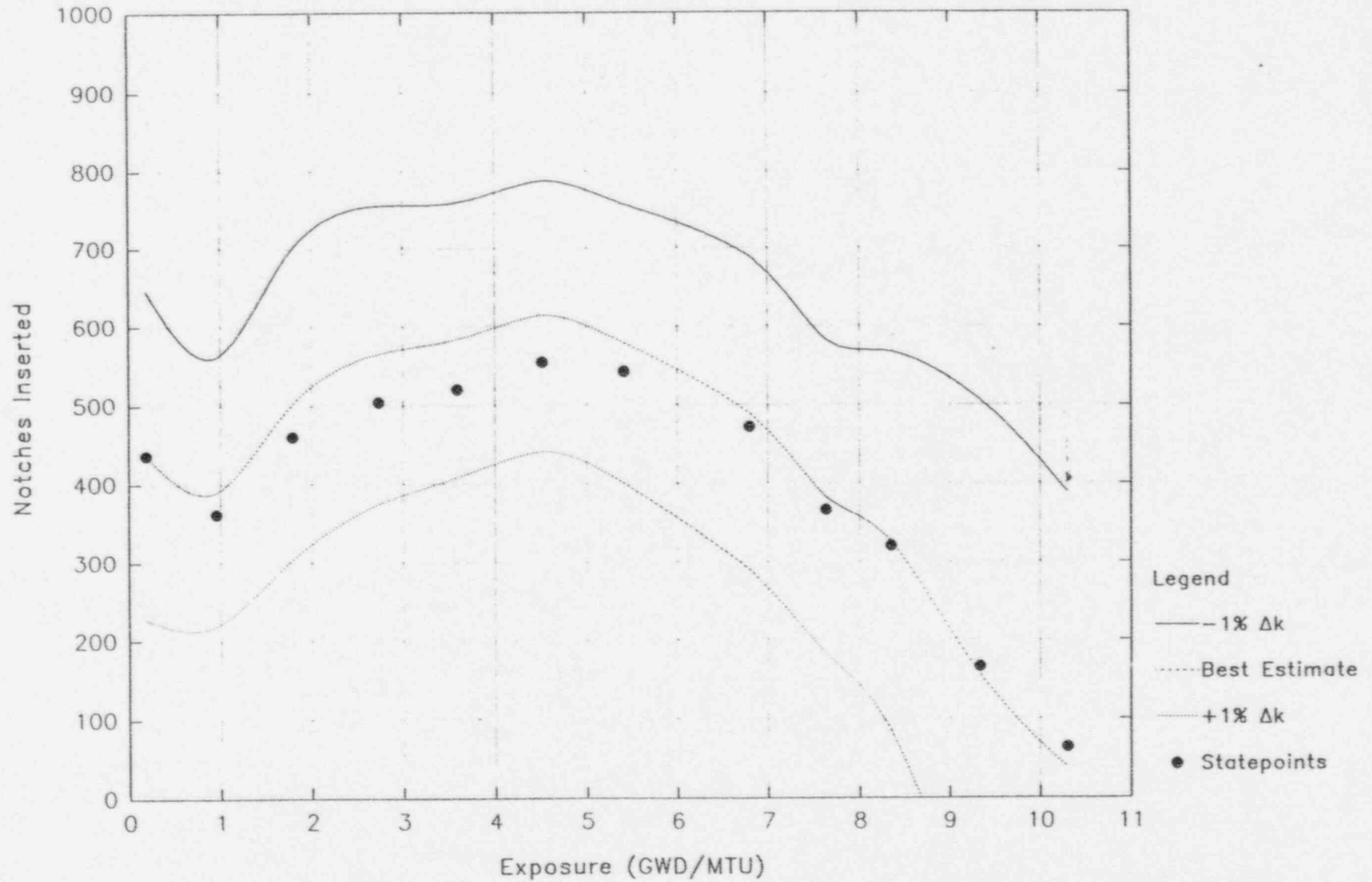




Figure 3.1.5  
Control Notch Worth Inventory Versus Exposure  
Cycle 15



### 3.2 Temperature Coefficient

The range of values of moderator temperature coefficients encountered in current BWR lattices does not include any that are significant from the safety point of view. The small magnitude of this coefficient, relative to that associated with steam voids and combined with the long time-constant associated with transfer of heat from the fuel to the coolant, makes the reactivity contribution of moderator temperature change insignificant during rapid transients.

For the reasons stated above, current core design criteria do not impose limits on the value of the temperature coefficient, and effects of minor design changes on the coefficient usually are not calculated.

### 3.3 Void Coefficient

The void coefficient in a BWR cannot be directly measured, i.e., there are always present the effects of other parameters such as control rods, Doppler coefficient, xenon etc. The magnitude of the uncertainty in the void coefficient can be inferred, however, from comparisons of predicted versus measured critical statepoints where the effect of the other parameters is minimized. Table 3.3.1 gives calculated values for the measured critical statepoints from EOC coastdown for cycles 11 through 15. The standard deviation of the calculated  $k_{eff}$ 's is  $\pm .0020 \Delta k$  for the coastdown cases. The total core reactivity held down by voids for the average void fraction (35%) at full power is on the order of 5%  $\Delta k$ . An average  $\% \Delta k / \% \Delta V$  can be calculated from Table 3.3.1 which represents the error in the predicted and measured value.  $\% \Delta k / \% \Delta V = .0083$ . Multiplying by the average percent void gives the error in terms of  $\Delta k$ .  $\% \Delta k = .0083 * 35\% = 0.29\%$ . Therefore the uncertainty in void can be calculated by dividing by the total void worth at 35% which gives  $0.29\% / 5\% = 5.8\%$  uncertainty. This uncertainty includes components of error from exposure, xenon and Doppler. Therefore, a reliability factor of 10% in void coefficient is deemed appropriately conservative for safety related calculation.

Table 3.3.1 EOC Coastdown Statepoints

Cycle	Cycle Exposure (GWD/MTU)	Power (%)	Void (%)	$k_{eff}$
11	5.624	100	34.5	1.0009
	6.352	99	36.9	1.0017
	6.756	92	34.3	1.0016
	7.256	84	31.0	1.0015
	7.764	74	27.6	1.0014
	8.159	66	24.7	1.0016
12	5.478	100	37.8	1.0002
	6.830	96	33.2	1.0004
	7.148	91	32.7	0.9999
13	7.373	100	36.7	0.9975
	8.229	87	31.4	0.9970
	8.724	78	28.3	0.9968
	9.103	71	25.7	0.9969
	9.729	59	21.4	0.9969
	10.165	51	18.4	0.9968
14	7.454	100	35.8	0.9992
	8.237	93	33.7	0.9990
	8.882	83	29.8	0.9988
15	9.332	100	32.1	0.9982
	10.301	91	29.8	0.9972
	11.197	73	25.0	0.9960

Mean  $K_{eff}$  = .9990  $\sigma$  = .0020

### 3.4 Doppler Coefficient

Measurements can be made in a power reactor which are directed at determining the Doppler coefficient at various power levels. In a BWR the uncertainty associated with such measurements (e.g. rod repositioning, void feedback) are such that results are not reliable for direct validation of the calculational model. Consequently, an indirect approach is taken.

The primary variable in the calculation of Doppler effects using the CASMO-3/SIMULATE-3 model is the fuel temperature. A change in fuel temperature associated with a power change results in a reactivity change due to the change in the resonance absorption.

The algorithm in SIMULATE-3 that determines the model change in reactivity due to the fuel temperature change uses data calculated by CASMO-3. The approach is to determine the accuracy of CASMO-3 in calculating the change in the resonance integral (RI) due to a known fuel temperature increase, then use engineering judgement to bound this uncertainty to assure conservatism.

Comparisons of CASMO-3 calculations to critical experiments (references 4, 23, 24, 25, 26, 27, 28, and 33) have determined that the uncertainty of CASMO-3 is well within the measurement uncertainty. In view of this, a 10% reliability factor placed on the Doppler coefficient is judged adequate to assure a conservative value.

### 3.5 Isotopics

The benchmarking of CASMO-3 to Yankee Rowe and Zion data is thoroughly discussed in references 4 and 36.

### 3.6 Power Distribution Reliability Factor Determination

The purpose of this section is to discuss the methods used to determine the power distribution reliability factors. Reliability factors have been determined for the local fuel pin power in a node and for the total fuel bundle power. These factors can then be applied to the calculation of the linear heat generation rate (LHGR), the average planar linear heat generation rate (APLHGR) and the critical power ratio (CPR) respectively.

The statistics presented in Sections 3.6.1 and 3.6.2 follow those presented in the Prairie Island Topical, see reference 1.

#### 3.6.1 Local Power Distribution

The model reliability factor for calculating power distributions is based on comparisons of measured and predicted traversing incore probe (TIP) flux detector signals for normal operating core conditions.

The signals from the detectors are corrected by the on-site process computer to account for such things as detector sensitivity, drift, and background. It is these corrected signals, or reaction rates, which have been compared to simulated reaction rates calculated with the NSP models in order to derive model reliability factors.

The reliability factor, RF, is defined as a single value of  $\Delta TPF/TPF_m$  such that  $TPF_c(I,J,K)$  times  $1 + \Delta TPF/TPF_m$  has a 95% probability at a 95% confidence level of being conservative with respect to  $TPF_m(I,J,K)$ . The subscripts c and m denote calculated and measured values.  $TPF(I,J,K)$  is the total pin peaking factor for all I,J,K locations in the core. This value cannot be measured directly. What is measured by the detector system is the



reaction rate in the instrument thimble. This measured reaction rate is a local value.  $RR_m = \phi \Sigma_f$  (measured).

These measurements are collapsed down to 24 axial nodal values in each thimble consistent with the nodalization of SIMULATE-3. The CASMO-3/SIMULATE-3 model has been used to calculate the reaction rates in the instrument thimbles:  $RR_c = \phi \Sigma_f$  (calculated). The observed difference distribution (ODD) has then been calculated by simply taking the relative difference of these two values:

$$ODD = (RR_m - RR_c) / RR_m$$

for all measured locations in the core.

It is important to note that the ODD is not the difference between nodal powers but rather is the difference between local fission rate values. It is assumed that the ODD is equal to  $\Delta TPF / TPF_m$ . This is a valid assumption since the calculated and measured reaction rates are local fission rate values as is the TPF, the only difference is the location.

The observed difference distribution determined above includes the uncertainties in the calculational model as well as the uncertainties in the measurement instrumentation. The calculational model uncertainty includes uncertainty in the calculation of the nodal power and in the conversion factors from nodal power to the pin power which is taken to be the same as the total uncertainty in the calculated reaction rates. Therefore, the total uncertainty in the local pin power can be written as follows:

$$RF_{TPF} = \sigma_{TPF,95}$$

where  $\sigma_{TPF,95}$  is determined from the ODD determined above.

The simulated detector signals are calculated in a manner which is consistent with the calculation of local power peaking factors for the purpose of safety evaluations; see Section 5.1. The first step is to compute the power distribution under consideration. The resolution used is 24 axial levels per fuel assembly.

The predicted detector signals are obtained directly from SIMULATE-3 calculated two group fluxes and fission cross sections in the instrument locations.

A total of 68 core statepoints, or TIP traces, were chosen for the purpose of comparing measured and simulated in-core reaction rates for the CASMO-3/SIMULATE-3 model. These statepoints span operating cycles 11 through 15 of Monticello. The specific core conditions for each of the statepoints are given in Table 3.6.1.

Typical examples of the comparisons of measured and predicted reaction rates are provided in Figures 3.6.1 through 3.6.15. The data is presented in sets of three figures, one set for each cycle, three TIP trace maps per cycle (BOC, MOC, EOC). Each figure in each set presents the differences between the measured and predicted axial reaction rates for all instrumented locations in the core and the core average axial reaction rates (lower right hand corner).

The measurements are represented as squares at the 24 axial levels. The predicted reaction rates are shown as lines.

The distribution of observed differences between measured and calculated instrument signals for all 68 core statepoints was determined. For each trace, 2 of the 24 axial values were excluded

from consideration. These excluded values correspond to the top and bottom nodes. These locations are areas of steep flux gradients, and small errors in instrument position result in large differences in measured to calculated values. Since the reaction rates in these areas are always smaller (i.e., the high power point will never occur in the top or bottom nodes) these values were excluded from the determination of the observed differences density function. The reliability factors developed here include the measurement uncertainty as well as the calculational uncertainty. However, known problems with the TIP measurement system such as TIP tube mislocation and channel bowing make the measurement uncertainty very large relative to the calculational uncertainty. A 95%/95% confidence level was determined from the observed difference density function determined above.

The method of normalizing the calculated and measured reaction rates was used to adjust the average of all 24 detectors at the remaining 22 axial locations to 1.0. This normalization technique was used to put the measured and predicted values on a common basis which is consistent with the definition of the local peaking factors. The measurement uncertainty in core thermal power is accounted for in the transient and LOCA analysis.

All data was retained in the data base. The total number of nodal observations used was 35,904. The total number of observations eliminated was 3,264.

All subsequent statistical analysis has been performed using the methods described in Appendix A.2. To ensure a conservative reliability factor at all power levels, the sample was divided into subsamples as a function of power (see Figure 3.6.22). A standard deviation was calculated for each subsample using the methods described in Appendix A.2. Figure 3.6.22 shows a distinct power dependence for the absolute difference. Therefore, to assure conservatism in the application, the reliability factor will be applied as a relative rather than an absolute value.

The distribution of observed differences is shown in Figure 3.6.16. The following statistics therefore represent the total data base as described above using relative differences. The first step using this method is to determine the mean relative difference of the measured to calculated values ( $\mu_{mc}$ ) and the standard deviation ( $\sigma_{mc}$ ):

$$\mu_{mc} = \frac{\sum_{i=1}^n e_i}{n} = 0.002$$

$$\sigma_{mc} = \sqrt{\frac{\sum_{i=1}^n (e_i - \mu_{mc})^2}{n-1}} = 0.071$$

where:  $e_i$  =  $i$ th observed difference  
 $n$  = total number of observations

The second step is to transform the  $e_i$  to standard measure using

the following formula:

$$Z_i = \frac{e_i - \mu_{mc}}{\sigma_{mc}}$$

and the resulting variates Z were then sorted into ascending order (see Figure 3.6.17). A value of Z was chosen as an estimate of the 95th percentile of the distribution,  $i = 34,109$ . This gives the 95th percentile of Z to be

$$Z_{34109} = Q_{95} = 1.689$$

which implies that 95% of the errors are likely to be less than 1.689 standard deviations from the mean. It remains then to calculate a 95% confidence interval on  $Q_{95}$  using the following formula

$$\text{Var}Q_{95} = \sigma_{Q_{95}}^2 = \frac{q(1-q)}{n f_1^2}$$

where:  $q =$  the quantile (.95)  
 $n =$  number of independent observations in sample  
 $f_1 =$  ordinate of the density function of the distribution function at the abscissa  $q$

Due to the dependence of the observed differences with axial height, the total number of observations was reduced by a factor of 5 to determine the total number of independent observations. The factor of 5 was chosen to conservative bound based on the Prairie Island topical, Reference 1, value of 3.0 which is applicable to 48 axial data points rather than 24.

It is necessary to obtain an estimate of  $f_1(.95)$ , and this was done by applying a linear regression analysis on a short interval of the cumulative distribution function (CDF) of Z in the region of the 95th percentile (see Figure 3.6.18). The estimated slope of the CDF (estimated from the straight line in Figure 3.6.18) is an estimate of the ordinate density function. The slope is calculated as 0.143.

This gives:

$$\text{Var}Q_{95} = \frac{0.95(1-0.95)}{\left[\frac{35904}{5}\right] 0.143^2} = 0.00032$$

and

$$\sigma_{Q_{95}} = \sqrt{\text{Var}Q_{95}} = 0.018$$

The estimate of the upper limit on  $Q_{95}$  is

$$K_c \sigma_{Q_{95}} = 1.645 \cdot 0.018 = 0.029$$

thus:  $\phi$

$$Q_{95} \leq 1.689 + 0.029$$

The upper limit is then  $1.689 + .029 = 1.718$  which gives the following as the 95% confidence level that the calculated reaction rate ( $RR_c$ ) will be conservative with respect to the measured reaction rate ( $RR_m$ ).

$$\begin{aligned} RR_m &= RR_c (1 + \mu_{mc} + (Q_{95} + K_c \sigma_{Q95}) \sigma_{mc}) \\ RF_m &= RR_c (1 + .124) \end{aligned}$$

Therefore  $\sigma_{T_{PF,95}} = .124$  with the bias absorbed into the reliability factor. Note that this value includes measurement error which adds conservatism to the calculation.

### 3.6.2 Integrated Power Distribution

The model reliability factors for calculating power distributions are based on comparisons of integrated measured and predicted TIP trace signals obtained from normal operating core conditions.

The reliability factor (RF) is defined as a single value of  $\Delta RPF/RPF_m$  such that  $RPF(I,J)$  calculated times  $1 + \Delta RPF/RPF_m$  has a 95% probability at a 95% confidence level of being conservative with respect to the measured  $RPF(I,J)$ . The subscripts c and m will be used to denote calculated and measured values.  $RPF(I,J)$  is the integrated peaking factor determined for all I,J locations in the core. This value cannot be measured directly. What is measured by the detector system is the reaction rate in the instrument thimble. This measured reaction rate is a local value.  $IRR_m = \phi \Sigma_f$  (measured). These values are determined at each thimble by integrating the central 22 measured axial locations. The three-dimensional model CASMO-3/SIMULATE-3 has been used to calculate the reaction rate in the instrument thimbles.  $IRR_c = \phi \Sigma_f$  (calculated).

The observed difference distribution (ODD) has then been calculated by simply taking the relative difference of these two values

$$ODD = (IRR_m - IRR_c)/IRR_m \text{ for all measured locations in the core.}$$

The observed difference distribution determined above includes the uncertainties in the calculational model, the uncertainties in the measurement instrumentation, and the uncertainties in conversion factors from nodal power to instrument value. The calculational model uncertainty includes uncertainty in the calculation of the nodal powers as well as uncertainties in the local pin powers. Therefore the uncertainty in the local integrated pin power can be written as follows:

$$RF_{\Delta RPF} = \sigma_{RPF,95}$$

where  $\sigma_{RPF,95}$  is determined from the ODD.

The distribution of observed differences between measured and calculated integrated instrument signals for all 68 statepoints was determined for the CASMO-3/SIMULATE-3 model and is shown in Figure 3.6.19. The total number of integrated observations used was 1,632.

All subsequent statistical analysis has been performed using the methods described in Appendix A.2 on the entire sample.

The cumulative distribution function and the CDF in the region of the 95th percentile are given in Figures 3.6.20 and 3.6.21 respectively. The significant parameters calculated for this distribution are as follows:

$\mu_{mc}$	=	0.001
$\sigma_{mc}$	=	0.043
$Q_{95}$	=	1.728
$\sigma_{Q95}$	=	0.035
$K_c \sigma_{Q95}$	=	0.058
$IRR_{.95}$	=	$IRR_c (1 + 0.079)$
$\sigma_{RPF.95}$	=	0.079

where:  $IRR_m$  = Integrated reaction rate measured  
 $IRR_c$  = Integrated reaction rate calculated

For conservatism the reliability factor will remain at the value determined for CASMO-2/NDH (reference 2) as

$$RF_{RPF} = 0.095 > \sigma_{RPF.95} = 0.079$$

No dependence of the observed difference with position was found. Therefore, n was not reduced.

### 3.6.3 Gamma Scan Comparisons

Gamma scan measurements are not available from Mnt cycles 11 through 15. The reliability factors for the CASMO-2/NDH methods (Reference 2) were determined from TIP comparisons which bounded the gamma scan comparisons. The greater measurement uncertainties associated with neutron TIPs results in larger measured to calculated variance as compared to gamma scan. Therefore, use of neutron TIP statistics, including the measurement uncertainty, will result in a conservative estimate of the power distribution uncertainty.

Other benchmarks of the CASMO-3/SIMULATE-3 power distribution predictions are available for gamma scan (references 4, and 35), critical experiments (references 4, 28, 32, 33, 34, 38, and 51), fine mesh PDQ (diffusion theory) (references 5, 37, 41, 42, 44, and 46), CASMO-3 color sets (references 5, 34, 41, 46, and 48), gamma TIPs (references 5, 6, 40, and 45), and neutron TIPs (references 5, 37, 38, 39, 41, 45, 47, 49, and 50). These comparisons include both BWR and PWR type cores and geometries.

### 3.6.4 Standard Power Distribution Comparison

The following is a presentation of the power distribution using the industry standard format. Published power distribution data is usually presented in tables of axial, radial and nodal comparisons and is usually compared at the 1 $\sigma$  level. Note that the entire data base is used.

#### 3.6.4.1 Axial Power Distribution Comparisons

Table 3.6.2 presents axial peak-to-average comparisons for selected statepoints from cycles 11 through 15. The following results are taken from the entire data base presented in sections 3.6.1, 3.6.2.

Simulator to measured TIP traces



Unrodded  
n = 912  
 $\mu = 0.009$   
 $\sigma = 0.048$

Rodded  
n = 720  
 $\mu = 0.010$   
 $\sigma = 0.052$

This data shows excellent agreement with other published data.

#### 3.6.4.2 Radial Power Distribution Comparisons

Table 3.6.3 presents radial peak-to-average comparisons from selected statepoints from cycles 11 through 15. The following results were taken from the entire data base presented in Section 3.6.1, 3.6.2 and 3.6.3.

Simulator to measured TIP traces

$\mu = 0.001$   
 $\sigma = 0.043$

This data shows excellent agreement to other published data.

#### 3.6.4.3 Nodal Power Distributions Comparisons

Table 3.6.4 presents the nodal standard deviations for the 20 axial planes from the entire data base presented in Sections 3.6.1, 3.6.2.

Simulator to measured TIP traces

$\mu = 0.002$   
 $\sigma = 0.071$

This data shows excellent agreement to other published data.

### 3.7 Delayed Neutron Parameters

This section deals with determining reliability factors for values which can be calculated but not measured. In these cases, an argument may be made for the general magnitude of the reliability factor without making direct comparisons between measured and predicted values.

The importance of the reliability of the calculated values of the delayed neutron parameters is primarily associated with the core  $\beta_{eff}$ . The uncertainties in the calculation of  $\beta_{eff}$  are composed of several components, the most important of which are listed below:

- a) Experimental values of  $\beta$ , and  $\lambda$ , by nuclide;
- b) Calculation of the spatial nuclide inventory;
- c) Calculation of core average  $\beta_{eff}$  as an adjoint-flux weighted average over the spatial nuclide inventory.

The experimental determination of the  $\beta$ 's and  $\lambda$ 's are assumed to be accurate to within 1%. The most important nuclide concentrations with respect to core  $\beta$  are  $U^{238}$ ,  $U^{235}$  and  $Pu^{239}$ . References 4 and 36 indicate that the uncertainty in the calculation of these parameters is about 0.3% for CASMO-3. Therefore, components a) and b) above are combined as 1.3% for CASMO-3.

The uncertainty in the calculation of a core average  $\beta$  depends on the

relative adjoint-flux weighting of the individual assemblies in the core. For demonstration purposes, consider a four region core, each with a different average burnup and average  $\beta$ . This is typical of advanced BWR cycles in that about a fourth of the core has seen three previous cycles, a fourth two previous cycles, a fourth one previous cycle and a fourth is the feed fuel. Typical regional  $\beta$ 's are given below:

Region 1 (fourth cycle fuel)	$\beta = 0.00543$
Region 2 (third cycle fuel)	$\beta = 0.00581$
Region 3 (second cycle fuel)	$\beta = 0.00633$
Region 4 (feed fuel)	$\beta = 0.00745$

The effect of errors in the calculated flux distribution can be evaluated in terms of the effect on the core average  $\beta_{eff}$ . As a base case, weighting factors are all set to 1.0. In this case, the core average  $\beta_{eff} = 0.00626$ . Using a maximum error in the regional flux weighting of 7.0%, the worst error in the calculation of the core average  $\beta_{eff}$  is obtained by increasing the weight of the Region 1 fuel and decreasing the weight of the Region 4 fuel. It should be noted that the average relative weighting factor is unity. The revised  $\beta$  is calculated as follows:

$$\begin{aligned} \beta(1) \times 1.07 &= .00581 \\ \beta(2) \times 1.00 &= .00581 \\ \beta(3) \times 1.00 &= .00633 \\ \beta(4) \times 0.93 &= .00693 \\ \beta &= .00622, \text{ which yields a } -0.6\% \text{ error for component c) above.} \end{aligned}$$

The sum of the errors for these four factors for CASMO is as follows:

$$1.3\%(a+b) + 0.5\%(c) = 1.8\%$$

For conservatism the reliability factor for delayed neutron parameters is set at 4%.

### 3.8 Effective Neutron Lifetime

An argument similar to the delayed neutron parameter argument is applied to the determination of the effective neutron lifetime ( $\Lambda$ ) uncertainty. The uncertainty components which go into the calculation of  $\Lambda$  are as follows:

- a) Experimental values of microscopic cross sections;
- b) Calculation of the spatial nuclide inventory; and
- c) Calculation of the core average effective neutron life-time as an adjoint-flux weighted average over the spatial nuclide inventory.

Uncertainties for components a) and b) are assumed to be the same as described for the calculation of  $\beta_{eff}$ , that is, 1% uncertainty in the experimental determination of nuclear cross section and .3% uncertainty in the determination of the spatial nuclide inventory for CASMO. The core average neutron lifetime depends on adjoint flux weighting of local absorption lifetimes. If a conservative estimate of the error in regional power sharing (7%) is used in determining the impact on the core average lifetime, the error in lifetime is on the order of 1.0%. Combining all of these uncertainties linearly results in a total uncertainty of 1.8% for CASMO-3. Therefore, a 4% reliability factor will be applied to the neutron lifetime calculation when applied to safety related calculations.

Table 3.6.1 Full Power Statepoints

Cycle	Cycle Exposure (GWD/MTU)	Power (%)	Rod Density (%)	k <sub>eff</sub>
11	.388	99.9	11.71	0.9989
	.819	100.0	8.26	0.9981
	1.331	99.9	8.75	0.9980
	1.759	100.0	7.85	0.9981
	2.251	100.0	7.71	0.9981
	2.659	100.0	7.61	0.9983
	3.223	100.0	7.37	0.9985
	3.716	100.0	7.30	0.9980
	4.128	100.1	7.23	0.9987
	4.631	100.0	6.71	0.9990
	5.301	99.9	4.58	1.0003
	5.624	100.0	4.17	1.0009
	6.352	98.6	0.03	1.0017
	6.756	92.1	0.03	1.0016
	7.256	83.5	0.03	1.0015
	7.764	74.0	0.03	1.0014
8.159	66.4	0.03	1.0016	
12	0.535	100.0	2.89	1.0006
	1.063	100.0	3.17	0.9994
	1.736	99.9	5.23	0.9988
	1.945	99.9	5.23	0.9993
	2.478	99.9	7.82	0.9992
	2.858	100.0	7.30	0.9998
	4.497	99.9	7.02	1.0000
	4.880	99.9	5.54	0.9998
	5.478	99.8	3.03	1.0002
	6.830	95.7	0.96	1.0004
	7.148	91.1	0.00	0.9999
13	0.783	100.0	7.58	0.9963
	1.408	100.0	8.26	0.9956
	2.149	100.0	9.09	0.9952
	2.672	100.0	10.47	0.9961
	3.351	100.0	10.74	0.9959
	3.967	99.9	10.47	0.9965
	4.956	99.9	8.26	0.9966
	6.165	100.0	6.06	0.9973
	6.707	100.0	3.58	0.9976
	7.373	99.9	0.00	0.9975
	8.229	86.8	0.00	0.9970
	8.724	77.8	0.00	0.9968
	9.103	70.6	0.00	0.9969
	9.729	58.9	0.00	0.9969
10.165	50.9	0.00	0.9968	
14	0.751	100.0	6.20	0.9970
	1.296	100.1	6.37	0.9962
	1.977	100.0	7.02	0.9955
	2.648	100.1	8.26	0.9958
	3.325	100.1	8.68	0.9956
	4.170	99.9	8.68	0.9962
	5.284	100.1	8.75	0.9970
	5.904	100.0	6.61	0.9969
	6.530	100.0	4.58	0.9983
	7.454	100.0	1.89	0.9992
	8.237	92.7	0.00	0.9990
	8.882	82.5	0.00	0.9988

Table 3.6.1 Full Power Statepoints (Continued)

Cycle	Cycle Exposure (GWD/MTU)	Power (%)	Rod Density (%)	$k_{eff}$
15	0.187	99.8	7.51	0.9979
	0.954	99.9	6.23	0.9963
	1.790	99.8	7.92	0.9958
	2.735	99.8	8.68	0.9947
	3.591	99.7	8.95	0.9943
	4.518	99.7	9.54	0.9944
	5.409	99.7	9.33	0.9959
	6.802	99.8	8.13	0.9971
	7.636	99.8	6.30	0.9971
	8.349	99.5	5.51	0.9977
	9.332	99.7	2.86	0.9982
	10.301	91.1	1.10	0.9972
	11.197	73.4	0.00	0.9960

Table 3.6.2 Axial Power Distribution Comparison

Cycle	Location	Rod	Peak to Average TIP	Peak to Average Calculated	% Difference
11	20-29	Out	1.185	1.143	3.5
11	28-13	Out	1.272	1.297	-2.0
12	28-29	Out	1.241	1.255	-1.1
12	20-21	Out	1.182	1.192	-0.8
12	12-21	Out	1.183	1.194	-1.0
13	44-29	Out	1.405	1.406	-0.1
13	12-29	Out	1.438	1.393	3.1
13	28-21	Out	1.155	1.163	-0.6
14	20-29	Out	1.318	1.302	1.2
14	44-29	Out	1.256	1.231	1.9
14	12-37	Out	1.289	1.275	1.1
15	36-29	Out	1.161	1.193	-2.8
15	36-37	Out	1.415	1.326	6.3
15	12-37	Out	1.361	1.349	0.9
11	20-37	In	1.611	1.598	0.8
12	20-21	In	1.225	1.259	-2.7
13	28-45	In	1.173	1.115	5.0
14	20-37	In	1.500	1.434	4.4
14	12-29	In	1.324	1.333	-0.6
15	28-29	In	1.195	1.181	1.1



Table 3.6.3

## Radial Power Distribution Comparisons

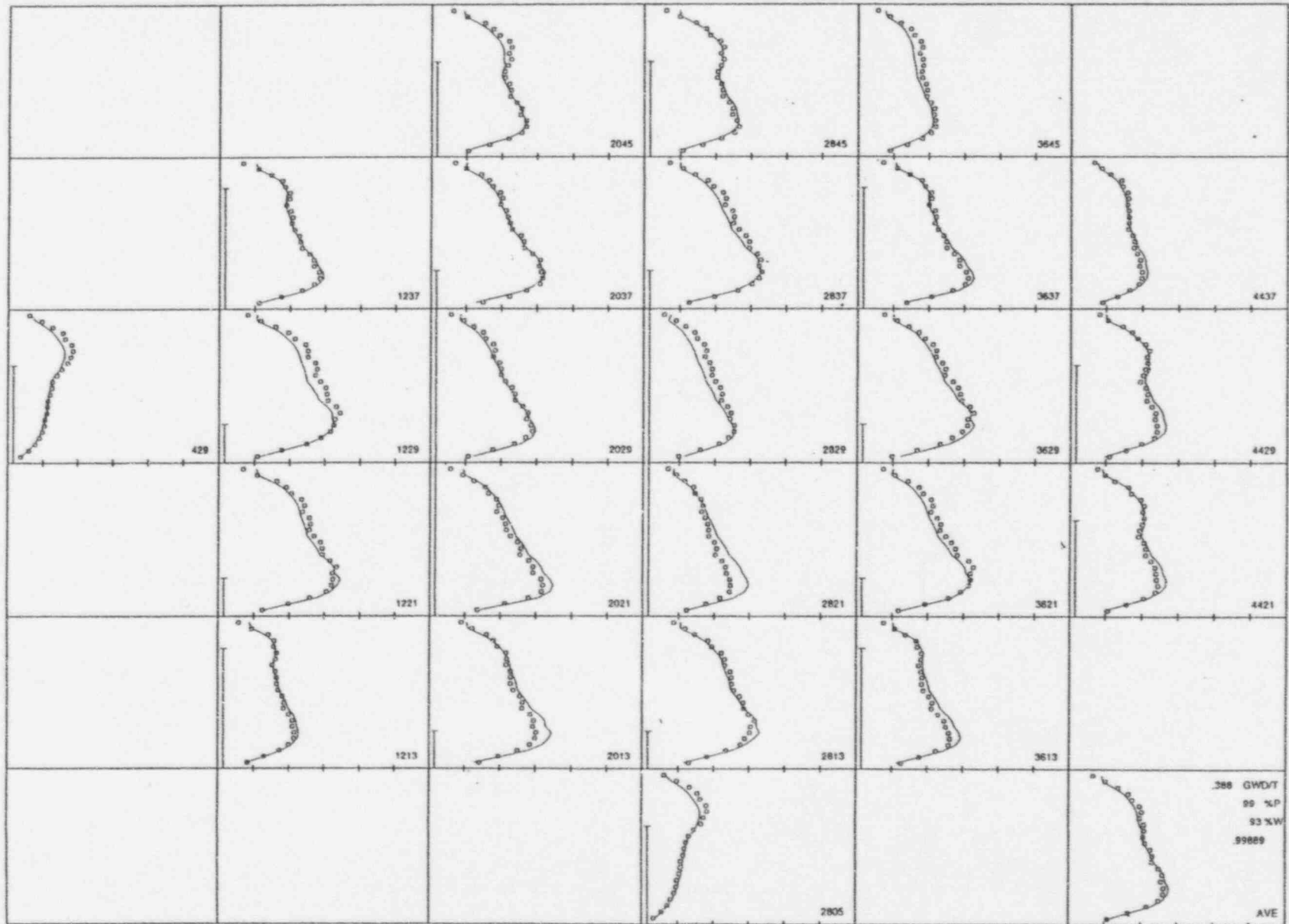
Cycle	Location	Exposure	TIP	Calculated	% Difference
11	20-37	0.388	1.118	1.103	1.4
11	36-13	1.331	1.151	1.185	-3.0
11	28-37	2.251	1.179	1.157	1.9
11	20-29	3.223	1.141	1.122	1.7
11	12-21	4.631	1.230	1.242	-1.0
11	12-29	7.764	1.228	1.176	4.2
12	36-29	1.063	1.159	1.139	1.7
12	36-29	2.478	1.187	1.150	3.1
12	12-21	4.880	1.155	1.131	2.1
12	28-21	6.830	1.131	1.199	-6.1
12	28-29	6.830	1.190	1.208	-1.6
12	28-37	7.148	1.159	1.208	-4.2
13	20-21	2.150	1.217	1.278	-5.0
13	28-37	2.672	1.136	1.149	-1.2
13	36-29	6.165	1.117	1.150	-3.0
13	36-29	6.707	1.125	1.147	-1.9
13	28-21	7.374	1.155	1.163	-0.7
13	28-37	10.165	1.120	1.127	-0.6
14	12-29	1.297	1.129	1.144	-1.3
14	36-29	1.977	1.117	1.168	-4.5
14	20-37	3.325	1.153	1.121	2.7
14	28-21	5.904	1.121	1.130	-0.8
14	28-13	7.454	1.110	1.130	-1.8
14	20-37	8.882	1.181	1.193	-1.0
15	12-29	0.954	1.111	1.168	-5.2
15	36-13	2.735	1.181	1.157	2.0
15	28-21	5.409	1.148	1.118	2.7
15	20-37	8.349	1.168	1.151	1.5
15	36-21	10.301	1.140	1.199	-5.2
15	20-37	11.197	1.233	1.201	2.6

Table 3.6.4

Power Distribution Standard Deviations in 20 Axial Planes

Planes	Planar Standard Deviation
3	0.062
4	0.061
5	0.056
6	0.054
7	0.055
8	0.054
9	0.056
10	0.060
11	0.058
12	0.060
13	0.062
14	0.064
15	0.062
16	0.060
17	0.066
18	0.061
19	0.060
20	0.062
21	0.063
22	0.074

Figure 3.6.1 Measured and Calculated Detector Responses BOC Cycle 11



STATEPOINT 1103 AT 0.3882 GWD/MTU

— SIMULATE-3  
 □ Measured

Figure 3.6.2 Measured and Calculated Detector Responses MOC Cycle 11

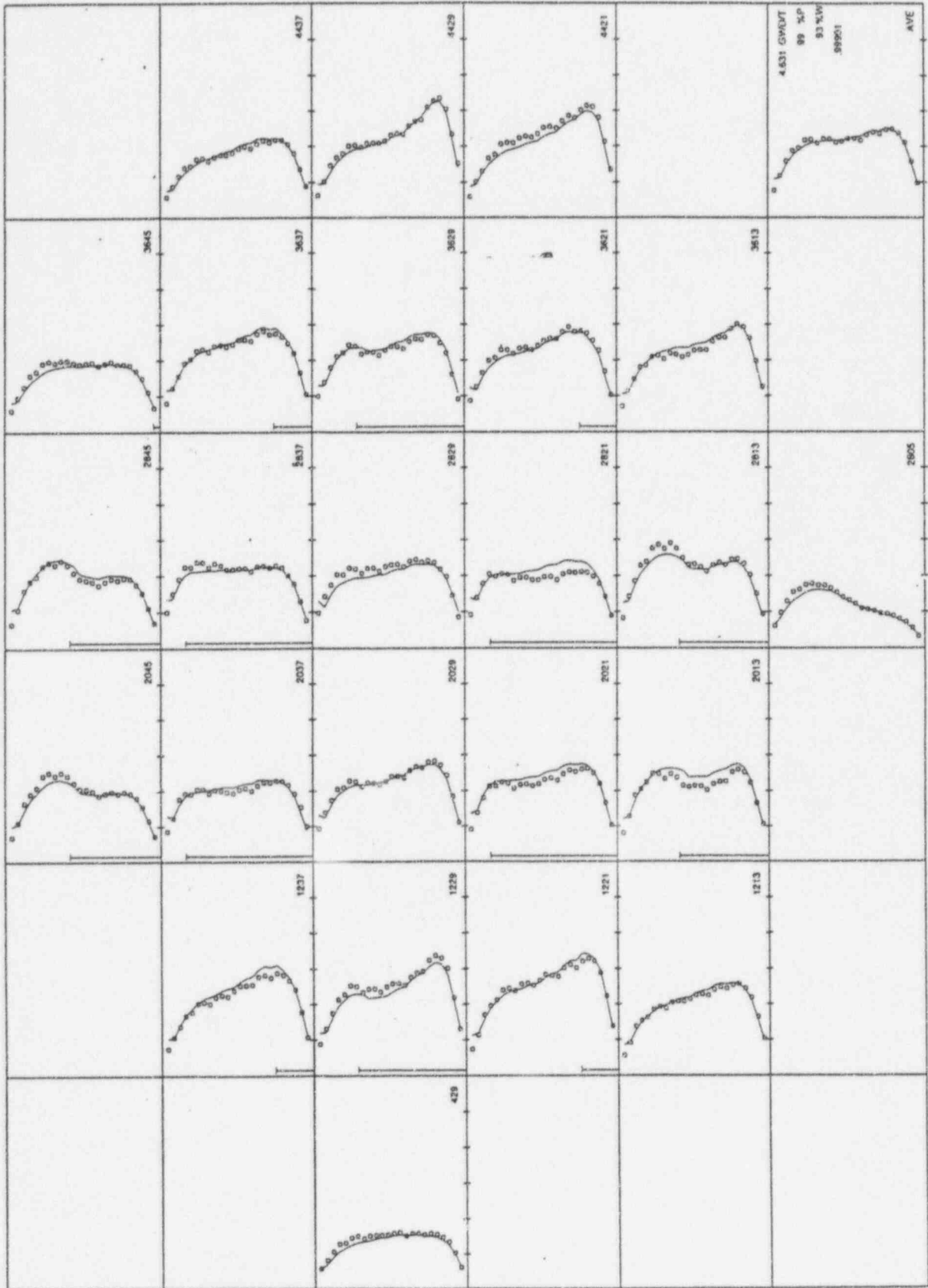
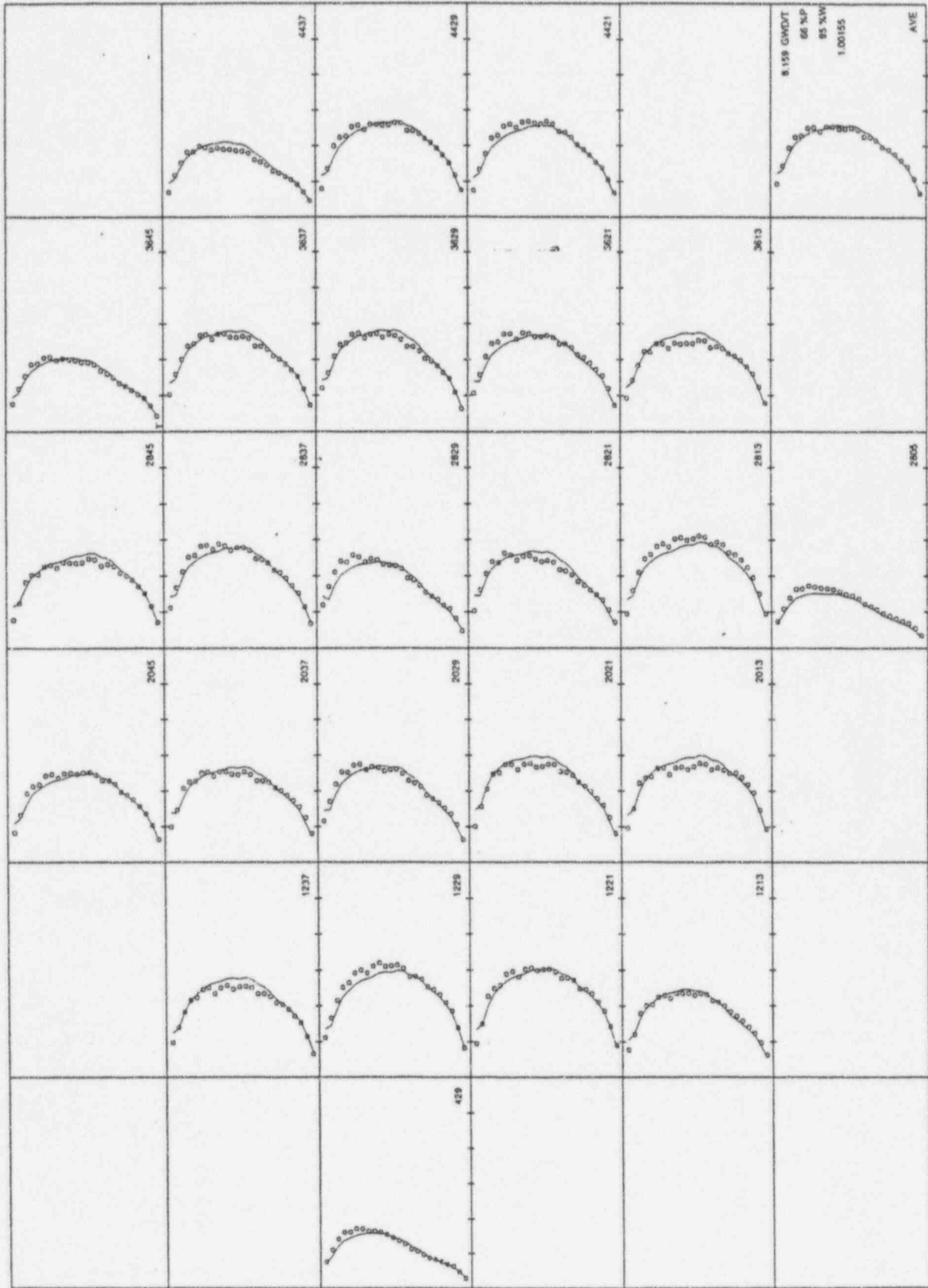


Figure 3.6.3 Measured and Calculated Detector Responses EOC Cycle 11



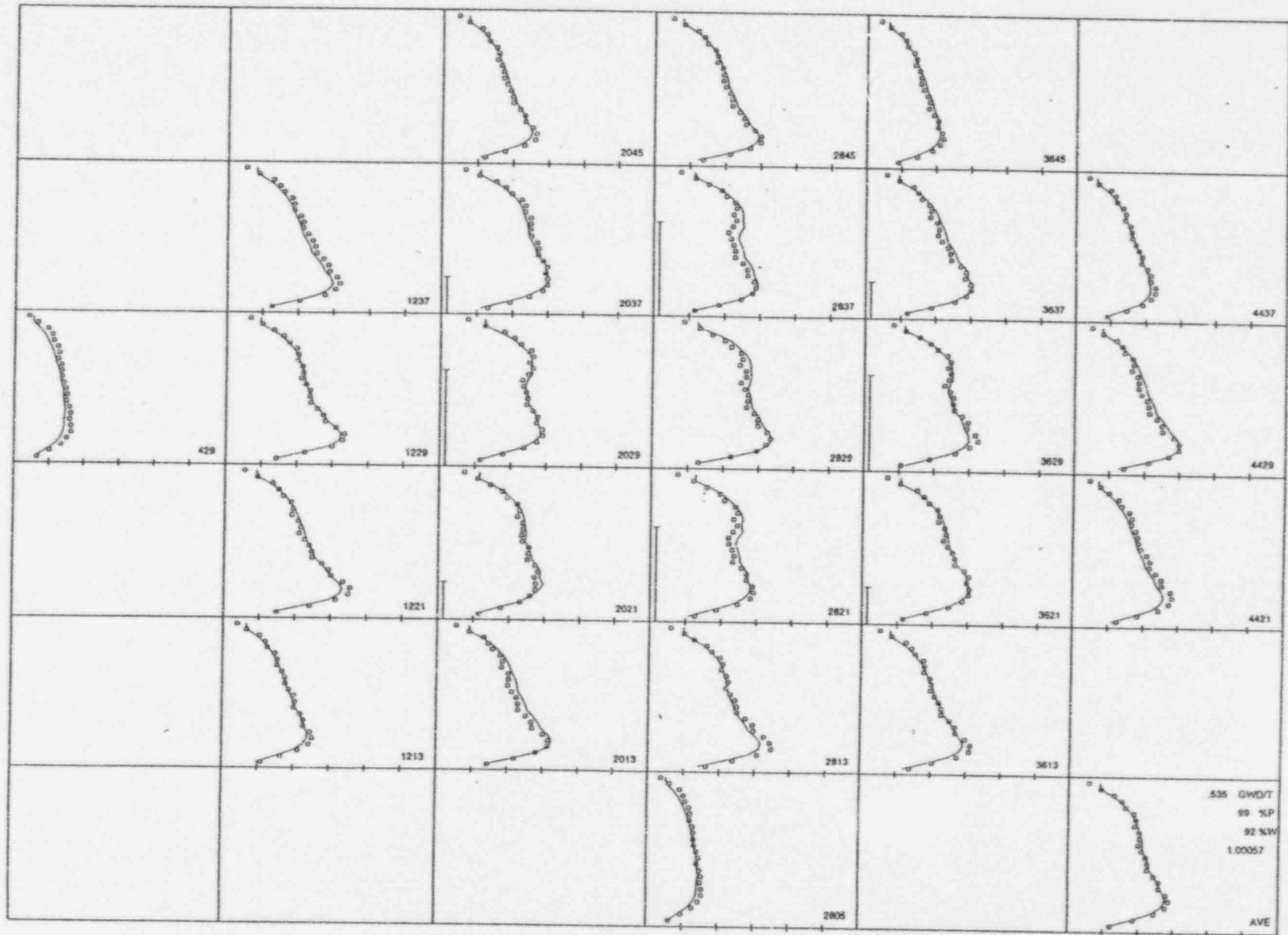
STATEPOINT 1121 AT 8.1586 GWD/MTU

— SIMULATE-3  
 □ Measured



Figure 3.6.4

Measured and Calculated Detector Responses BOC Cycle 12



STATEPOINT 1201 AT 0.5350 GWDMTU

— SIMULATE-3  
□ Measured

Figure 3.6.5 Measured and Calculated Detector Responses MOC Cycle 12

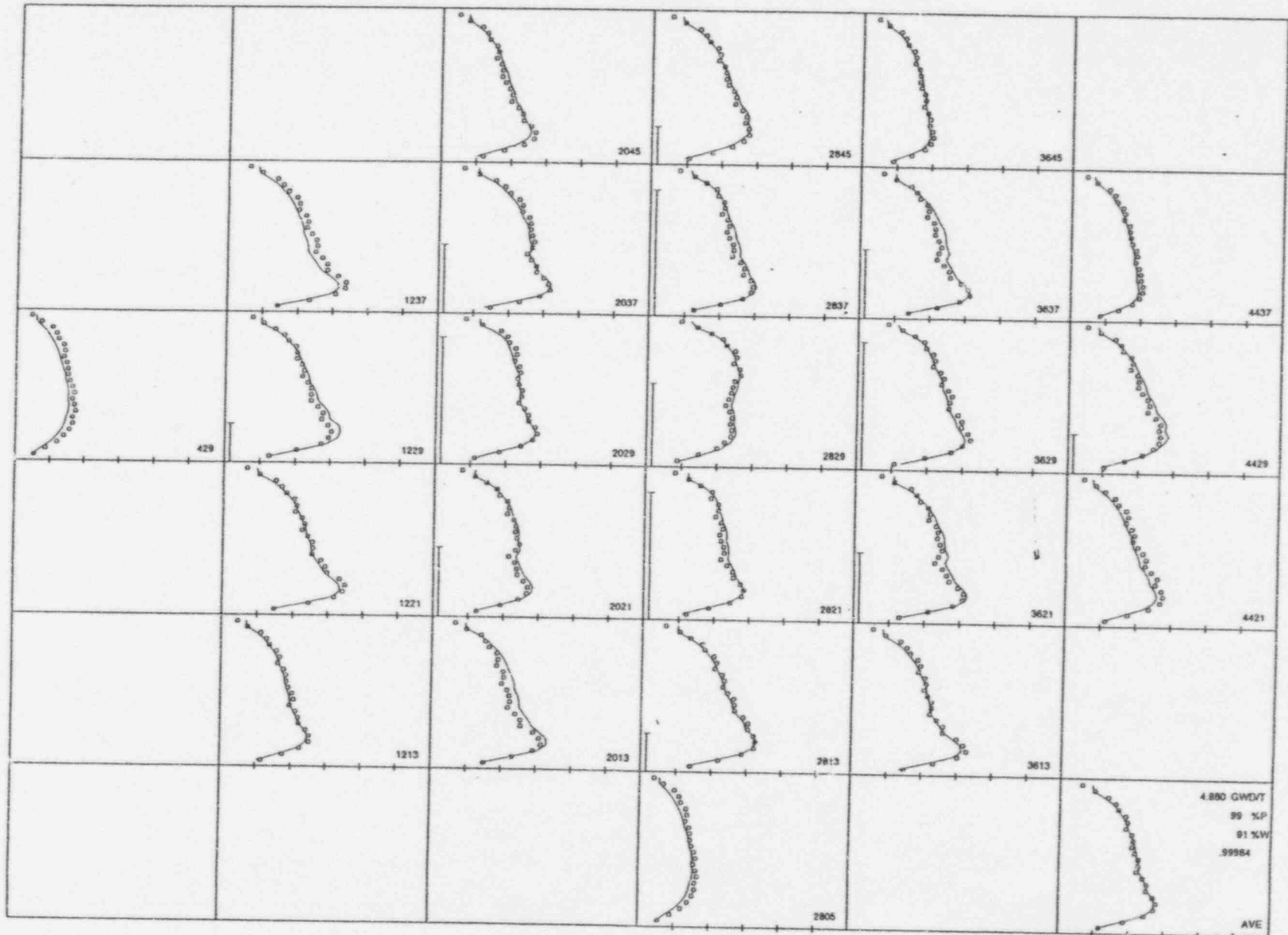


Figure 3.6.6 Measured and Calculated Detector Responses EOC Cycle 12

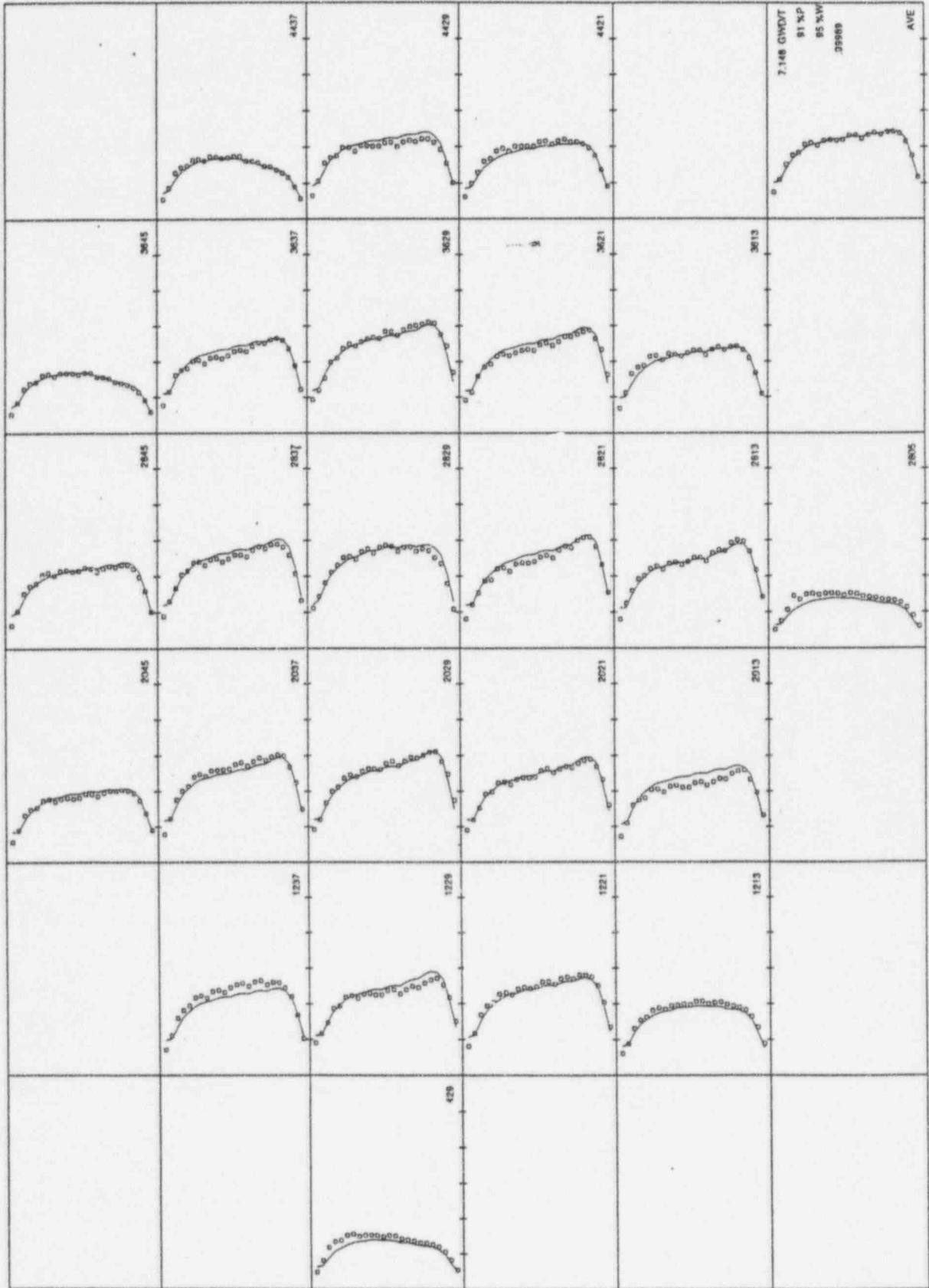
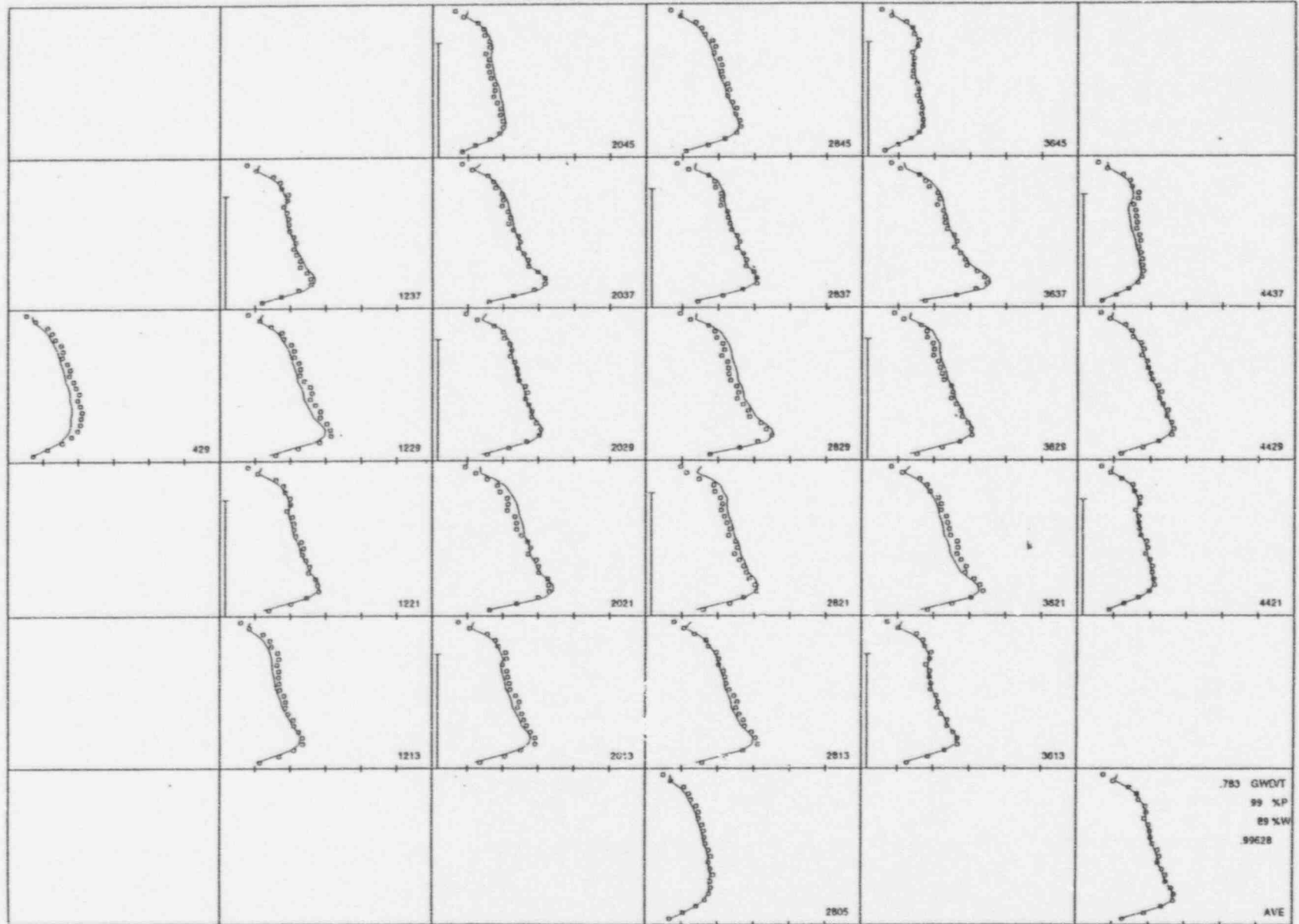


Figure 3.6.7

Measured and Calculated Detector Responses BOC Cycle 13

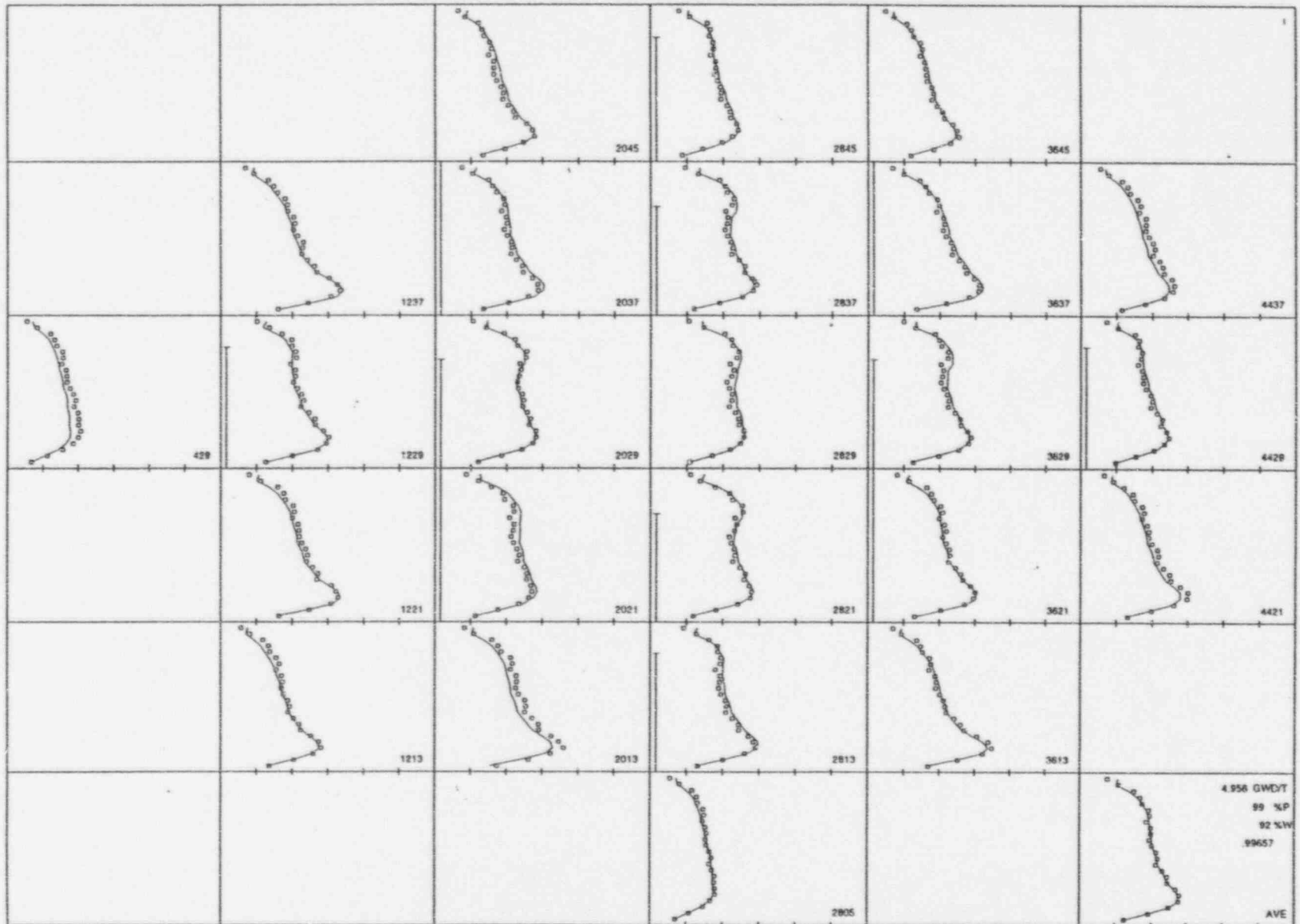


STATEPOINT 1301 AT 0.785 GWD/MTU

— SIMULATE-3  
 □ Measured

Figure 3.6.8

Measured and Calculated Detector Responses MOC Cycle 13

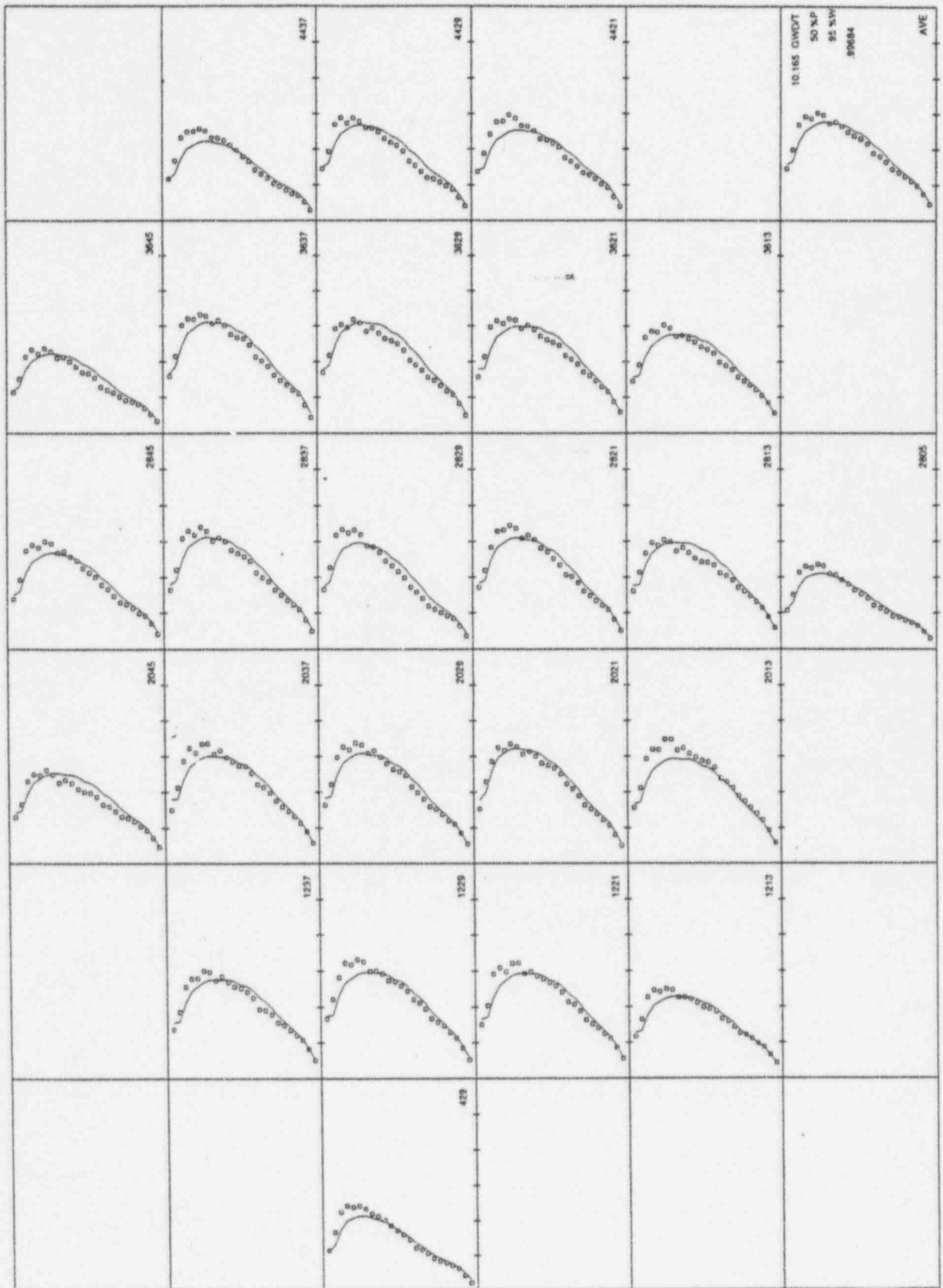


STATEPOINT 1308 AT 4.9558 GWD/MTU

— SIMULATE-3  
 □ Measured



Figure 3.6.9 Measured and Calculated Detector Responses EOC Cycle 13



STATEPOINT 1318 AT 10.1651 GWD/MTU

— SIMULATE-3  
 □ Measured

Figure 3.6.10 Measured and Calculated Detector Responses BOC Cycle 14

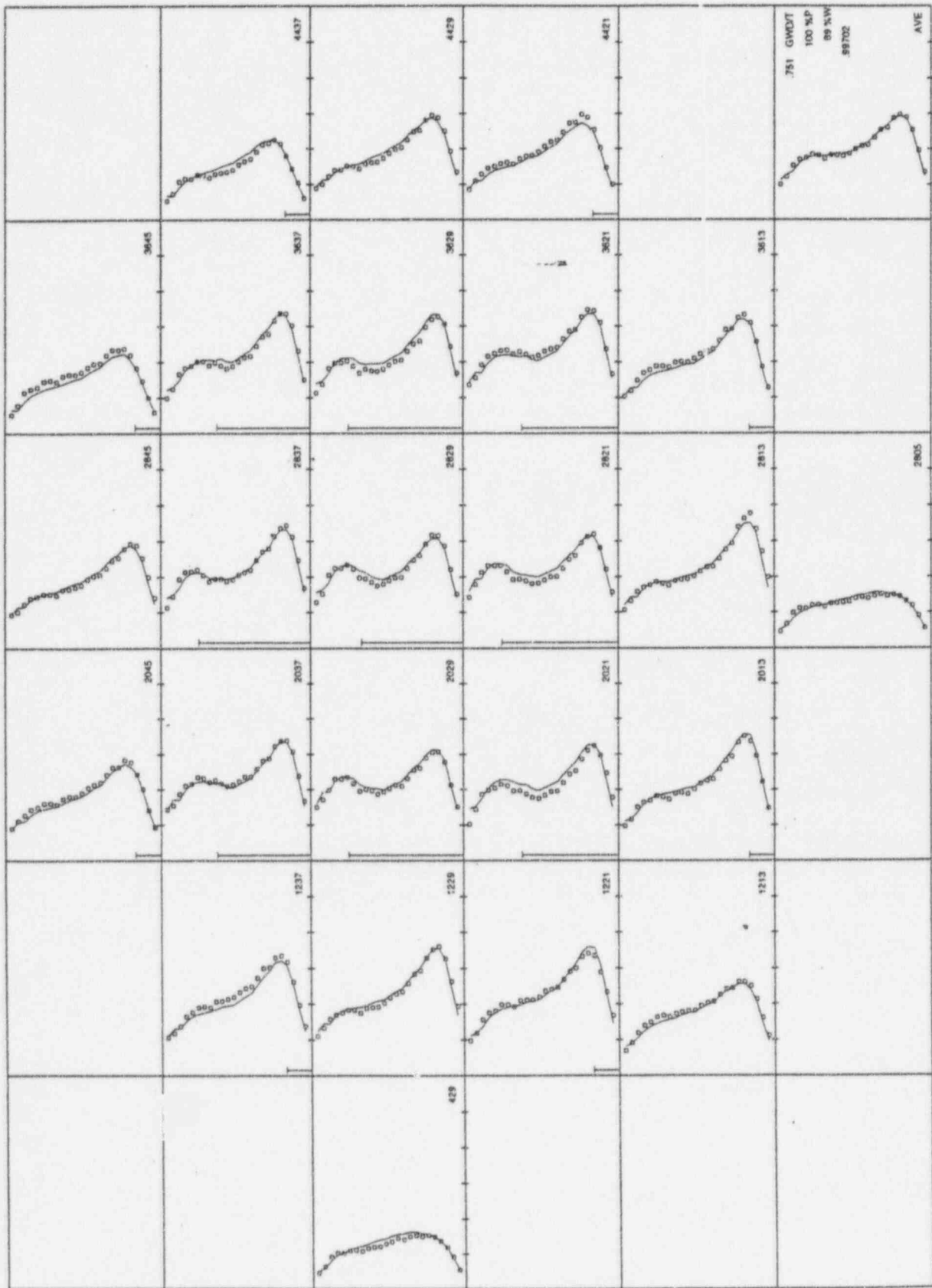


Figure 3.6.11 Measured and Calculated Detector Responses MOC Cycle 14

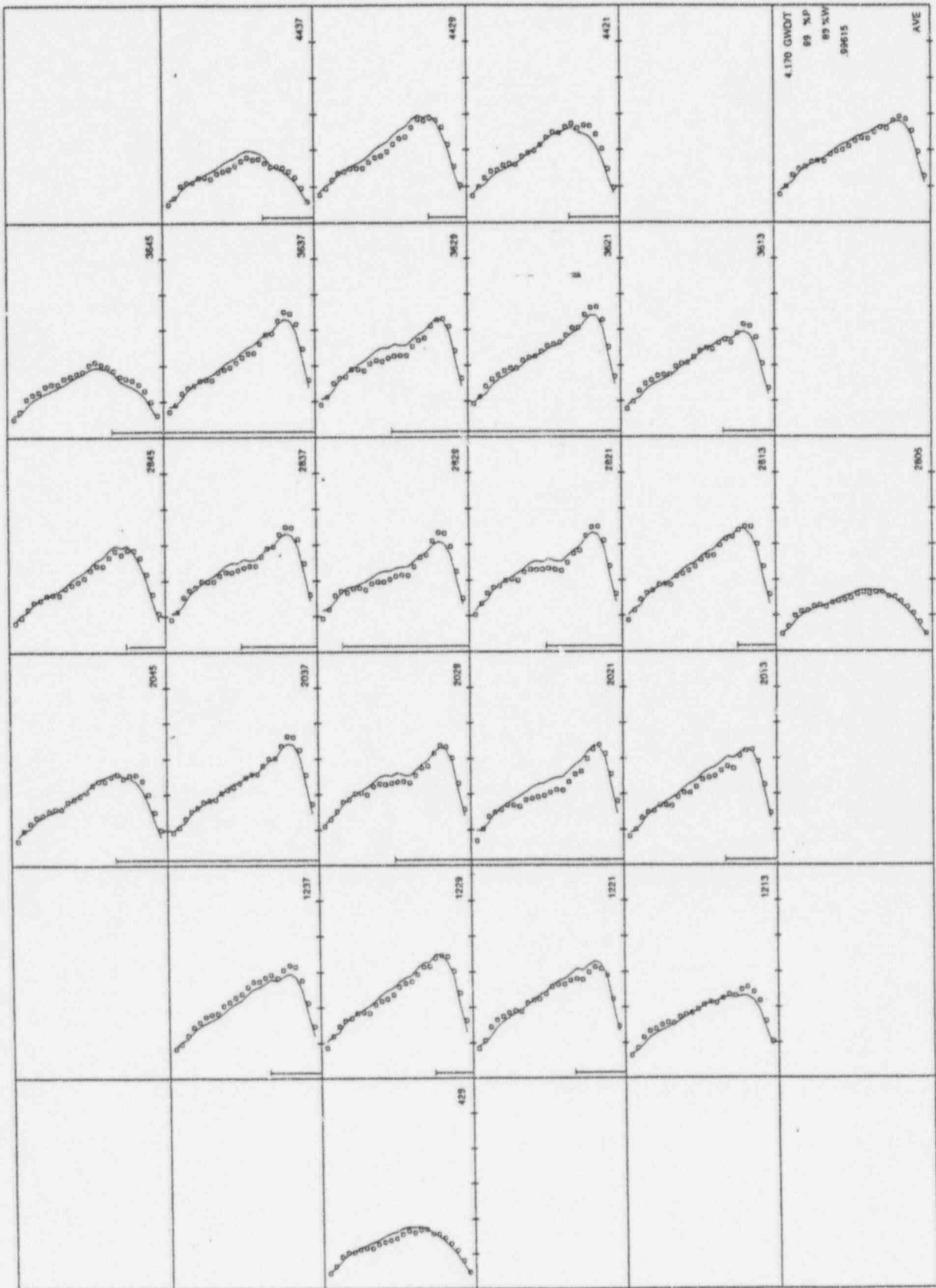
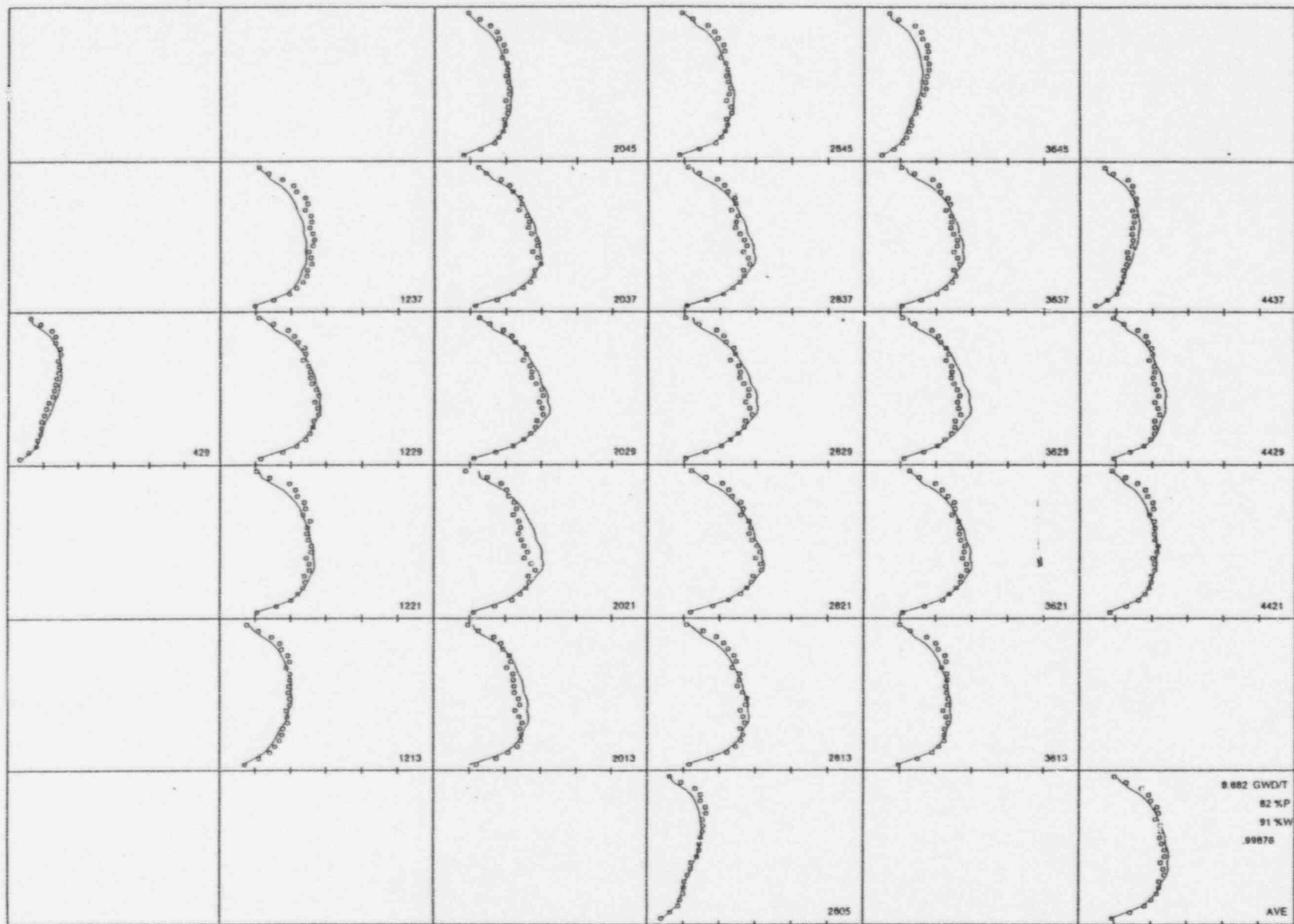


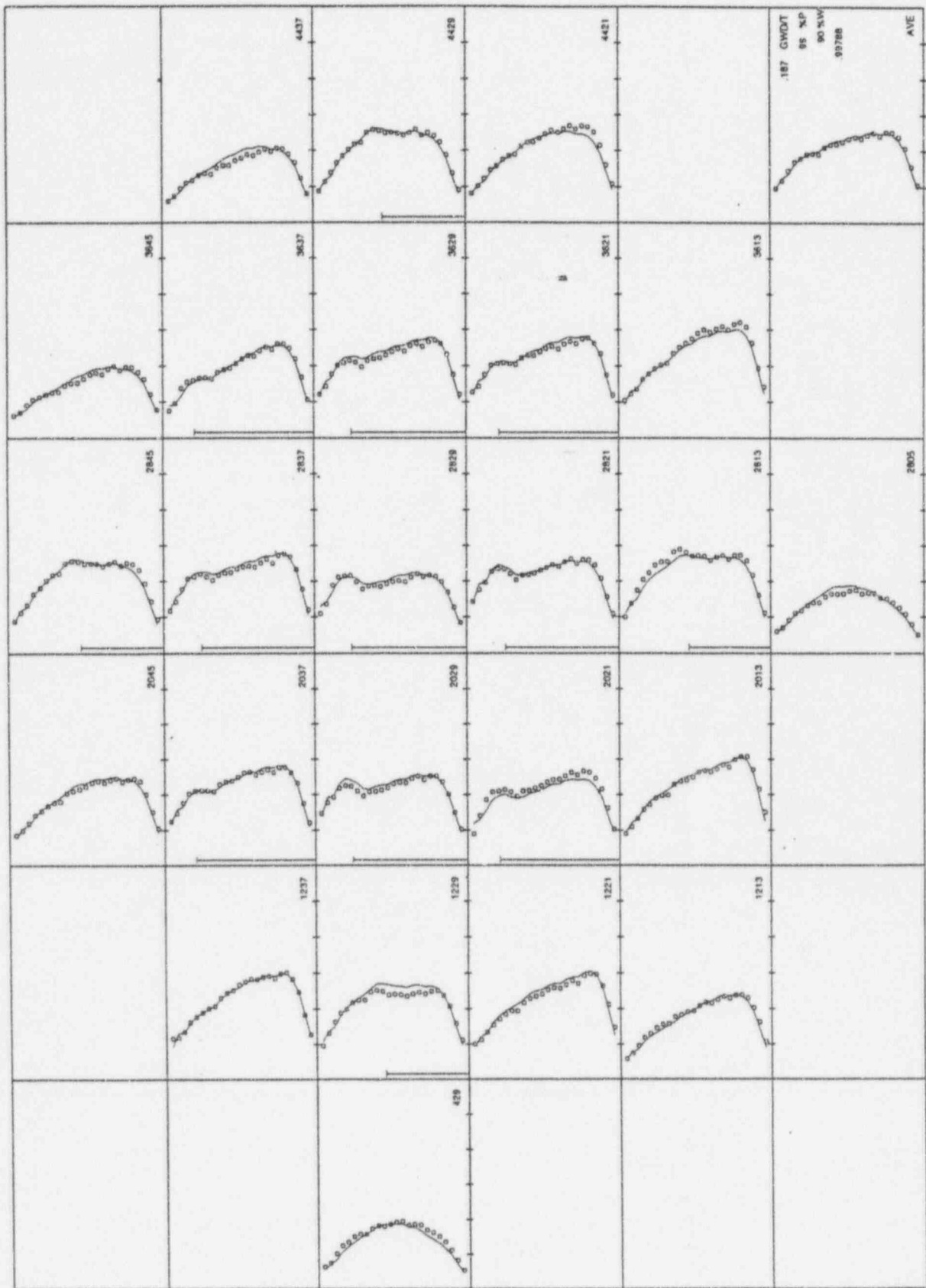
Figure 3.6.12 Measured and Calculated Detector Responses EOC Cycle 14



STATEPOINT 1413 AT 8.8822 GWD/MTU

— SIMULATE-3  
 □ Measured

Figure 3.6.13 Measured and Calculated Detector Responses BOC Cycle 15

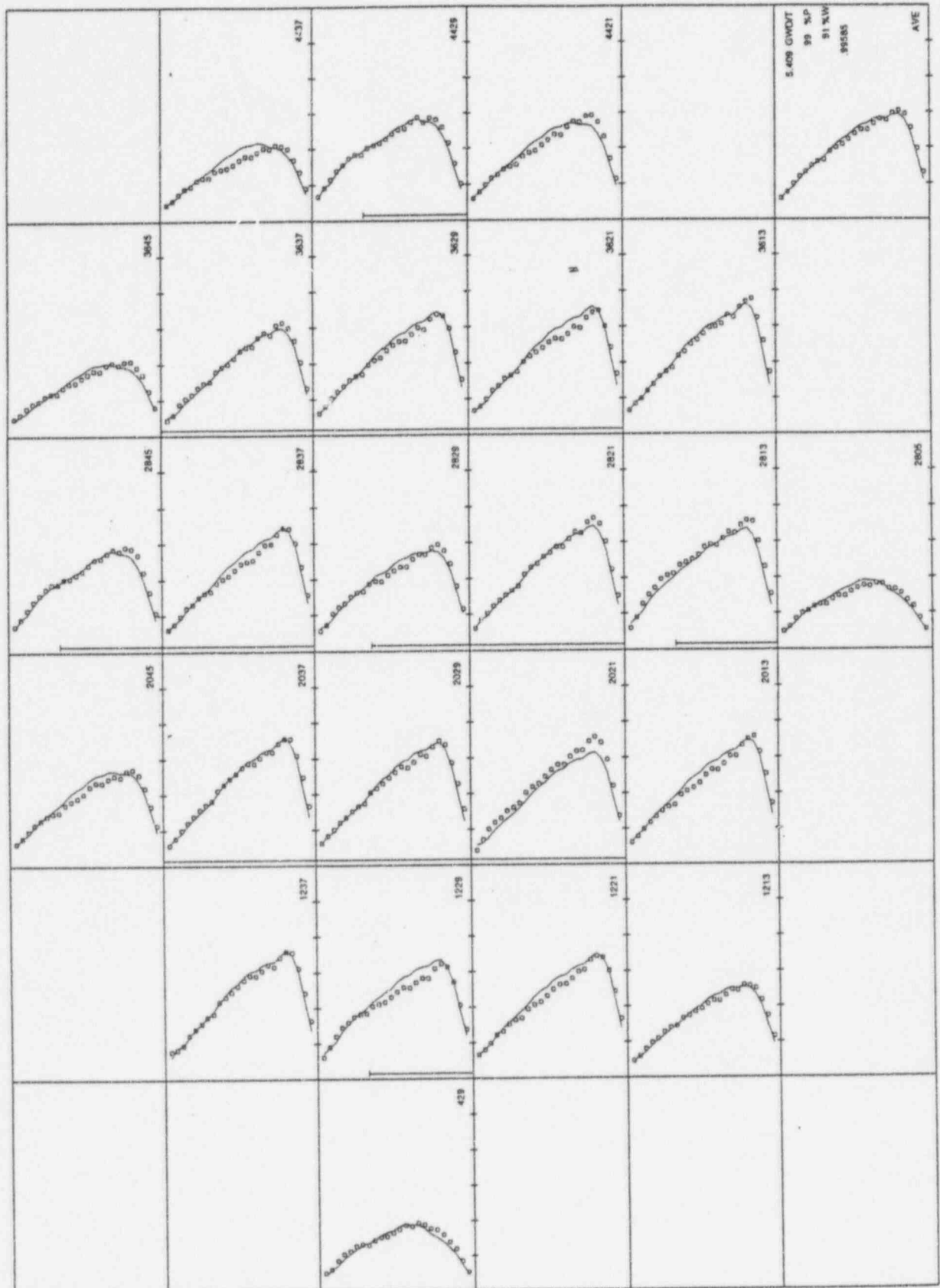


STATEPOINT 1501 AT 0.1870 GWD/MTU

— SIMULATE-3  
 □ Measured



Figure 3.6.14 Measured and Calculated Detector Responses MOC Cycle 15



STATEPOINT 1507 AT 5.4086 GWDMTU

— SIMULATE-3  
 □ Measured

Figure 3.6.15 Measured and Calculated Detector Responses EOC Cycle 15

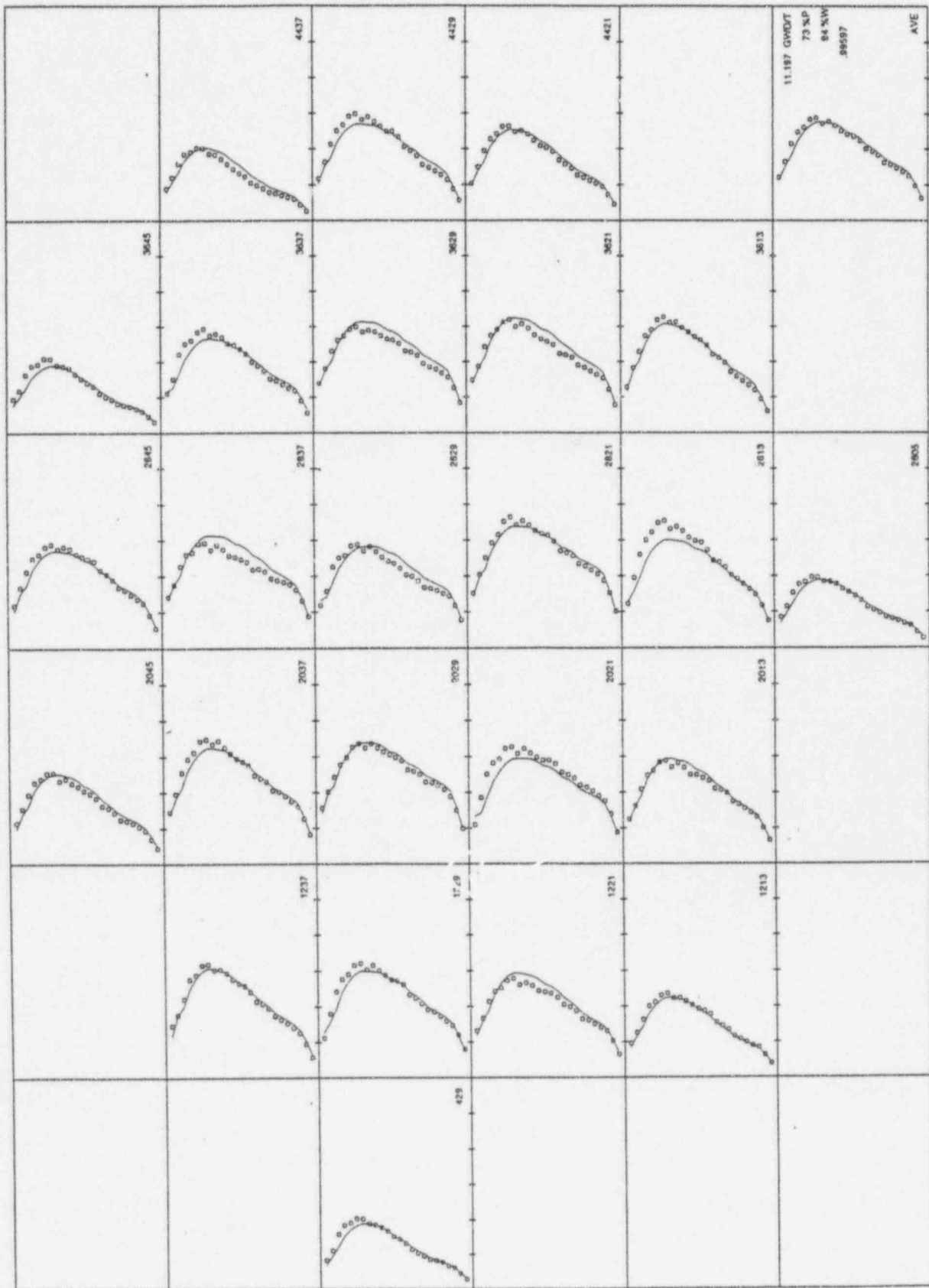


Figure 3.6.16

# Observed Differences Density Function Comparison

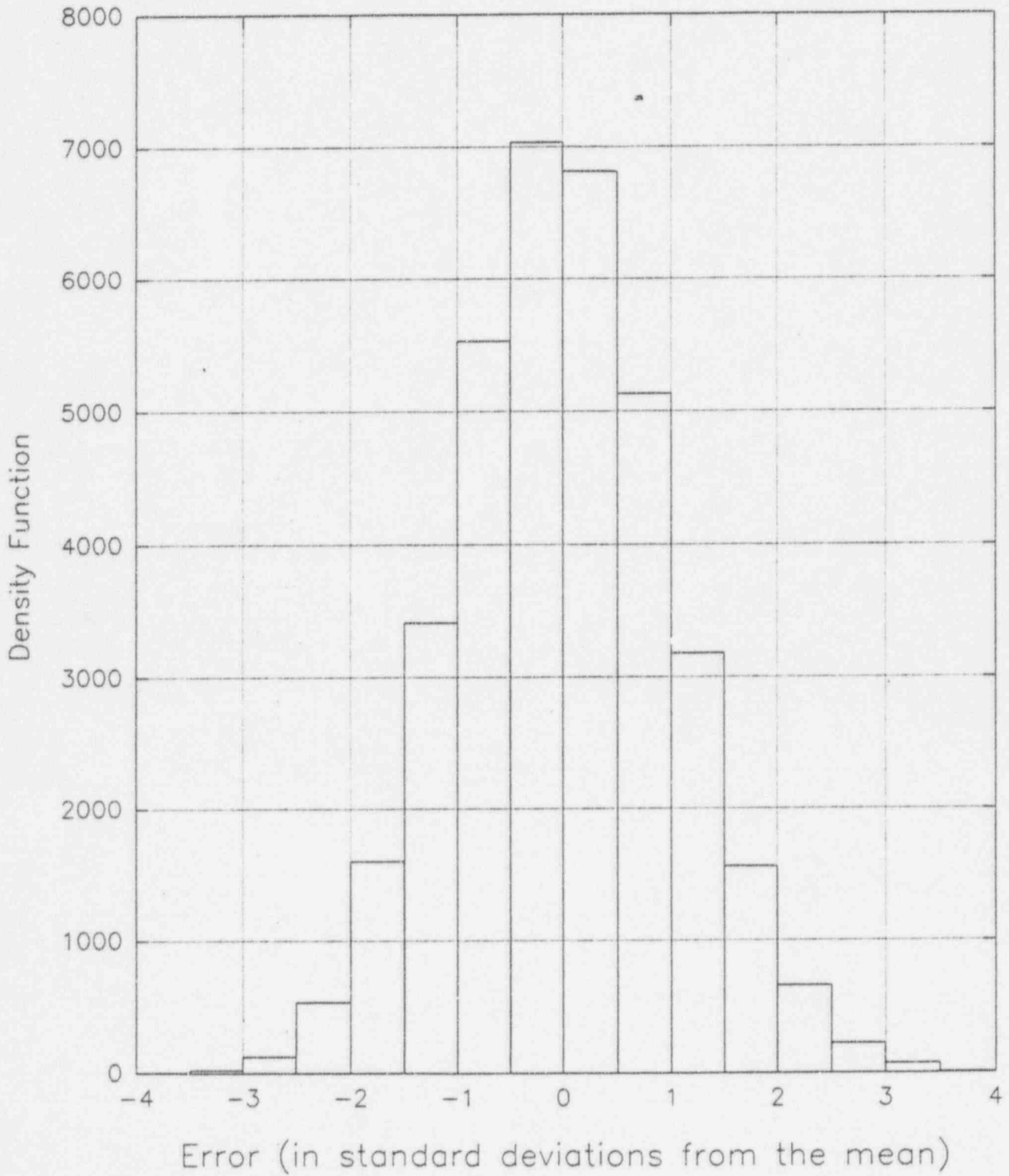


Figure 3.6.17

### Cumulative Distribution Function (CDF) Comparison

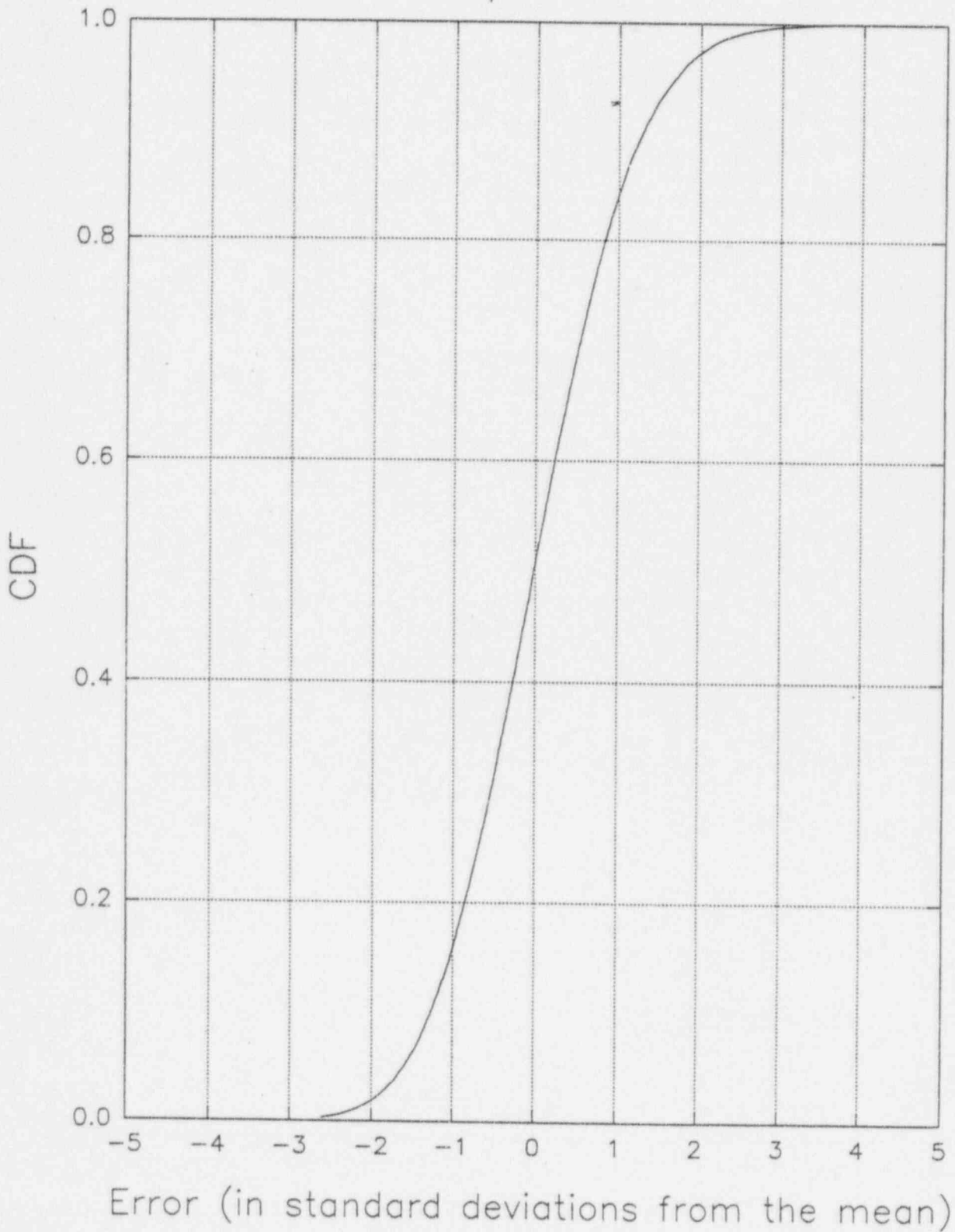


Figure 3.6.18

### CDF in the Region of the 95th Percentile Model Comparison

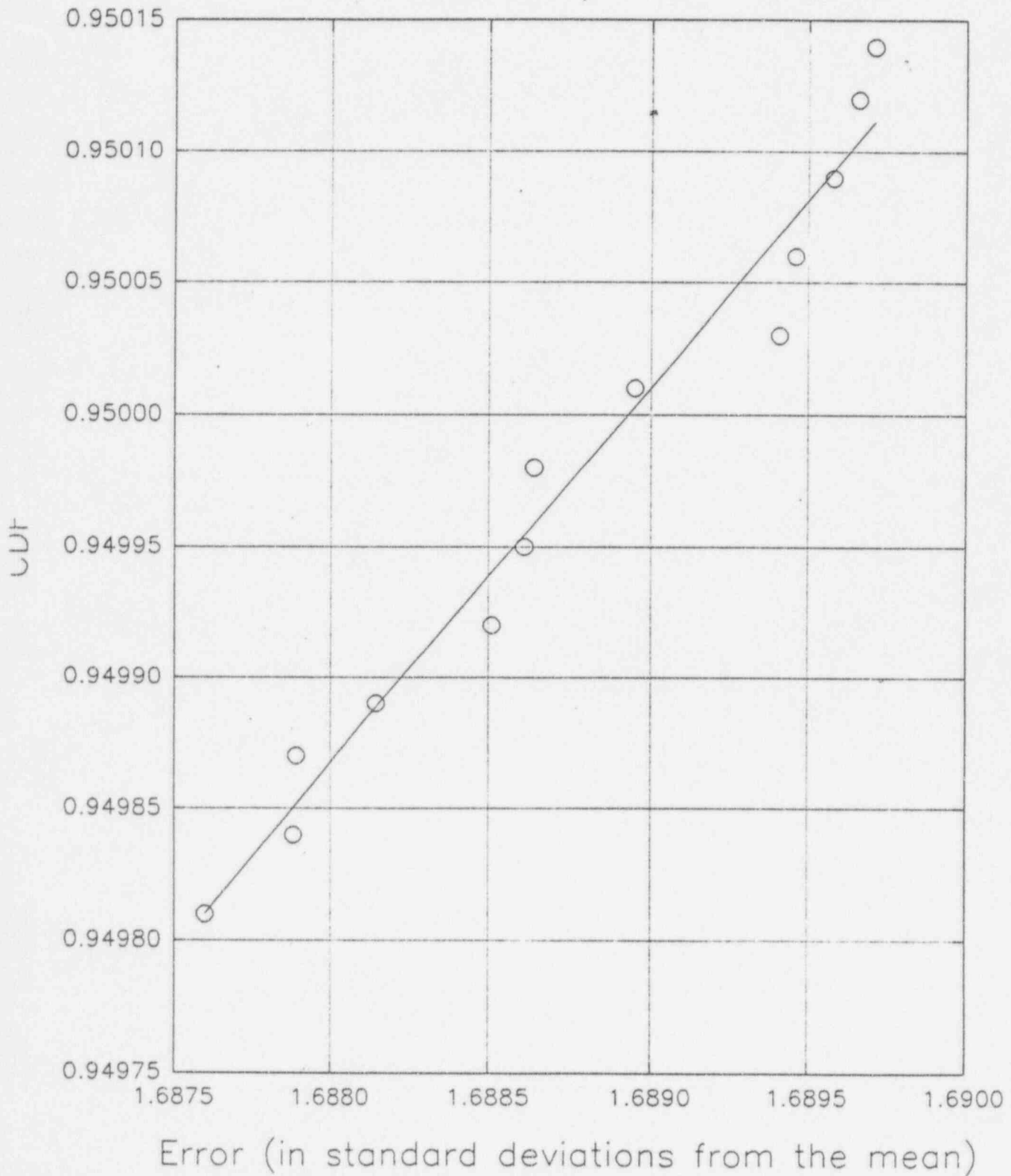




Figure 3.6.19

# Observed Differences Density Function Integrated Reaction Rates Comparison

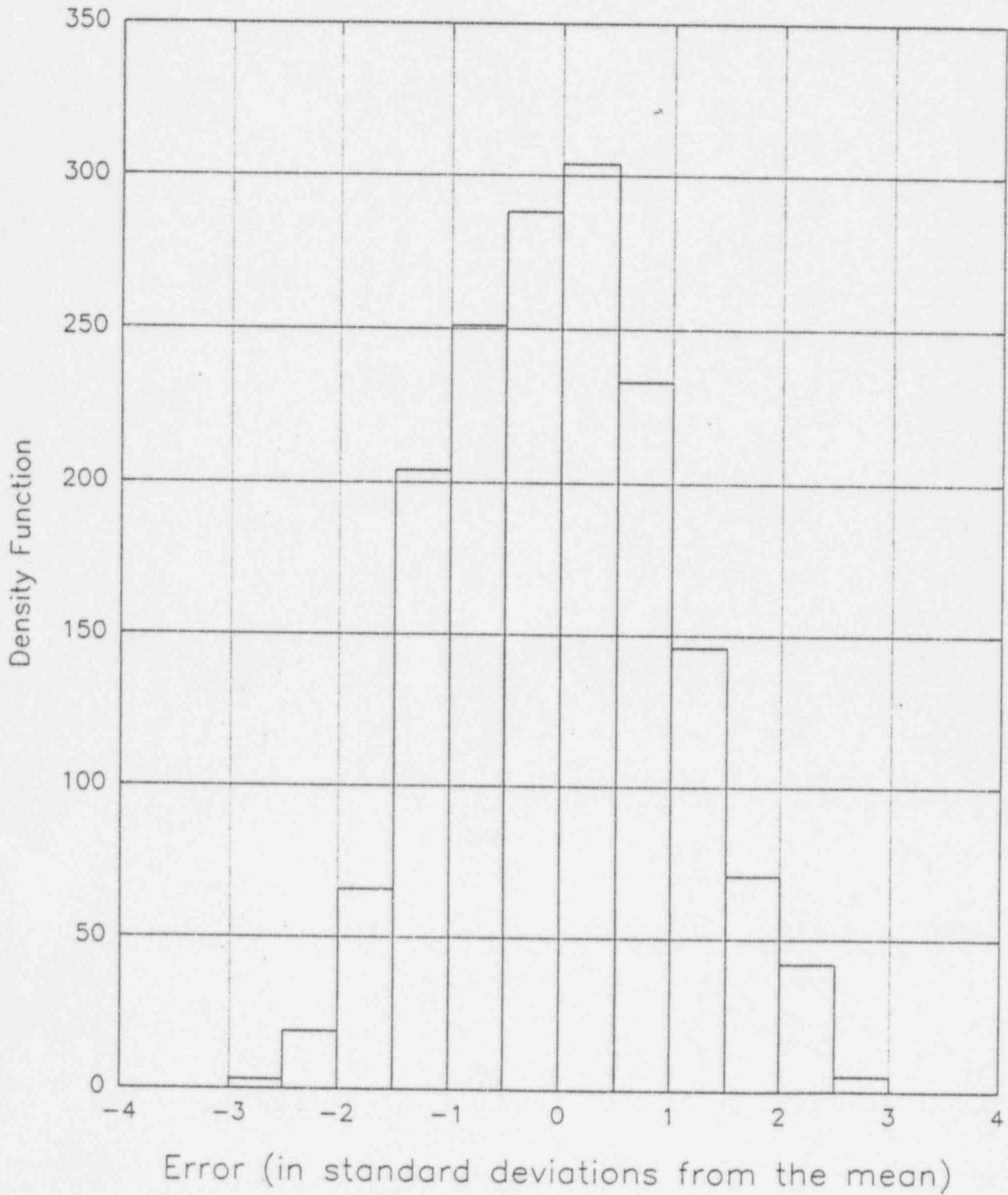


Figure 3.6.20

Cumulative Distribution Function (CDF)  
Integrated Reaction Rates Comparison

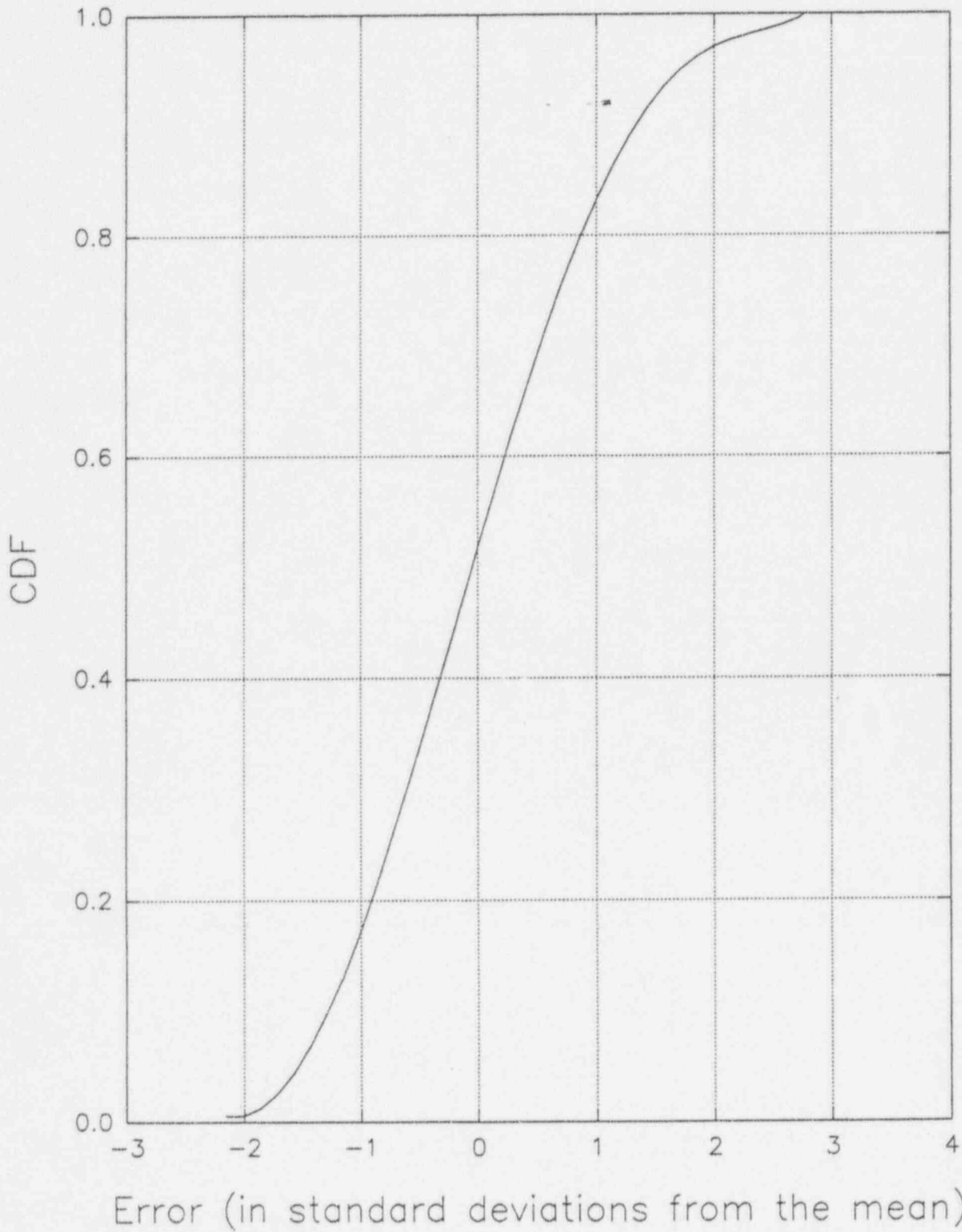


Figure 3.6.21

CDF in the Region of the 95th Percentile  
For Integrated Reaction Rates

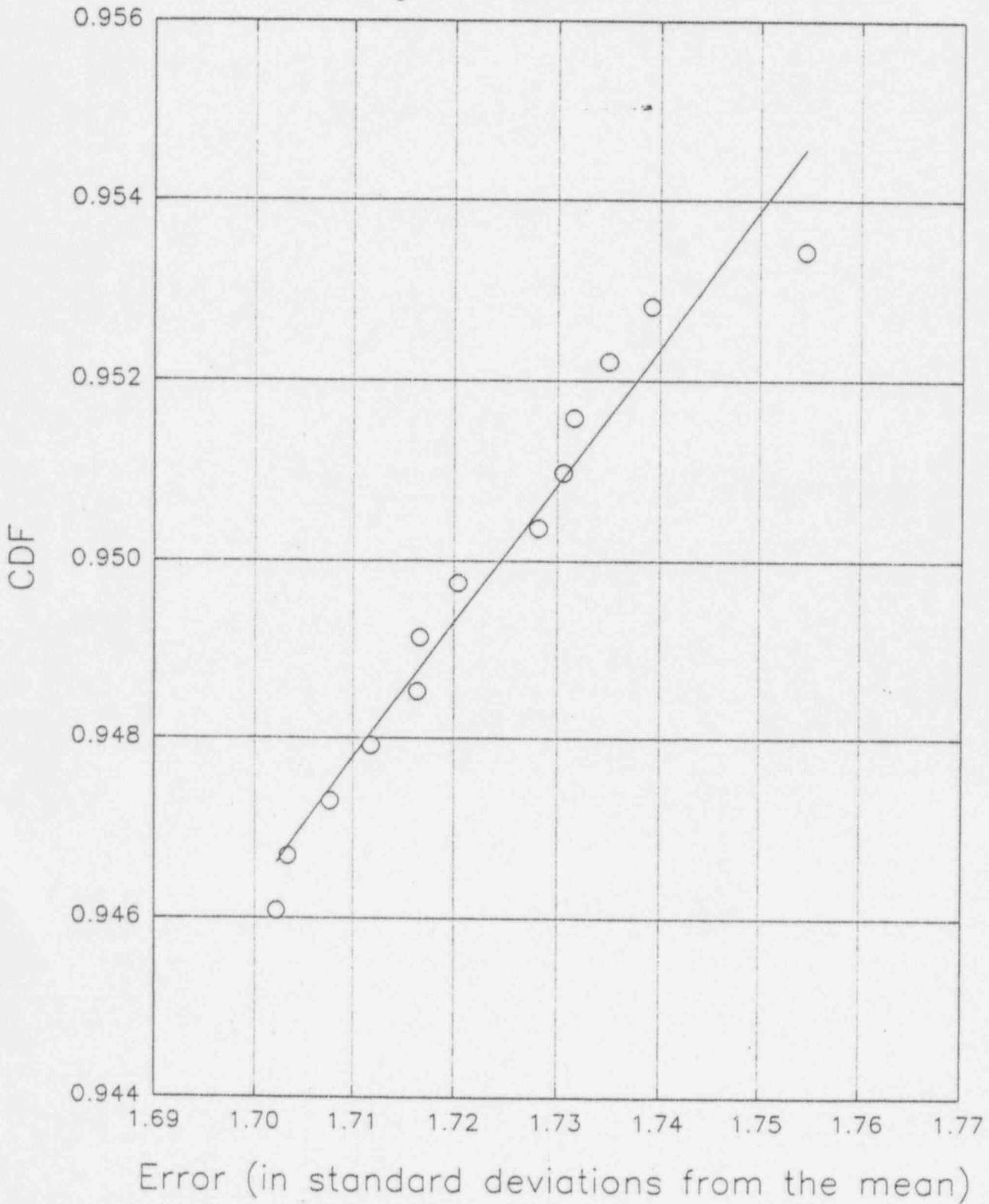
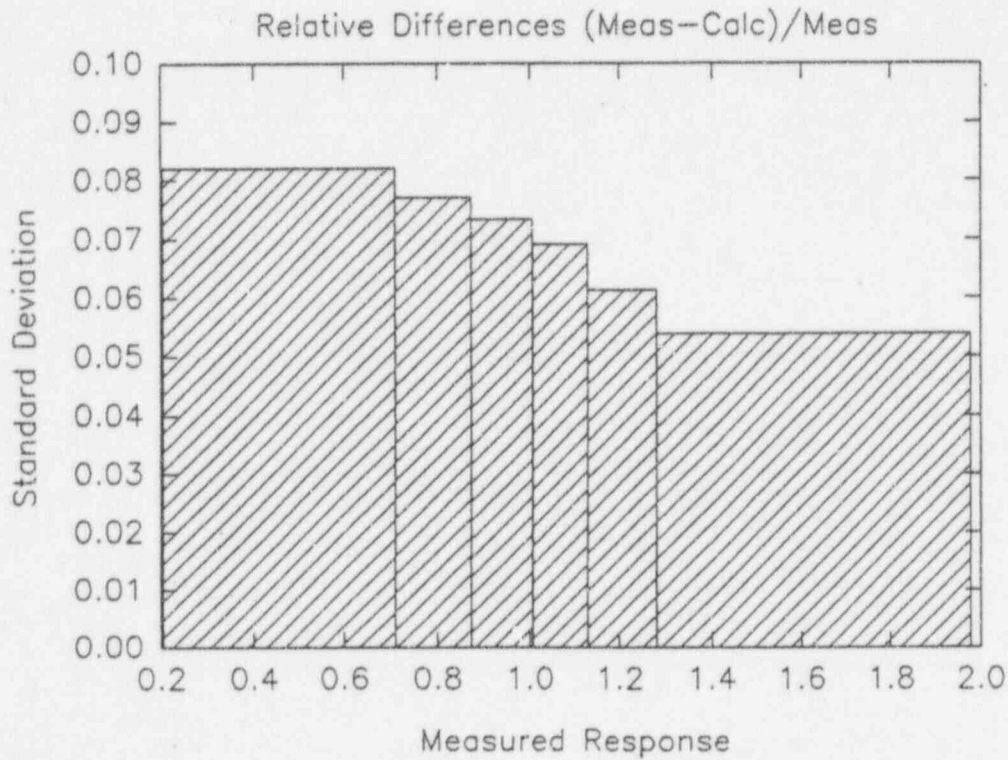
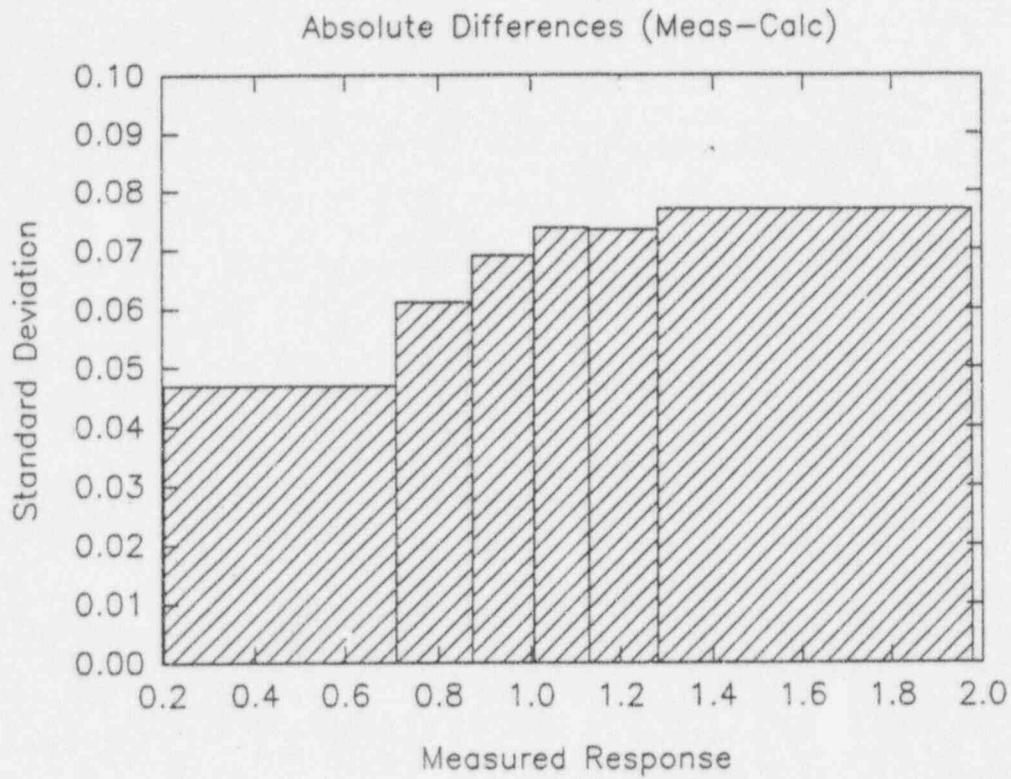


Figure 3.6.22  
 Standard Deviation  
 vs Measured Instrument Response



#### 4.0 MODEL APPLICATIONS TO REACTOR OPERATIONS

This section describes the methods used in applying the reliability factors and biases to reactor operations. It is not the intent of this section to define the procedures used. However, some aspects of these procedures are presented in order to clarify the approach taken in applying the model reliability factors and biases.

The model will be applied to reactor operations in two primary modes, predictive and monitoring. Cold critical comparisons, including few rod and in-sequence criticals; and hot criticals at power are given below to verify this mode of application.

In the monitoring mode, process computer support and isotopic inventory calculations must be considered.

#### 4.1 Predictive Applications

##### 4.1.1 Cold Criticals

NSP has predicted few rod cold criticals around the high worth rod for each cycle of operation in order to verify the predicted model. The resultant cold critical  $k_{eff}$  for all few rod criticals calculated for cycles 11 through 15 is:

$$k_{eff} = 0.9929 \pm .0023$$

NSP has predicted in-sequence withdrawals to cold critical for each cycle of operation to verify the rod withdrawal pattern and to prevent the withdrawal of a high notch worth rod that could scram the reactor.

The resultant cold critical  $k_{eff}$  for all in-sequence criticals calculated for cycles 11 through 15 is:

$$k_{eff} = 0.9922 \pm .0028$$

The combined statistics of few rod and in-sequence criticals calculated for cycles 11 through 15 is:

$$k_{eff} = 0.9923 \pm .0027$$

Table 4.1.1 gives the detailed information for each critical.

Figure 4.1.1 gives the graphical representation of the criticals for each cycle.

##### 4.1.2 Hot Full Power Criticals

NSP has predicted the hot at-power critical conditions throughout each cycle.

The resultant hot critical  $k_{eff}$  for all criticals calculated for cycles 11 through 15 is:

$$k_{eff} = 0.9979 \pm .0019$$

Table 3.6.1 gives the detailed information for each critical. Figure 4.1.2 gives the graphical representation of the criticals for each cycle. Circled points indicate coastdowns.



## 4.2 Monitoring Applications

### 4.2.1 Process Computer

The General Electric 3D-Monicores System recently installed at Monticello will be retained. NSP is currently evaluating several options for support of this system for cycles 18 and beyond. GE will supply support for cycle 17. The support options are as follows:

1. Continue to have GE supply all support.
2. NSP will support with system as installed.
3. NSP will support with system modified by replacing Panacea with an approved core model (i.e. SIMULATE-3 or NDH).

### 4.2.2 Isotopic Inventory

The isotopic inventory calculation will be performed by NSP if either option 2 or 3 is decided upon in Section 4.2.1. The calculation of the isotopic inventory for Monticello is based upon a two-dimensional, CASMO-3 calculation. This is the same model as is used to calculate the TIP trace design input. Therefore, the accuracy of the burnup distribution can be verified by the agreement of the measured and calculated reaction rates which is used to evaluate the measurement uncertainties, see Section 3.6 above. The accuracy of the isotopics versus local exposure is described in references 4 and 36 based on measurements at Yankee Rowe.

TABLE 4.1.1

## Few Rod and In-sequence Cold Criticals

Cycle	Cycle Exposure (GWD/MTU)	Temperature (°F)	F = Few Rod S = Sequence	$k_{eff}$
11	0.000	85	F	0.9921
	0.000	106	F	0.9936
	0.000	106	S	0.9948
	0.000	113	S	0.9936
12	0.000	129	F	0.9964
	0.000	128	S	0.9928
	0.000	128	S	0.9938
	3.256	141	S	0.9903
	6.260	203	S	0.9896
13	0.000	91	F	0.9905
	0.000	91	F	0.9904
	0.000	91	S	0.9897
	0.000	91	S	0.9908
	8.853	201	S	0.9876
	9.764	164	S	0.9851
14	0.000	109	F	0.9907
	0.000	111	S	0.9913
	0.000	118	S	0.9936
	4.569	122	F	0.9924
	4.569	123	S	0.9919
	5.811	152	S	0.9895
	6.647	209	S	0.9905
	8.510	154	S	0.9923
	8.510	142	S	0.9920
15	0.000	108	F	0.9933
	0.000	108	F	0.9963
	0.000	113	S	0.9939
	0.000	107	S	0.9963
	0.093	200	S	0.9979
	0.093	147	S	0.9962
	1.616	182	S	0.9939
	4.151	137	S	0.9922
	6.202	129	S	0.9928

Statistics			
Type	N	Mean	$\sigma$
Few Rod	9	0.9929	0.0023
Sequence	24	0.9922	0.0028
Combined	33	0.9923	0.0027

Figure 4.1.1 Cold Criticals vs Core Average Exposure

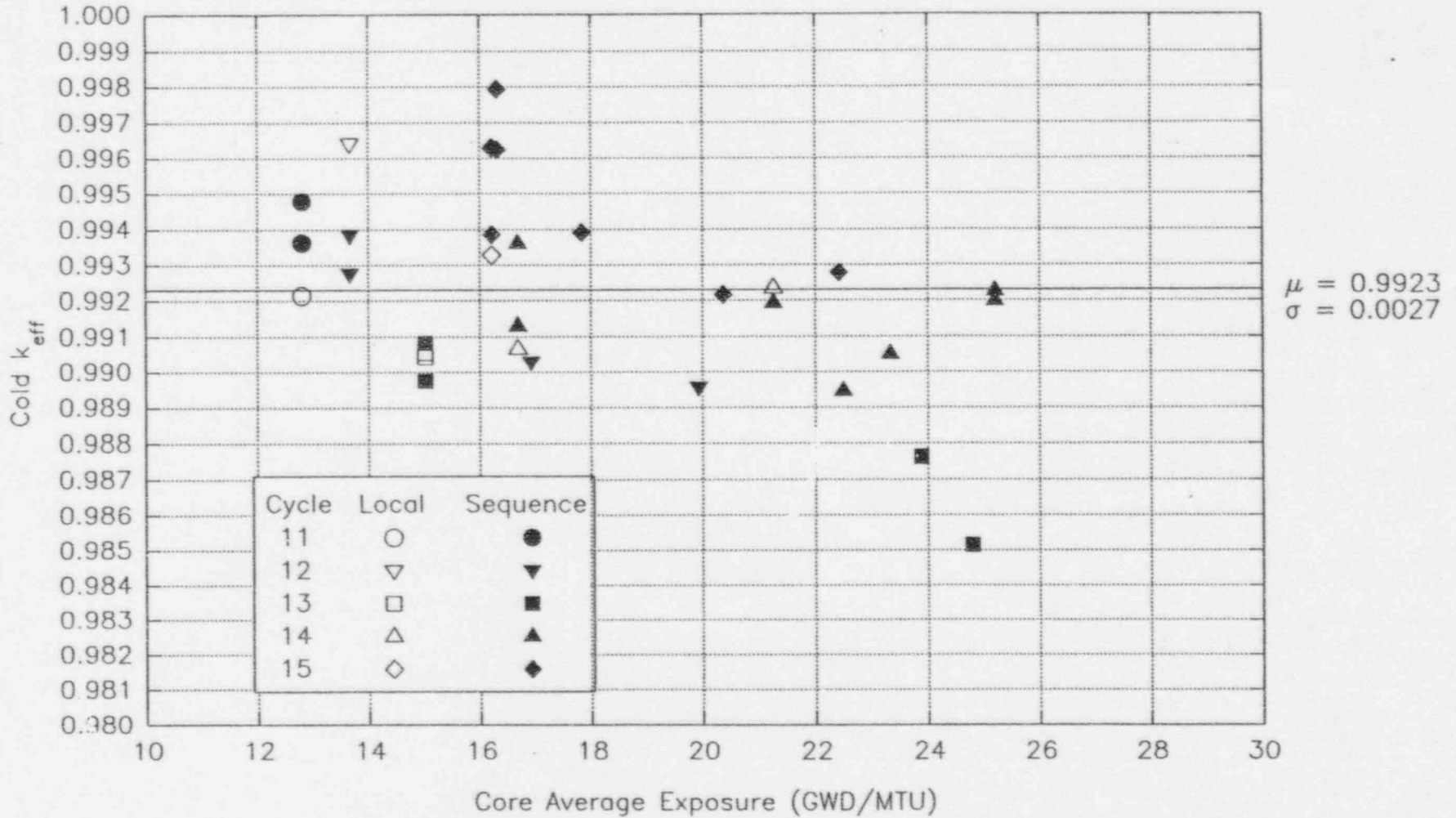
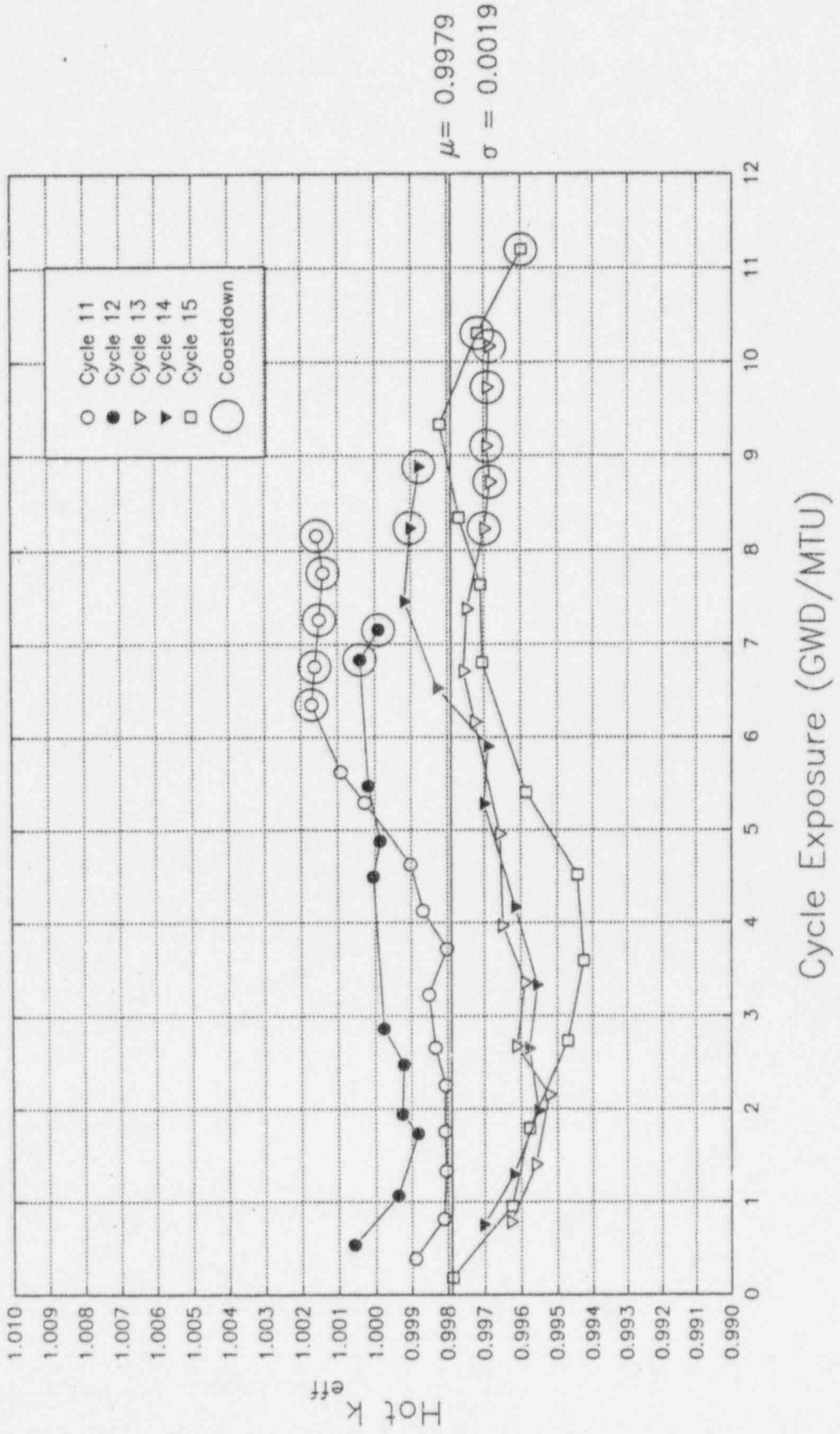


Figure 4.1.2 Hot Criticals



## 5.0 MODEL APPLICATIONS TO SAFETY EVALUATION CALCULATIONS

This section describes the methods used in applying the reliability factors and biases to the results of safety related physics calculations. It is not the intent of this section to define the procedures to be used in performing the physics calculations. However, some aspects of these procedures are presented in order to clarify the approach taken in applying the model reliability factors and biases.

In such applications, the question is generally: Will the reload core maintain a safe margin to established safety limits (i.e., peak linear heat generation rate, minimum CPR, shutdown margin, etc.) under normal and non-normal or accident conditions? The question is usually answered by performing cycle specific safety analyses for the limiting transients and accidents.

For each parameter of interest,  $RF_x$  and  $Bias_x$  are given in Table 3.0.1. The application of the  $RF_x$  and  $Bias_x$  for each parameter of interest is shown below.

### 5.1 Linear Heat Generation Rate (LHGR and APLHGR)

The Linear Heat Generation Rate (LHGR) and the Average Planar Linear Heat Generation Rate (APLHGR) are calculated directly in SIMULATE-3.

The model reliability factor and bias listed in Table 3.0.1 are then applied as follows:

$$LHGR = LHGR(model) (1 + Bias + RF_{TPF})$$

$$APLHGR = APLHGR(model) (1 + Bias + RF_{TPF})$$

where model signifies the best estimate value directly calculated with the 3D simulator.

### 5.2 Critical Power Ratio (CPR)

The Critical Power Ratio is defined as the ratio of the bundle power required to produce onset of transition boiling somewhere in the bundle (critical power) to the actual bundle power, i.e.:

$$CPR(I,J) = P_c(I,J) / P(I,J)$$

where:

$P_c(I,J)$  is the critical bundle power in assembly (I,J)

$P(I,J)$  is the actual bundle power in assembly (I,J)

The minimum critical power ratio, MCPR, is defined as the minimum value of CPR in the core, i.e.:

$$MCPR = (P_c(I,J) / (P(I,J)))_{\min}$$

The model reliability and bias listed in Table 3.0.1 are then applied as follows:

$$CPR = [P_c(I,J) / P(I,J)] (1 + Bias + RF_{RPF})$$

### 5.3 Control Rod Worth

Rod worth are calculated using the three-dimensional nodal model. Worth are determined by varying the rod position while the independent core parameters such as core power, flow, and void distribution are held constant.



The model reliability factor and bias listed in Table 3.0.1 are then applied as follows:

$$\Delta K_{\text{ROD}} = \Delta K_{\text{ROD}}(\text{MODEL}) (1 + \text{Bias}) (1 \pm \text{RF}_{\text{ROD}})$$

The reliability factor is either added or subtracted, whichever is most conservative for each particular application.

#### 5.4 Void Reactivity

The model reliability and biases listed in Table 3.0.1 are applied to  $\Delta k/\Delta U$  as

$$\Delta k/\Delta U (1 + \text{Bias}) (1 \pm \text{RF}_{\text{voids}})$$

The reliability factor is either added or subtracted, whichever is most conservative, for each application.

#### 5.5 Fuel Temperature (Doppler) Coefficient

The Doppler coefficient is a measure of the change in neutron multiplication associated with a change in fuel temperature. Reactivity is changed mainly due to Doppler broadening of the U-238 parasitic resonance absorption cross section due to increases in fuel temperature.

The model reliability factor and bias listed in Table 3.0.1 are then applied at each point as follows:

$$\Delta k/\Delta t_r^h (1 + \text{Bias}) (1 \pm \text{RF}_D)$$

Again, the reliability factor is either added or subtracted, whichever is most conservative for each particular application.

#### 5.6 Delayed Neutrons

The delayed neutron constants;  $\beta_{\text{eff}}$ , and  $\lambda_1$ , are assumed to be constant in time during a transient. The use of constant delayed neutron constants corresponding to the initial conditions is justified by the results in Reference 29 which show that  $\beta_{\text{eff}}$  does not change significantly during a transient until the scram is over. Adjoint flux weighting is used to obtain these constants.

The reliability factor listed in 3.0.1 is applied as shown:

$$\beta_{\text{eff}} (\text{model}) (1 + \text{Bias}) (1 \pm \text{RF}_\beta)$$

#### 5.7 Prompt Neutron Lifetime

The prompt neutron lifetime  $\Lambda$  is assumed to be constant in time.

The reliability factor listed in Table 3.0.1 is applied as follows:

$$\Lambda(\text{model}) (1 + \text{Bias}) (1 \pm \text{RF}_\Lambda)$$

## 6.0 REFERENCES

1. NSP Topical "Qualification of Reactor Physics Methods for Application to PI Units", NSPNAD-8101P, Rev. 1, December, 1982.
2. NSP Topical "Qualification of Reactor Physics Methods for Application to Monticello", NSPNAD-8609, Rev. 1, April, 1992.
3. NSP Topical "Monticello Nuclear Generating Plant Safety Evaluation Methods," NSPNAD-8608, Rev. 1, August, 1988.
4. A. S. DiGiovine, K. B. Spinney, D. G. Napolitano, J. Pappas, "CASMO-3G Validation and Verification", YAEC-1653-A, Yankee Atomic Electric Company, 1990.
5. A. S. DiGiovine, J. P. Gorski, M. A. Tremblay, "SIMULATE-3 Validation and Verification", YAEC-1659-A, Yankee Atomic Electric Company, 1990.
6. B. Y. Hubbard, D. J. Morin, J. Pappas, R. C. Potter, "MICBURN-3/CASMO-3/TABLES-3/SIMULATE-3 Benchmarking of Cycles 9 Through 13," YAEC-1683-A, Yankee Atomic Electric Company, 1990.
7. M. Edenius, and B. H. Forssen, "CASMO-3 A Fuel Assembly Burnup Program User's Manual", Studsvik AB, NFA-89/3 Rev.2, March, 1992.
8. M. Edenius, H. Häggblom, and B. H. Forssen, "CASMO-3 A Fuel Assembly Burnup Program Methodology", Studsvik AB, NFA-89/2 Rev.1, January, 1991.
9. M. Edenius, A. Ahlin, and H. Häggblom, "CASMO-2 User's Manual, Studsvik AB, NR-81/3, 1981.
10. M. Edenius, and C. Grägg, "MICBURN-3 Microscopic Burnup in Burnable Absorber Rods User's Manual", Studsvik AB, NFA-89/12, November, 1989.
11. J. A. Umbarger, A. S. DiGiovine, K. S. Smith, and J. T. Cronin, "SIMULATE-3 Advanced Three-Dimensional Two-Group Reactor Analysis Code Users Manual", Studsvik of America, SOA-92/01 Rev.0, April, 1992.
12. K. S. Smith, J. T. Cronin, and J. A. Umbarger, "SIMULATE-3 Advanced Three-Dimensional Two-Group Reactor Analysis Code Methodology", Studsvik of America, SOA-92/02 Rev.0, April, 1992.
13. J. A. Umbarger, and K. S. Smith, "TABLES-3 Library Preparation Code for SIMULATE-3", Studsvik of America, SOA-92/03 Rev.0, April, 1992.
14. "S3POST SIMULATE-3 Summary File Postprocessor", Studsvik of America, SOA-91/04, 1991
15. I. B. Fiero, M. A. Krammen, H. R. Freeburn, et al, "ESCORE-The EPRI Steady-State Core Reload Evaluator Code: General Description", Electric Power Research Institute, EPRI NP-5100-L-A, April, 1991.
16. M. A. Krammen, H. R. Freeburn, et al, "ESCORE-The EPRI Steady-State Core Reload Evaluator Code Volume 1: Theory Manual", Electric Power Research Institute, EPRI NP-4492-CCMP Volume 1, August, 1986.
17. M. A. Krammen, R. B. Fancher, N. T. Yackle, et al, "ESCORE-The EPRI Steady-State Core Reload Evaluator Code Volume 2: User's Manual", Electric Power Research Institute, EPRI NP-4492-CCMP

Volume 2, August, 1986.

18. M. A. Krammen, R. B. Fancher, M. W. Kennard, et al, "ESCORE-The EPRI Steady-State Core Reload Evaluator Code Volume 3: Programmer's Manual", Electric Power Research Institute, EPRI NP-4492-CCMP Volume 3, August, 1986.
19. D. B. Jones, "ARMP-02 Documentation Part II, Chapter 7-MICBURN-E Computer Code Manual Volume 1: Theory and Numerics Manual", Electric Power Research Institute, EPRI NP-4574-CCM, Part II, Ch. 7 Volume 1, December, 1986.
20. D. B. Jones, "ARMP-02 Documentation Part II, Chapter 7-MICBURN-E Computer Code Manual Volume 2: User's Manual", Electric Power Research Institute, EPRI NP-4574-CCM, Part II, Ch. 7 Volume 2, December, 1986.
21. D. B. Jones, "ARMP-02 Documentation Part II, Chapter 7-MICBURN-E Computer Code Manual Volume 3: Programmers Manual", Electric Power Research Institute, EPRI NP-4574-CCM, Part II, Ch. 7 Volume 3, December, 1986.
22. M. Edenius, and H. Häggblom, "Benchmarking of CASMO Resonance Integrals for U-238 Against Hellstrand's Measurements", Studsvik of America, SOA-91/05, December, 1991.
23. M. A. Edenius, "Benchmarking of CASMO Resonance Integrals for U-238 Against Hellstrand's Measurements. Comparison between CASMO-3 Versions 4.4 and 4.7", Studsvik of America, SOA-93/04, March, 1993.
24. M. A. Edenius, "CASMO Doppler Coefficients versus MCNP-3A Monte Carlo Calculations", Studsvik of America, SOA-93/06, October, 1993.
25. M. Edenius, "Studies of the Reactivity Temperature Coefficient in Light Water Reactors," AE-RF-76-3160, AB Stomenergi, 1976.
26. M. Edenius, "Seminar on U-238 Resonance Capture," S. Pearlstein, Editor, page 87, BNL-NCS-50451, 1975.
27. M. Edenius, "Temperature Effects in Thermal Reactor Analysis," Internal Report presented to Oskarshamnuerkets Kraftgrupp AB(OKG), Stockholm, Sweden, employed by AB Stomenergi Studsvik, Sweden.
28. M. Edenius, and A. Ahlin, "CASMO-3: New Features, Benchmarking, and Advanced Applications," *Nuclear Science and Engineering*, 100, No. 3, p. 342, November, 1988.
29. J. M. Holzer, et.al. "A Code System to Produce Point Kinetics Parameters for LWR Calculations," *ANS Trans*, 39, 946-7, 1981.
30. M.G. Kendall, A. Stuart, "The Advanced Theory of Statistics," Vol. 1, 5th. ed., Hafner Publishing Co. N.Y., 1987.
31. D.B. Owen, "Factors for One-Sided Tolerance Limits and for Variables Sampling Plans" Sandia Corporation, March 1963.
32. K. S. Smith, "SIMULATE-3 Pin Power Reconstruction: Benchmarking Against B&W Critical Experiments," *Trans. Am. Nuc. Soc.*, 56, p. 531, San Diego, CA, June, 1988.
33. M. Edenius, "CASMO-3 Benchmarking," *Trans. Am. Nuc. Soc.*, 56, p. 536, San Diego, CA, June, 1988.
34. K. R. Rempe, K. S. Smith, and A. F. Henry, "SIMULATE-3 Pin Power

- Reconstruction: Methodology and Benchmarking," *Nuclear Science and Engineering*, 103, No. 4, p. 334, December, 1989.
35. T. Uegata, E. Saji, and H. Tanaka, "Verification of the CASMO-3/SIMULATE-3 Pin Power Accuracy by Comparison with Operating Boiling Water Reactor Measurements," *Nuclear Science and Engineering*, 114, No. 1, p. 81, May, 1993.
  36. P. J. Rashid, "CASMO-3 Benchmark Against Yankee Rowe Isotopics", Studsvik of America, SOA-86/05, September, 1986.
  37. "Nuclear Design Methodology Using CASMO-3/SIMULATE-3P," Duke Power Company DPC-NE-1004A, November, 1992.
  38. D. J. Edwards, L. E. Kostynak, F. A. Monger, R. M. Rubin, and C. E. Willingham, "Steady State Reactor Physics Methodology," Texas Utilities Electric Company, RXE-89-003-NP, July, 1989.
  39. R. Y. Chang, C. W. Gabel, "PWR Reactor Physics Methodology Using CASMO-3/SIMULATE-3," Southern California Edison Company, SCE-9001-A, September, 1992.
  40. M. Edenius and P. J. Rashid, "Benchmarking of the Gamma-TIP Calculation in CASMO Against the Hatch BWR," *Trans. Am. Nuc. Soc.*, 49, p. 431, Boston, MA, June, 1985.
  41. K. S. Smith and K. R. Rempe, "Testing and Applications of the QPANDA Nodal Model," *Nuclear Science and Engineering*, 100, No. 3, p. 324, November, 1988.
  42. A. S. DiGiovine and D. G. Napolitano, "SIMULATE-3 Pin Power Reconstruction and Comparison to Fine-Mesh PDQ," *Trans. Am. Nuc. Soc.*, 54, p. 361, Dallas, TX, June, 1987.
  43. K. R. Rempe and K. S. Smith, "SIMULATE-3: Power Distributions and Detector Response Modeling," *Trans. Am. Nuc. Soc.*, 54, p. 355, Dallas, TX, June, 1987.
  44. D. G. Napolitano, A. S. DiGiovine, K. R. Rempe, and K. S. Smith, "SIMULATE-3: Pin Power Reconstruction Applied to Seabrook Station," *Trans. Am. Nuc. Soc.*, 55, p. 590, Los Angeles, CA, November, 1987.
  45. R. Hakanson and E. Kurcyusz-Ohlofsson, "Forsmark 1 Core Analysis with the Studsvik Code Package," *Proceedings of the 1988 International Reactor Physics Conference*, Jackson Hole, WY, September, 1988.
  46. A. S. DiGiovine, J. P. Gorski, and M. A. Tremblay, "Verification of the SIMULATE-3 Pin Power Distribution Calculation.," *Nuclear Science and Engineering*, 103, No. 4, p. 324, December, 1989.
  47. E. Kurcyusz-Ohlofsson, "Analysis of Advanced PWR Cores with CASMO-3/SIMULATE-3," *PHYSOR 90*, Vol.2, p. XIV-1, Marseille, France, April, 1990.
  48. K. S. Smith and K. R. Rempe, "Mixed-Oxide and BWR Pin Power Reconstruction," *PHYSOR 90*, Vol.2, p. VII-11, Marseille, France, April, 1990.
  49. H. Grubel, R. Rippler, G. Skoff, B. Wikes, and G. Wupperfeld, "Umstellung der nuklearen Kernausslegung für das KfW Mülheim-Kärlich (KMK) auf das Studsvik-Programmsystem CASMO/SIMULATE," *Tagungsbericht Proceedings, Jahrestagung Kerntechnik '91*, p. 3, Bonn, Germany, May, 1991.

50. Y. Wang, J. Yang, Y. Yeh, and S. Yaur, "Neutronic Model Verification for Maanshan Power Plant with Advanced In-core Fuel Management Package," *Proceedings of the 1992 Topical Meeting on Advances in Reactor Physics*, p. 1-13, Charleston, SC, March, 1992.
51. A. Jonsson, D. R. Harris, R. Y. Chang, O. J. Thomsen, "Analysis of Critical Experiments with Erbia-Urania Fuel," *Trans. Am. Nuc. Soc.*, 65, p. 415, Boston, MA, June, 1992.

APPENDIX A Statistical Methods for the Determination and Application of  
Uncertainties

The purpose of using statistical methods is to determine the value  $X_c$  (calculated) such that there is a 95% probability at the 95% confidence level that  $X_c$  will be conservative with respect to  $X_T$  (true value) when applying the calculational methods to safety related reactor analyses.

The first step is to determine whether or not a distribution is normal. If it is, the methods described in Section A.1 are used. If the distribution cannot be treated as normal, but the distributions are known, then the methods described in Section A.2 are used.

If neither of the above methods apply, then the parameter in question is conservatively bounded.



## A.1 Application of Normal Distribution Statistics

### Separation of Measurement and Computational Uncertainties

Comparison of measured and calculated reactor parameters includes the effects of both the measurement and calculational uncertainties. Methods used in this report to isolate the calculational uncertainties are described below in terms of the following definitions:

$X_i$  = true reactor parameter

$X_m$  = measured reactor parameter

$X_c$  = calculated reactor parameter

$e_m = (X_m - X_i) / X_i$  = measurement error

$e_c = (X_c - X_i) / X_i$  = calculation error

$e_{mc} = (X_m - X_c) / X_m$  = observed differences

$$\mu = \frac{\sum_{i=1}^n e_i}{n}$$

$$\sigma = \left( \sum_{i=1}^n (e_i - \mu_i)^2 / (N-1) \right)^{1/2} = \text{standard deviation}$$

If  $e_m$  and  $e_c$  are independent, then the following relationships exist. (Note that these relationships apply for non-normal distributions as well).

$$\sigma_c^2 = \sigma_{mc}^2 - \sigma_m^2$$

$$\mu_c = \mu_c - \mu_{mc}$$

Once the  $\sigma_c$  and  $\mu_c$  have been calculated from historical data, they could be used to apply conservatism to future calculations of reactor parameters,  $X_c$ , as follows:

$$X_c - X_c (1 + \mu_c) (1 \pm K_c \sigma_c)$$

The factor  $K_c$  is defined as described in Table A.1.14 to provide a 95% probability at the 95% confidence level that  $X_c$  is conservative with respect to the true value,  $X_i$ .

### Reliability Factors

It is the objective to define reliability factors which are to be used to increase/decrease calculated results to the point where there is a 95% probability at the 95% confidence level that they are conservative with respect to actual reactor parameters.

For any given application, there is concern only with one side of the component; that is, if the calculated value is too large or too small.

Therefore, one-sided tolerance limits based on normal distributions may be used to find a  $K_c$  which will give a 95% probability at the 95% confidence level to the reliability factor defined by:

$$RF = K_c \sigma_c$$

Numerical values of  $K_c$  for various sample sizes used to calculate  $\sigma_c$  are provided on Table A.1.

TABLE A.1

Single-Sided Toleranc. Factors (Reference 31)

n	$K_c$
2	26.26
3	7.66
4	5.15
5	4.20
6	3.71
7	3.40
8	3.19
9	3.03
10	2.91
11	2.82
12	2.74
15	2.57
20	2.40
25	2.29
30	2.22
40	2.13
60	2.02
100	1.93
200	1.84
500	1.76
$\infty$	1.645

n = Number of data points used for  $\sigma$

## A.2 Application of Non-Normal Distribution Statistics

If a distribution is determined to be other than normal, the requirement is that there is a 95% confidence level that  $X_c$  will be conservative with respect to the true value  $X_m$ . (In the following, the notation used is consistent with that defined in Section A.1). It is thus required that a 95% upper confidence limit be determined for the 95th percentile of the distribution of errors.

In the calculation, a set of error observations ( $e_i$ ) are determined. The mean ( $\mu_{mc}$ ) and the standard deviation ( $\sigma_{mc}$ ) are calculated using the following formulation:

$$\mu_{mc} = \frac{\sum_{i=1}^n e_i}{n}$$

$$\sigma_{mc} = \left( \frac{\sum_{i=1}^n (e_i - \mu_{mc})^2}{n-1} \right)^{1/2}$$

Note that the  $e_i$  above are determined from the following:

$$e_i = e_{mc} = (X_m - X_c) / X_m = \text{observed differences}$$

Generally, the  $e_{mc}$  are taken from several cycles of operation; thus, they represent the true distribution. The  $e_i$  are then transformed to standard measure by the following formula:

$$Z_i = \frac{e_i - \mu_{mc}}{\sigma_{mc}}$$

and the resulting variates ( $Z$ ) are sorted into ascending order and the  $k$ th (such that  $k \geq .95n$ ) variate is chosen as an estimate of the 95th percentile of the distribution (See reference 30, page 50-51). This gives a 95th percentile of  $Z$  to be  $Q_{95}$ . This implies that 95% of the errors are likely to be less than  $Q_{95}$ .

It remains to calculate a 95% confidence interval on  $Q_{95}$ . (The formula for this calculation is taken from reference 13 page 236-243 (See references section 6.0).

$$\text{Var } Q_{95} = \frac{q(1-q)}{n f_1^2}$$

where:  $q$  = the quantile (.95)  
 $n$  = number of independent observations in the sample  
 $f_1$  = ordinate of the density function of the distribution of observed differences at abscissa  $q$

It is necessary to determine if the observations are independent. If they are not independent, it is necessary to reduce the sample size to account for the dependence in the determination of the 95% confidence level.

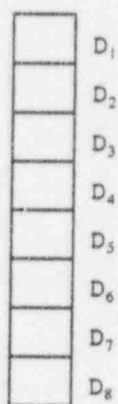


Figure A.2.1. Differences for Nearby Positions

To set notation, let  $\delta_{.95}$  be the population 95th percentile for the observed differences, that is  $P[D_i \leq \delta_{.95}] = .95$ . We wish to determine a 95% upper confidence limit for  $\delta_{.95}$  when some of the differences are dependent. For differences observed at adjacent positions, the appropriate measure of association for our analysis can be shown to be

$$C(1) = P[D_1 \leq \delta_{.95} \text{ and } D_2 \leq \delta_{.95}] - (.95)^2$$

We also consider the association of differences observed at locations two apart

$$C(2) = P[D_1 \leq \delta_{.95} \text{ and } D_3 \leq \delta_{.95}] - (.95)^2$$

and, more generally,

$$C(k) = P[D_1 \leq \delta_{.95} \text{ and } D_{1+k} \leq \delta_{.95}] - (.95)^2$$

for  $k = 1, 2, 3, 4, 5, 6, 7$  locations apart. In this example, there are 8 differences  $D_i$ , 7 adjacent pairs  $(D_i, D_{i+1})$ , 6 pairs with indices two apart  $(D_i, D_{i+2}) \dots$ , 1 pair  $D_1, D_8$ .

Let  $d_{(s)}$  be the sample 95th percentile with  $s$  selected to be the smallest integer not less than  $.95n$ . The large sample distribution of  $d_{(s)}$  depends on that of

$T(x)$  = number of differences,  $D_i$ , that are less than or equal  $x$ .

Even with dependence among the  $D_i$ ,

$$\frac{T(x) - nF(x)}{s.d. [T(x)]} = \frac{\frac{1}{\sqrt{n}} (T(x) - nF(x))}{\frac{1}{\sqrt{n}} s.d. [T(x)]}$$

will be approximately standard normal. Here  $F(x) = P[D_i \leq x]$  and  $f(x)$  is the probability density function for the observed differences.

It follows that

$$P[\sqrt{n}(d_{(s)} - \delta_{.95}) \leq z] = 1 - P[T(\delta_{.95} + n^{-1/2}z) \leq s-1]$$

$$= 1 - \Phi \left[ \frac{-f(\delta_{.95})z}{\frac{1}{\sqrt{n}} \text{s.d.}[T(\delta_{.95})]} \right]$$

where

$$\left[ \frac{1}{\sqrt{n}} \text{s.d.}[T(\delta_{.95})] \right]^2 = \frac{1}{n} [n(.95)(.05) + 2 \frac{7}{8}nC(1) + 2 \frac{6}{8}nC(2) + \dots + \frac{2}{8}nC(7)]$$

$$= (.95)(.05) + \frac{14}{8}C(1) + \frac{12}{8}C(2) + \frac{10}{8}C(3) + \dots + \frac{2}{8}C(7)$$

Under independence  $0 = C(1) = C(2) = \dots = C(7)$  and this expression reduces to its customary value  $(.95)(.05)$ . If the differences are dependent, the variance of  $d_{(s)}$  is

$$\frac{(.95)(.05)}{nf^2(\delta_{.95})} \left[ 1 + \sum_{k=1}^7 \frac{2(8-k)C(k)}{8(.95)(.05)} \right]$$

In order to apply this result, we estimate  $C(1)$  by

$$C(1) = \frac{\text{number of adjacent pairs } (D_i, D_{i+1}) \text{ where both } \leq d_{(s)} - (.95)^2}{\text{Total number of adjacent pairs}}$$

The estimate of  $C(2)$  is

$$C(2) = \frac{\text{number of pairs } (D_i, D_{i+2}) \text{ where both } \leq d_{(s)} - (.95)^2}{\text{Total number of pairs } (D_i, D_{i+2})}$$

and

$$C(k) = \frac{\text{number of pairs } (D_i, D_{i+k}) \text{ where both } \leq d_{(s)} - (.95)^2}{\text{Total number of pairs } (D_i, D_{i+k})}$$

for  $k = 3, 4, 5, 6, 7$ . The value of  $f^2(\delta_{.95})$  can be estimated as previously suggested. Then, the large sample upper 95% confidence limit for  $\delta_{.95}$ , adjusted for dependence among differences by location is given by

$$d_{(s)} + \frac{1.645}{\sqrt{n}} \left[ \frac{(.95)(.05)}{f^2(\delta_{.95})} \left( 1 + \sum_{k=1}^7 \frac{2(8-k)C(k)}{8(.95)(.05)} \right) \right]^{1/2}$$

One interpretation of this confidence limit, or the variance expression, is that the total sample size  $n$  is effectively reduced by the dependence. We estimate the effective sample size to be



$$\frac{n}{1 + \sum_{k=1}^7 \frac{2(8-k)C(k)}{8(.95)(.05)}}$$

If only two terms are used, the effective sample size is estimated to be

$$n \left[ \frac{(.95)(.05)}{(.95)(.05) + \frac{14}{8}C(1) + \frac{12}{8}C(2)} \right]$$

It is necessary to obtain an estimate of  $f_1(.95)$  on a short interval of the cumulative distribution function of  $Z$  in the region of the 95th percentile. The slope of the cumulative distribution function is an estimate of the ordinate of the density function since the density function is simply the derivative of the cumulative distribution function. Thus

$$\sigma_{Q_{95}}^2 = \text{Var } Q_{95}$$

This value then allows an estimate of the 95% confidence limit on  $Q_{95}$ . Even though nothing is known about the distribution of  $Q_{95}$ , the distribution can be shown to be normal using the following derivation.

$$P[D_1 \leq \delta_{.95} \text{ and } D_2 \leq \delta_{.95}]$$

where  $\delta_{.95}$  is the 95th percentile of the distribution of differences. If the differences  $D_1$  and  $D_2$  are independent

$$\begin{aligned} P[D_1 \leq \delta_{.95} \text{ and } D_2 \leq \delta_{.95}] &= P[D_1 \leq \delta_{.95}] P[D_2 \leq \delta_{.95}] \\ &= (.95)(.95) = (.95)^2 \end{aligned}$$

The difference

$$P[D_1 \leq \delta_{.95} \text{ and } D_2 \leq \delta_{.95}] - (.95)^2$$

is a measure of association (dependence) from position to adjacent position. Note that if

$$\begin{aligned} I(D_1 \leq \delta_{.95}) &= \begin{cases} 1 & \text{if } D_1 \leq \delta_{.95} \\ 0 & \text{if } D_1 > \delta_{.95} \end{cases} \\ I(D_2 \leq \delta_{.95}) &= \begin{cases} 1 & \text{if } D_2 \leq \delta_{.95} \\ 0 & \text{if } D_2 > \delta_{.95} \end{cases} \end{aligned}$$

then the covariance is

$$C(1) = \text{Cov}(I(D_1 \leq \delta_{.95}), I(D_2 \leq \delta_{.95})) = P[D_1 \leq \delta_{.95} \text{ and } D_2 \leq \delta_{.95}] - (.95)^2$$

We assume the same covariance for

$$I(D_2 \leq \delta_{.95}) \text{ and } I(D_3 \leq \delta_{.95}) \dots I(D_7 \leq \delta_{.95}) \text{ and } I(D_8 \leq \delta_{.95}).$$

There are about  $n \cdot 7/8$  such pairs among the whole set of  $n$  observed

differences.

Let  $d_{(s)}$  be the sample 95th percentile where  $s$  is the smallest integer not less than  $n(.95)$ . When  $n$  is large

$$C(1) = \frac{\text{number of pairs } (D_i, D_{i+1}) \text{ where both } \leq d_{(s)}}{\text{Total number of pairs } (D_i, D_{i+1})} - (.95)^2$$

is a good estimate of  $C(1)$ . Similarly, for the approximately  $6n/8$  pairs  $(D_i, D_{i+2})$

$$C(2) = \text{Cov}[I(D_1 \leq \delta_{.95}), I(D_3 \leq \delta_{.95})]$$

is estimated by

$$C(2) = \frac{\text{number of pairs } (D_i, D_{i+2}) \text{ where both } \leq d_{(s)}}{\text{Total number of pairs } (D_i, D_{i+2})} - (.95)^2$$

and

$$C(k) = \frac{\text{number of pairs } (D_i, D_{i+k}) \text{ where both } \leq d_{(s)}}{\text{Total number of pairs } (D_i, D_{i+k})} - (.95)^2$$

Let us now see how to modify the proof that  $d_{(s)}$  is asymptotically normal in order to account for the dependence among adjacent differences. It is still true that

$$(A1) \quad P[d_{(s)} \leq x] = 1 - P[d_{(s)} > x] = 1 - P[s-1 \text{ or fewer } D_i \leq x] \\ = 1 - P[T(x) < s]$$

where  $T(x) = \sum_{i=1}^n I(D_i \leq x) = \# \text{ differences } D_i \leq x$ . Moreover,  $T(x) - nF(x)$

has mean 0 and, for large samples, is approximately normal under a wide range of dependence structures. Consequently, the

sums  $\sum_{i=1}^g I(D_i \leq x)$  are independent of one another and each has the same

distribution. Since  $T(x)$  is just the sum of these group sums, the central limit theorem gives

$$\frac{T(x) - nF(x)}{s.d. [T(x)]} \text{ is approximately standard normal.}$$

Consequently, from (A1) and the normal approximation

$$(A2) \quad P[\sqrt{n}(d_{(s)} - \delta_{.95}) \leq Z] = P[d_{(s)} \leq \delta_{.95} + n^{-1/2}Z] \\ = 1 - P[T(\delta_{.95} + n^{-1/2}Z) < s] \\ = 1 - \Phi \left[ \frac{s - nF(\delta_{.95} + n^{-1/2}Z)}{s.d. [T(\delta_{.95} + n^{-1/2}Z)]} \right]$$

Now, note that

$$\begin{aligned} \frac{1}{\sqrt{n}} (s - nF(\delta_{.95} + n^{-1/2}z)) &= \frac{1}{\sqrt{n}} (s - nF(\delta_{.95}) - nf(\delta_{.95})n^{-1/2}z + o(1)) \\ &= \frac{1}{\sqrt{n}} (s - n(.95) - n^{1/2}zf(\delta_{.95})) + o(1) \\ &= -zF(\delta_{.95}) + o(1) \end{aligned}$$

Furthermore,

$$\begin{aligned} \frac{1}{n} \text{Var}[T(\delta_{.95} + n^{-1/2}z)] &= \text{Var}[I(D_1 \leq \delta_{.95} + zn^{-1/2})] \\ &+ \sum_{k=1}^7 \frac{2(8-k)}{8} \text{Cov}[I(D_1 \leq \delta_{.95} + n^{-1/2}z), I(D_{1..k} \leq \delta_{.95}n^{-1/2}z)] \end{aligned}$$

which converges to

$$\begin{aligned} F(\delta_{.95}) - F^2(\delta_{.95}) + \sum_{k=1}^7 \frac{2(8-k)}{8} (P[D_1 \leq \delta_{.95}, D_{1..k} \leq \delta_{.95}] - (.95)^2) \\ = (.95)(.05) + \sum_{k=1}^7 \frac{2(8-k)}{8} C(k) = \lim \frac{1}{n} \text{Var}[T(\delta_{.95})] \end{aligned}$$

Therefore, by (A2),

$$P[\sqrt{n}(d_{(s)} - \delta_{.95}) \leq z] \sim 1 - \Phi \left[ \frac{-zf(\delta_{.95})}{\frac{1}{\sqrt{n}} \text{s.d.}[T(\delta_{.95})]} \right]$$

or  $\sqrt{n}(d_{(s)} - \delta_{.95})$  is approximately normal with mean 0 and variance

$$\frac{1}{n} \left[ \frac{(.95)(.05) + \sum_{k=1}^7 2(8-k)C(k)/8}{f^2(\delta_{.95})} \right]$$

As was indicated above, the  $C(k)$  may be estimated by  $C(k)$  and the large sample normality will still hold. Therefore using Table A.1 to obtain  $K_c$ :

$$\lambda_{Q_{95}} = K_c (\text{Var } Q_{95})^{1/2}$$

Thus it is 95% certain that  $Q_{95}$  lies in the interval

$$Q_{95} \leq Q_{95} + \lambda \sigma_{Q_{95}}$$

therefore it is safe to say that we are 95% confident that the 95th percentile of the differences is:

$$\mu_{mc} + \sigma_{mc.95} \leq \mu_{mc} + (Q_{95} + \lambda \sigma_{Q_{95}}) \sigma_{mc}$$

APPENDIX B Computer Code Summary Description

<u>COMPUTER CODE</u>	<u>DESCRIPTION</u>
CASMO-3	<p>CASMO-3 is a multigroup two-dimensional transport theory code for depletion and branch calculations for a single assembly. It calculates the cross sections, nuclide concentrations, pin power distributions, and other nuclear data used to calculate input to the SIMULATE-3 program. Some of the characteristics of CASMO-3 are:</p> <ol style="list-style-type: none"> <li>1. 40 energy group cross section library.</li> <li>2. 7 energy groups are used during the two-dimensional transport calculations.</li> <li>3. Gadolinium effective cross sections are generated by the MICBURN-3 program.</li> <li>4. The predictor-corrector approach is used for depletion.</li> <li>5. Effective resonance cross sections are calculated individually for each pin.</li> </ol>
ESCORE	<p>ESCORE is a steady-state fuel performance code capable of modeling the thermal and mechanical response of LWR fuel and used to provide fuel temperature inputs.</p>
MICBURN-3	<p>MICBURN-3 calculates the burnup of a fuel pin containing gadolinium and generates 40 group effective cross sections as a function of number density for gadolinium to be input to CASMO-3.</p>
SIMULATE-3	<p>A two-group 3D nodal program based on the QPANDA neutronics model. Some of the features of SIMULATE-3 are:</p> <ol style="list-style-type: none"> <li>1. Explicit reflector cross model.</li> <li>2. Pin power reconstruction.</li> <li>3. Fourth order expansion of intranodal flux distribution.</li> <li>4. No input normalization from higher order calculations or benchmark results.</li> </ol>
SPM	<p>Receives input from S3POST of the predicted, measured, and difference of the TIP reaction rates and calculates the biases and reliability factors.</p>
S3POST	<p>Reads output SIMULATE-3 and generates summaries and comparisons to measured incore TIP response. Modified by NSP to generate a file containing measured and predicted incore TIP response for input to the SPM program.</p>
TABLES-3	<p>Reads CASMO-3 output files and generates the input tables and curve fits for each fuel type for the SIMULATE-3 computer program.</p>